Order Number 9026014

Grain growth in sintered ZnO ceramics

Nunes, Silvia Irene, Ph.D.

University of Washington, 1989

U·M·I

300 N. Zeeb Rd.
Ann Arbor, MI 48106

Grain Growth in Sintered ZnO Ceramics

by

Silvia Irene Nunes

A dissertation submitted in partial fulfillment

of the requirements for the degreee of

Doctor of Philosophy

University of Washington

1990

Approved by Robert C. Bradt
(Chairperson of Supervisory Committee)

Program Authorized
to Offer Degree Materials Science and Engineering

Date December 18, 1989

DOCTORAL DISSERTATION

In presenting this dissertation in partial fulfillment of the requirements for the doctoral degree at the University of Washington, I agree that the Library shall make its copies freely avaiable for inspection. I further agree that extensive copying of this dissertation is allowable only for scholar purposes, consistent with "fair use" as prescribed in the U.S. Copyright Law. Requests for copying or reproduction of this dissertation may be referred to University Microfilms, 300 North Zeeb Road, Ann Arbor, Michigan 48106, to whom the author has granted "the right to reproduce and sell (a) copies of the manuscript in microfilm and/or (b) printed copies of the manuscript made from microform."

Signature Silvia Irene Mejias

Date December 18, 1989

University of Washington

ABSTRACT

by

Silvia Irene Nunes

GRAIN GROWTH IN SINTERED ZnO CERAMICS

Chairperson of the
Supervisory Committee

Prof. MSE Dr. R. C. Bradt
Dean, Mackay School of Mines
University of Nevada - Reno
Reno, NV. 89557-0047

The effects of the ZnO initial powder particle size and the spinel forming additives, Nb_2O_5 and Al_2O_3, on the ZnO grain growth processes and grain growth kinetics in pure ZnO and ZnO + 6 wt% Bi_2O_3 were studied. Two different initial ZnO particle sizes, 0.11 μm and 2.0 μm, were employed. Samples were fired at 900 °C, 1030 °C, 1192 °C, and 1400°C. The levels of the Nb_2O_5 and Al_2O_3 additives varied from 0.05 wt% to 0.80 wt%.

During solid state sintering of the "pure" ZnO the grain growth process is a normal one. The presence of the

Bi_2O_3-rich liquid phase promoted discontinuous grain growth when the initial ZnO particle size was 0.11 μm. Increasing the initial ZnO particle size, from 0.11 μm to 2.0 μm, suppressed the tendency for discontinuous grain growth. These observations were explained in terms of capillary forces excerted by the Bi_2O_3-rich liquid phase on the solid particles.

Additions of Nb_2O_5 to the ZnO + 6 wt% Bi_2O_3 system enhances the ZnO discontinuous grain growth when the Nb_2O_5 content is less than about 0.40 wt%. However, the grain growth is inhibited and appears normal when the Nb_2O_5 content is increased to 0.80 wt%. It is suggested that the grain growth enhancement might be due to enhanced Zn^{2+} diffusivity caused by the Nb^{5+} ions in solid solution. The presence of the spinel phase, $Zn_3Nb_2O_8$, at high Nb_2O_5 contents was confirmed by x-ray diffraction. Grain growth inhibition was attributed to spinel phase grain boundary drag mechanisms.

Al_2O_3 additions to ZnO + 6 wt% Bi_2O_3 prevent the occurrence of ZnO discontinuous grain growth and inhibit normal grain growth as well. The grain growth inhibition by the Al_2O_3 was explained in terms of segregation of the Al^{3+} ions to the grain boundaries and by grain boundary drag mechanisms due to the $ZnAl_2O_4$ spinel phase.

Higher values of the activation energies for grain growth, from 350 kJ/mol to 400 kJ/mol, are encountered for

systems in which the grain growth process is normal, while lower values of the activation energy, from 150 kJ/mol to 35 kJ/mol, occur for those systems with discontinuous grain growth. It is concluded that grain growth in the ZnO + 6 wt% Bi_2O_3 ceramics is controlled by drag mechanisms and that the activation energy decreases because during the earlier stages of the discontinuous grain growth process many pores are left behind by highly mobile grain boundaries.

The effects of the spinel forming additives, Nb_2O_5 and Al_2O_3, are expressed in terms of a general schematic diagram containing three regions. In the first region, grain growth is inhibited through solute segregation to the grain boundaries creating reduced grain boundary mobility through a solute drag mechanism. In the second region, additive solubility was accompanied by increased lattice vacancy concentration and enhanced cation diffusivity leading to an increased rate of grain growth. The third region is one of grain boundary pinning by spinel crystals at the grain boundaries, inhibiting grain growth.

TABLE OF CONTENTS

LIST OF FIGURES

LIST OF TABLES

ACKNOWLEDGEMENTS

The author wishes to express sincere appreciation to her advisor Prof. Richard D. Bradt for his guidance and support throughout this research. The constant assistance and invaluable advice of Prof.O.J.Whittemore are also deeply appreciated. Special thanks are extended to Prof. W.D.Scott, Prof.D.B.Fishbach and Prof.O.Vilches for their support, Prof. Robert Dunnel for the use of the Image Analyser and to Larry Kniffen for the beautiful SEM photographs.

Great thankfulness is sent to her fellow graduate students, Sue Laurich-McIntyre, Hong Li, Pixie Austin, and Asish Ghosh for their friendship and helpful discussions. The author is also greatly indebted to Chery Berg from the Minority Engineering Program, to Dr. Suzanne Brainard and the WIE Group, whose support helped me to overcome hardships and finish this project.

The financial support of the Mineral Institute of the University of Washington is deeply appreciated. The financial support of the Brazilian Government through CNPq in making possible this project is greatfully acknowledged.

Finally, the author is indebted to her friends, relatives, parents, brother and sister, and especially my husband and sons for the moral support, encouragement and love.

DEDICATION

To my husband Akio Ueno, my sons Paulo, Marcos and Carlos. To my parents, Bernardino F. Nunes Jr. and Maria Joana Sylvestre Nunes. To my brother Bernardino F. Nunes Neto and my sister Eliana Sylvestre Nunes. To my aunt Maria Sylvestre and my friend Darci Motta.

CHAPTER I - INTRODUCTION AND STATEMENT OF THE PROBLEM

The use of ceramic varistors which are based on ZnO is widespread throughout the world, but the electrical conduction mechanisms and the microstructural control of ZnO during processing are far from being fundamentally understood. This is partially due to the complicated microstructure of the multicomponent commercial ZnO varistor ceramics. To optimize the electrical properties of ZnO varistors it is necessary to maintain control of the grain size and perhaps also the grain size distribution during manufacture. Microstructural control is a critical issue facing the designer of practically all advanced ceramics.

Control of the grain size of ZnO during the manufacture of ceramic varistors is not a simple task. Several factors, including the initial ZnO powder particle size and its distribution, the particle shape, additives, impurities, the nature of the initial particle surfaces, compaction pressures, the state of agglomeration and the sintering atmosphere may all assume important roles in defining the final microstructure of ZnO varistors. Therefore, the ability to control the microstructure during processing translates into the ability to understand and to control all of these factors and more specifically to understand and control the effects which

these factors have on the densification and microstructural development including the grain growth of ZnO.

Analysis of the grain growth process in ZnO ceramics with regard to the microstructural development, the kinetic exponents and the activation energies is far from comprehensive and merits further research in a systematic fashion. Within that perspective it is possible to define the purpose of this thesis as twofold. First is to investigate the effects of the initial ZnO particle size on the microstructural development and on the grain growth kinetics of ZnO in sintered ZnO-Bi_2O_3 ceramics. Since the driving force for grain growth is the excess surface free energy, ZnO powders with different particle sizes (radii), and thus also different surface areas, may be expected to exhibit different sintering and grain growth kinetics. By varying the initial ZnO particle size and maintaining other process variables constant (i.e. compaction, atmosphere, composition, etc) and then measuring the grain sizes after firing at different times and temperatures it will be possible to quantitatively understand some of the effects of the ZnO initial particle size on the grain growth kinetics and the final ZnO microstructure.

The second objective is to address the role of several important additives on the grain growth of ZnO. Since Matsuoka [1] first reported that oxide additives

could improve the nonlinear characteristics of ZnO-Bi_2O_3 varistor ceramics, considerable information concerning the roles of various oxide additives on the sintering processes and on the electrical properties of these materials has been accumulated. However, only a portion of that information has been generated in a systematic fashion to quantitatively yield the necessary descriptive parameters. For example, it has been reported that some oxide additives promote the grain growth of ZnO, while others inhibit its microstructural coarsening. Of particular importance in this latter category appear to be some of the spinel-forming oxide additives. It is evident that the presence of second phases with the spinel structure at the grain boundaries of ZnO ceramics may strongly influence the grain growth kinetics, the final ZnO microstructure and consequently also the electrical properties of ZnO-based varistor ceramics.

The effects of the addition of Sb_2O_3 on the ZnO grain growth have been addressed by previous authors [2-5,70]. Asokan et al [2-5] have concluded that the presence of Sb_2O_3 leads to the formation of the $Zn_7Sb_2O_{12}$ spinel phase, which is present at the grain boundaries as small faceted inclusions and severely inhibits the grain growth of the ZnO. Senda and Bradt [70] have addressed the effect of Sb_2O_3 and confirmed the formation of the $Zn_7Sb_2O_{12}$ spinel, inhibition of ZnO grain growth and an

increase of the activation energy for grain growth.

The effects of additions of Nb_2O_5 on the grain growth of ZnO was also studied by Asokan et al [5]. They have concluded that Nb_2O_5 leads to the formation of the $Zn_3Nb_2O_8$ spinel phase. However, its effect on the microstructure appears to be a complicated one. Small additions of Nb_2O_5 are known to enhance the non-ohmic behavior of the ZnO. A maximum value of the non-linearity coefficient is achieved for compositions containing about 0.2 wt% Nb_2O_5 and sintered at 1100°C. Variation of the ZnO grain size with Nb_2O_5 content was also reported to exhibit similar behavior, i.e. the average grain size increased with additions of Nb_2O_5 to about the 0.2 wt% level, then decreased at higher Nb_2O_5 additions for all sintering temperatures. This ZnO grain growth behavior has been attributed to the presence of the $Zn_3Nb_2O_8$ spinel phase.

In combination with ZnO, Al_2O_3 is well known to form a compound with the spinel structure ($ZnAl_2O_4$), but the effects of this spinel phase on the grain growth kinetics of ZnO has not been systematically studied. Details are not well known in spite of additions of Al_2O_3 to many commercial ZnO varistor compositions. Komatsu et [8,9] suggest that Al_2O_3 may inhibit sintering through solid solution in the ZnO structure. However, the phase diagram suggests only very limited solid solubility of Al_2O_3 in

ZnO, thus considerable $ZnAl_2O_4$ must also form. Quadir and Readey [7] have confirmed that additions of Al_2O_3 inhibit the grain growth of ZnO. They have attributed this inhibition of the ZnO grain growth to the presence of the $ZnAl_2O_4$ spinel phase.

The two spinel-forming additives Nb_2O_5 ($Zn_3Nb_2O_8$) and Al_2O_3 ($ZnAl_2O_4$) are both worthy of more extensive study relative to their effects on grain growth of ZnO ceramics. While both Nb_2O_5 and Al_2O_3 are well known to affect the microstructural development of ZnO in varistor compositions, the quantitative analyses of the grain growth kinetics of ZnO in varistor ceramics with regard to the grain growth kinetic exponents and the activation energies are far from comprehensive. It requires further systematic investigation. In this thesis the effects of those two spinel forming additives, Nb_2O_5 and Al_2O_3, on the grain growth kinetics of ZnO in ZnO-Bi_2O_3 ceramics which develop a Bi_2O_3 liquid phase during firing will be addressed in a quantitative manner.

CHAPTER II - LITERATURE REVIEW

II.1 - Varistor

Metal oxide varistors represent a new type of semiconducting material with highly non-linear current-voltage characteristics. These devices are widely used for transient voltage protection of electronic circuits and electrical machinery. Figure (II.1.1) illustrates the typical application of a ZnO varistor as a transient protective element. Figure (II.1.2) illustrates the response of a ZnO varistor to a fast-rise-time (500 psec) pulse. Trace 1 is in the absence of the varistor and Trace 2 is with the varistor protection present.

The observed current-voltage characteristics of a varistor are often empirically described by the power law relation:

$$I = K V^{\alpha} \qquad (1)$$

where the parameter $\alpha = [d(\ln I)/d(\ln V)]$ is a measure of the varistor nonlinearity. The parameter α varies with the voltage. In the breakdown region it can attain values well in excess of 50 and can exceed 100 under special conditions. Figure (II.1.3) illustrates several typical current-voltage characteristic curves for varistors with different α values. When α is unity, Equation (1)

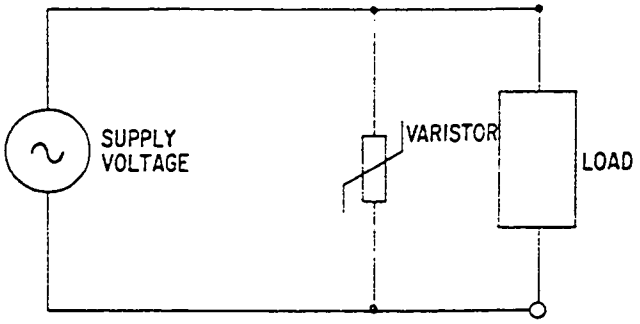

Figure II.1.1

Typical Application of ZnO Varistors as a Transient Protective Element [93].

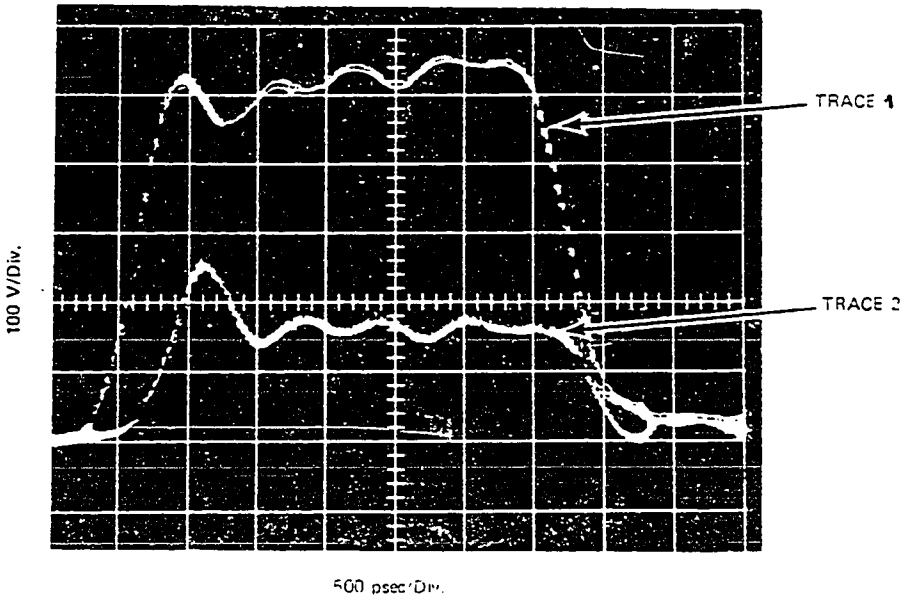

Figure II.1.2

Response of a ZnO Varistor to a Fast-Rise-Time Pulse (500 psec).

Trace 1 in the Absence of the Varistor.

Trace 2 with the Varistor Protection [93].

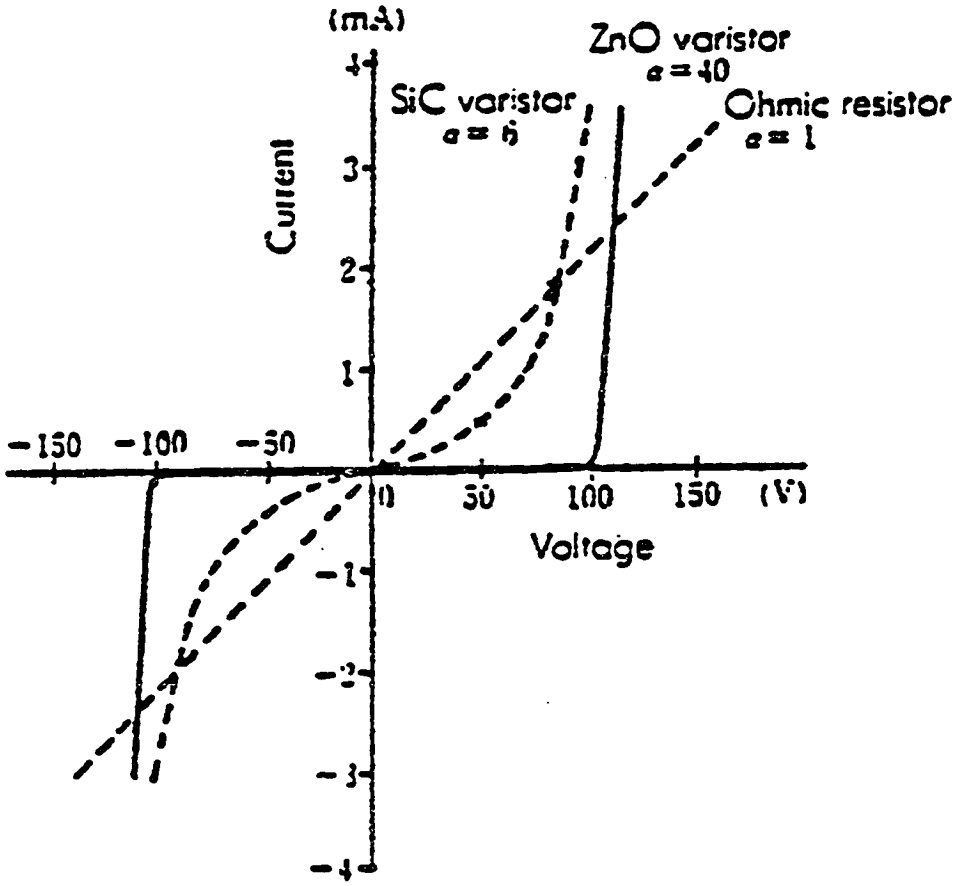

Figure II.1.3 -

Representative V-I Curves with Various α Values [13].

represents a standard ohmic device, i.e. the current is proportional to the applied voltage. As α approaches infinity the device characteristics approach those of a perfect varistor, for which the current varies substantially for small changes in voltage.

Ceramic varistors can be classified into several types for which the major constituents are either SiC, $BaTiO_3$, $SrTiO_3$, or ZnO. ZnO varistors are ZnO-based ceramic semiconductor devides with highly nonlinear current/voltage characteristics. They may be considered similar to back-to-back Zener diodes, but with much greater current and energy handling capabilities. ZnO-based ceramic varistors can also withstand much larger surge currents than most of the other varistor types.

Fabrication of ZnO varistors follows standard ceramic powder processing techniques. Calcined powders of ZnO, Bi_2O_3 and the other metal oxide additives are mixed, granulated, pressed and then fired at temperatures between 1100°C and 1400°C. Finally, a silver electrode is applied to the sintered ceramic body.

The microstructure of ZnO varistor ceramics is the result of a liquid phase sintering process in which the low melting temperature components (Bi_2O_3, etc.) constitute the initial liquid phase that dissolves some ZnO and also the other oxide additives during sintering. During cooling the liquid phase solidifies at the ZnO

multi-grain junctions and grain boundaries. The simplified sketch in Figure (II.1.4) [10] depicts ZnO grains and a low melting point component such as Bi_2O_3 at the grain-junctions. Although the actual phase assemblage of a commercial ZnO varistor can be very complex, in the case of Bi_2O_3-containing ZnO ceramics the microstructure is essentially comprised of:

(a) - Fine ZnO grains (Typical average ZnO grain sizes are only about 10 μm.)

(b) - A Bi_2O_3-rich intergranular layer from the Bi_2O_3-liquid phase sintering additions.

(c) - Spinel phases at the grain boundaries, often $Zn_7Sb_2O_{12}$, $Zn_3Nb_2O_8$ or $ZnAl_2O_4$.

The varistor properties are believed to be controlled by the electrical characteristics of the depletion layers situated within the ZnO grains at the grain-grain interfaces. To consider the varistor electrical behavior it is useful to represent the varistor microstructure by the block model [11] shown in Figure (II.1.5). This model presumes the device to be assembled of conducting ZnO cubes, of the size d, which are separated from each other by an insulating barrier region of a thickness t. These electrical insulating barriers, arising from the liquid phase sintering and subsequent ZnO grain growth, are known

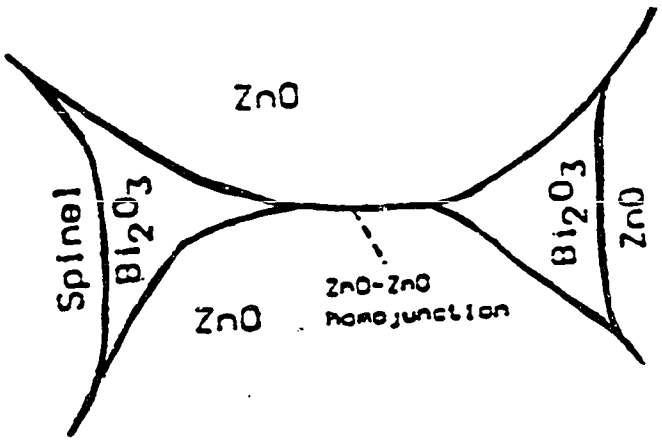

Figure II.1.4 - Schematic Arrangement of Phases in a ZnO Varistor Ceramic[10].

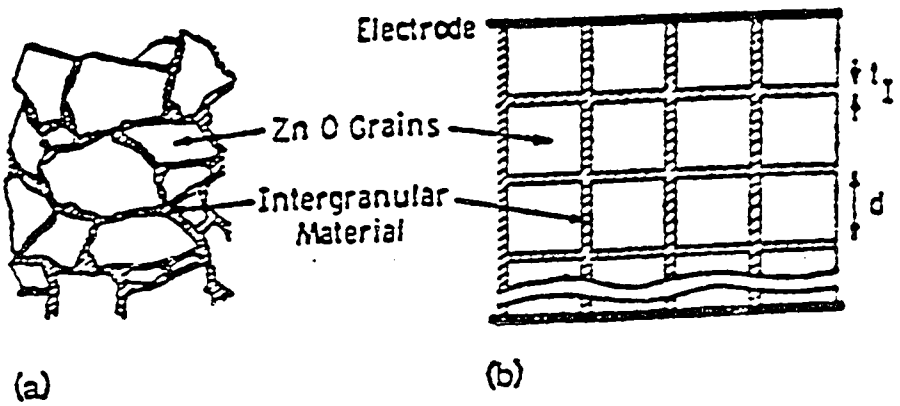

Figure II.1.5 - Sketches of (a) Actual and (b) Idealized Structures of the ZnO Varistors[11].

as back-to-back (double) Schottky barriers. These barriers can be physically attributed to the grain boundaries in the microstructure. Atomic defects exist, either intrinsic to the ZnO or arising from the additives in solid solution within the ZnO lattice to form localized defect state levels in the grain boundary regions. Depletion regions on both sides of the grain boundaries originate from these ionized defects causing the double Schottky barriers in this electronic device.

Eda [12] has proposed a SIS (semiconductor-insulator-semiconductor) structure for non-ohmic ZnO ceramics. This structure is described as an intergranular layer that is sandwiched between a forward-biased Schottky barrier and a reverse-biased Schottky barrier formed at the surface of n-type semiconducting ZnO grains. It is schematically depicted in Figure (II.1.6). Eda's studies have revealed that the insulator may have many traps and that the Schottky barriers at the grain boundaries are induced by the additive elements.

Conduction mechanisms can be described as follows: electrons ejected from the conduction band of the ZnO grain to the surface states at the forward biased Schottky barrier flow through the intergranular layer by multitunneling via traps or impurity levels and reach the surface states at the opposite side of the intergranular layer. Then, the electrons tunnel through the reverse-

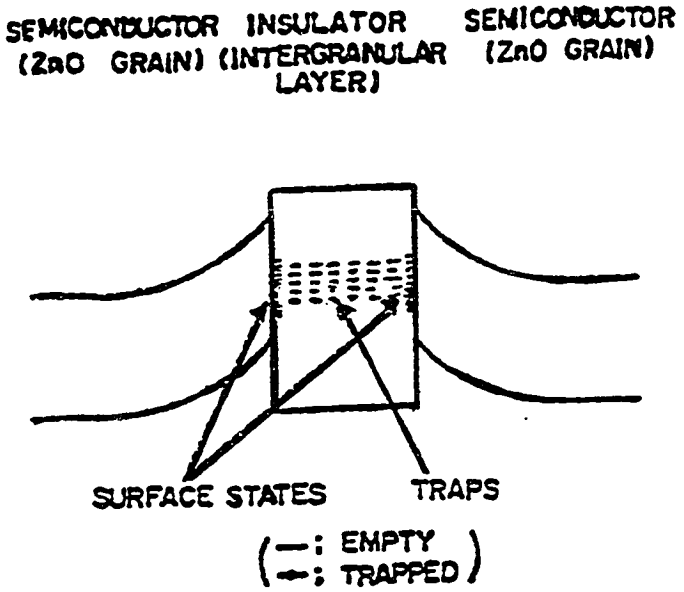

Figure II.1.6

- SIS-Type Model for Non-Ohmic ZnO Ceramics [12].

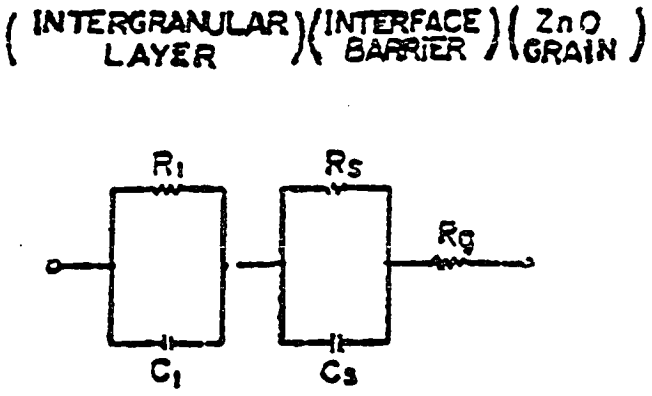

Figure II.1.7

- Equivalent Circuit of Non-Ohmic ZnO Ceramics [12].

biased Schottky barrier from the surface states to the conduction band of the ZnO grain. According to this model the V-I curves of the non-ohmic ZnO ceramics are mainly governed by the reverse-biased Schottky barriers.

From studies of the frequency dependence of the dielectric loss, an equivalent circuit for non-ohmic ZnO ceramics has been proposed [12]. It is shown in Figure (II.1.7). In Figure (II.1.7) R_g, R_i, C_i, R_s, C_s are, respectively, the resistance for the ZnO grains, the resistance and the capacitance of the intergranular layers and the interfacial surface barrier. The intergranular layer has a high resistance and a high capacitance while the individual ZnO grains have low resistance and a low capacitance. The intergranular layer dominates for low frequencies and the ZnO grains for high frequencies.

The characteristic V-I curve for ZnO varistors, as shown in Figure (II.1.8), can be divided into three separate regions on the basis of the current level. Region I can be expressed by:

$$I = C \exp(-E/KT) \qquad (2)$$

where I is the current, C is a constant, E is the applied field, T is the temperature and K is a constant. The current in this region depends mainly upon the high resistance (10^{12}-10^{13} ohm-cm) Bi_2O_3-rich layers separating

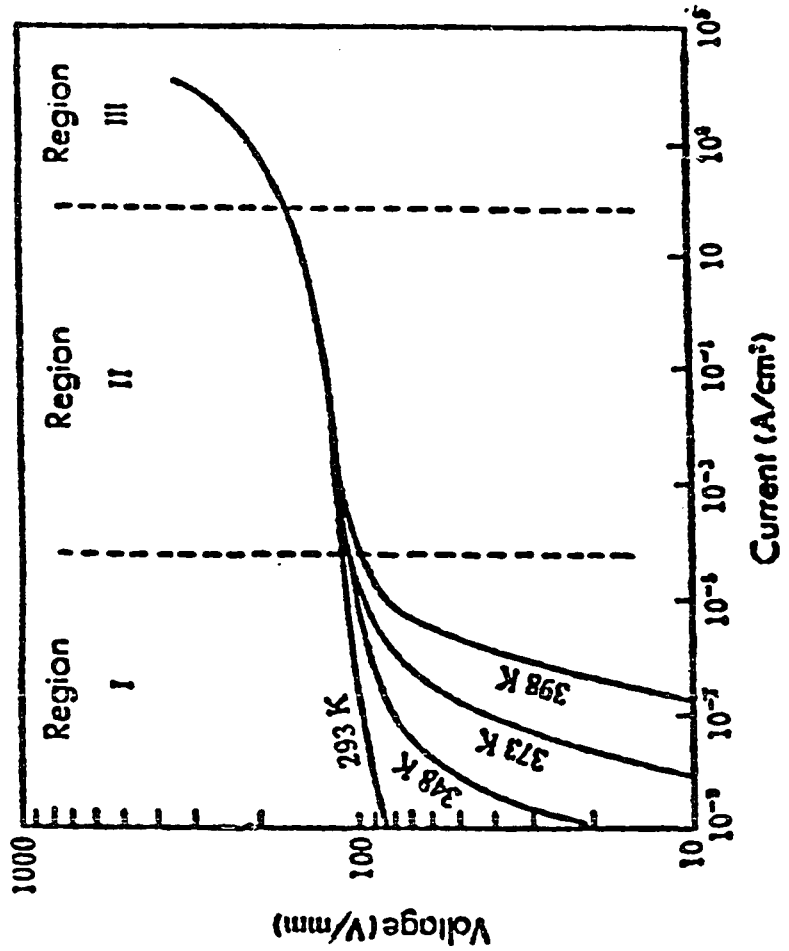

Figure II.1.8 - Current-Voltage Characteristics of ZnO Varistors [13].

the individual ZnO grains. Region II is believed to express the electronic properties related to the surfaces of the ZnO grains and is described by Equation (1). The exponent α in this region usually varies from 20 to 100 at current levels of 10^{-6} to 10 A/cm^2. The V-I character of Region III depends on the specific resistance of the ZnO grains (1-10 ohm-cm).

ZnO based varistors are highly complex multicomponent oxide ceramics whose electrical characteristics are generally accepted to be directly related to the phase assemblage of the ceramic microstructure and to the detailed processes occurring at the various boundaries within that structure. For example, it has been established that the ZnO grain size determines the varistor voltage per unit thickness. The ZnO grain size can be controlled by the sintering time and temperature, subsequent thermal treatments and the levels of metal oxide additives. This is the practical reason for studying the grain growth of ZnO and the effects of additives in these systems.

II.2 - Grain Growth

Grain growth is the process by which the mean grain size of an aggregate of crystals increases. The driving force is the decrease in the surface free energy which accompanies the reduction in total grain boundary area. Two types of grain growth have been discussed in the literature and are generally categorized as abnormal and normal. Abnormal grain growth is sometimes referred to as discontinuous grain growth. Abnormal, or discontinuous grain growth is the process by which a few individual grains grow very large relative to others in the structure. The process is also occasionally described as secondary recrystallization, particularly in metal systems. Normal grain growth is defined as having two main attributes. One is a uniform appearance. Secondly, there exists a relatively narrow range of grain sizes of similar shapes. There is a direct scaling in that a simple change of scale is sufficient to make the distributions of the grain sizes of two widely separate points in time to coincide. The form of the grain size distribution is time invariant. It is usually lognormal.

As an illustrative example, the total free energy of a model spherical particle (grain) can be expressed as a sum of two terms, one that represents the surface energy and another that represents the volume energy. This can be written as:

$$F = A_1 r^2 + A_2 r^3 \qquad (3)$$

where F is the total free energy of the particle, A_1 and A_2 are constants and r is the particle radius. The free energy per unit volume of the particle, F_v, is the above quantity, F, divided by the particle volume, $V = 4/3\ \pi\ r^3$:

$$F_v = F/V = A'_1/r + A'_2, \qquad (4)$$

where A'_1 and A'_2 are constants. The free energy per atom, F_a, is proportional to the free energy per unit volume, so that:

$$F_a = A''_1/r + A''_2, \qquad (5)$$

where A''_1 and A''_2 are constants. From Equation (5) it is evident that the free energy per atom varies inversely as the radius of the grain or particle size. That is, the larger the grain size, the lower is the free energy of the atoms and the more stable is the grain. Conversely, the smaller the grain size, the higher is the free energy and the lower is the stability of the grain. Therefore, a reduction in free energy is possible by enlarging the scale of the microstructure that is, by increasing the mean size of the grains.

II.2.1 - Normal Grain Growth

II.2.1.1 - Intrinsic Grain Boundary Migration

Curved grain boundaries tend to migrate towards their center of curvature to reduce the total grain boundary area and thus their surface free energy. The atomic mechanism for intrinsic grain boundary migration is schematically depicted in Figure (II.2.1) [14]. The term intrinsic implies the simple atomic (ionic) transfer from the edge of the shrinking grain, across the grain boundary, to the edge of the growing grain. Grain boundary migration or motion is thus the result of atomic jumps from one grain to the other.

The mobility of the grain boundary, μ, is defined as the velocity of the grain boundary under a unit driving force. It has been expressed as [14]:

$$\mu = (A\ n\ \Omega\ V_M^2/N\ R\ T)\ \exp\ (-\ Q_a/R\ T), \qquad (6)$$

where: A is the probability of a successful atomic jump across the grain boundary, n is the average number of atoms per unit area at the grain boundary, Ω is the jump frequency, V_M is the molar volume of the species diffusing across the grain boundary, N is Avogadro's number, Q_a is the activation free energy per atom to leave the grain boundary, R is the gas constant, and T is the absolute

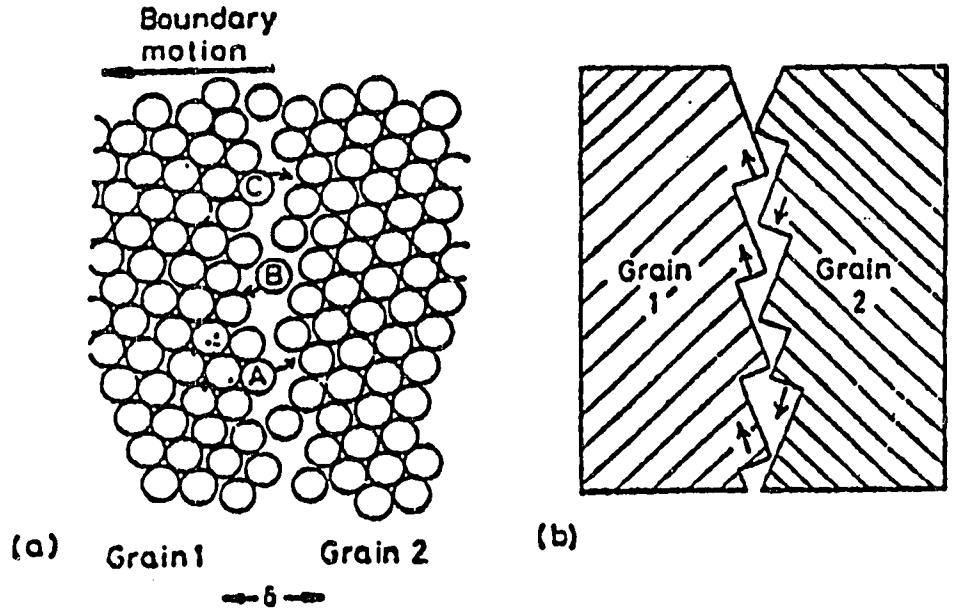

(a) - The boundary migrates to the left if the jump rate from grain 1 to grain 2 is greater than 2 to 1. Note that the free volume within the boundary has been exagerated for clarity.
(b) - Step-like structure where close packed planes protude into the boundary.

Figure II.2.1 - Atomic Mechanism of Grain Boundary Migration [14].

temperature.

The average velocity, V_{av}, of grain boundary motion under a driving force, f, is related to the mobility, μ, through the following equation :

$$V_{av} = g \mu f, \tag{7}$$

where g is a geometrical factor that is equal to unity for a spherical grain. The driving force, f, is the chemical potential gradient caused by the pressure difference across the curved grain boundary. This difference in pressure can be described by Laplace's equation as:

$$P = \gamma (1/r_1 + 1/r_2), \tag{8}$$

where γ is the surface free energy per unit area. The radii r_1 and r_2 are the major radii of curvature measured at a given point. By convention $r > 0$ for a convex surface and for a spherical droplet, $r_1=r_2=r$, so that for a spherical droplet Equation (8) reduces to the familiar form:

$$P = 2 \gamma/r. \tag{9}$$

The driving force, f, is expressed by :

$$f = d\ (V_a\ \ P)/dx = (V_a\ \gamma)/K'G\ w \qquad (10)$$

where V_a is the atomic volume, w is the grain boundary thickness, K' is a constant, and G is the grain size.

Einstein's expression for atomic mobility is:

$$\mu = (\ 1/V_a)\ D_a/kT, \qquad (11)$$

where D_a is the atomic self-diffusion coefficient, k is the Boltzmann constant, and T is the absolute temperature. Combining Equations (7), (10) and (11) yields the average velocity for intrinsic grain boundary migration, V_{av}. It is expressed by:

$$V_{av} = g\ D_a\ \gamma\ /\ K'G\ w\ k\ T. \qquad (12)$$

From Equation (12) it is evident that the average velocity of intrinsic grain boundary migration is a function of the diffusion coefficient of the atoms across the grain boundary, the surface energy, the grain size, and the grain boundary thickness, w.

II.2.1.2 - Grain Boundary Migration During Liquid Phase Sintering

Often a liquid phase coexists with the particulate solid at the firing temperature. Although a number of

physical and chemical processes may occur during the different stages of liquid phase sintering, one of the characteristic stages includes the phenomenon of grain growth. During grain growth, atoms are transfered through the liquid phase from the smaller grains to the larger grains. During grain growth in the presence of a liquid phase the transfer of atoms from the smaller grains to the larger grains involves the following three steps :

(i)-Initially, atoms or ions must surpass the free energy barrier of the small grain surface to escape the small grains. This step corresponds to the dissolution of the small grains into the liquid phase.

(ii)-Atoms or ions must then diffuse through the liquid phase from the small grains to the larger grains.

(iii)-Finally the atoms or ions must surpass the free energy barrier at a large grain surface to join the large grain. This step corresponds to the process of precipitation on the larger grains.

If the time required for atomic transfer across the interface is long compared to that required for diffusion through the liquid, then the reaction at the interface will be the rate controlling mechanism. Conversely, if

diffusion through the liquid is the slowest step, it will be the rate controlling mechanism. Therefore grain growth in the presence of a liquid phase can be controlled by either:

(a) - the interfacial or phase boundary reactions at either the dissolving smaller grains, or at the growing larger grains, or

(b) - the diffusion of the atoms or ions through the liquid phase.

Example of both situations have been reported in the literature.

According to Equation (5), grains of smaller dimensions, those with a smaller radius of curvature are less stable than larger ones. Consequently, the smaller grains will have a higher solubility in the liquid phase than the larger grains. The grain solubility dependence on the particle size for a spherical particle is described by the Thomson-Freundlich equation:

$$\ln (S / S_0) = 2 \gamma V_a / r k T, \qquad (13)$$

where S is the solubility of the particle, and S_0 is the equilibrium solubility which corresponds to that for a flat surface. Since smaller particles will dissolve

preferentially to the larger ones, this gives rise to a concentration gradient across the liquid layer. It is this concentration gradient which is the driving force for mass transport and grain growth during liquid phase sintering.

If Equation (6), which expresses the grain boundary mobility in the case of intrinsic grain boundary migration is to be applied to grain boundary migration in the presence of a liquid phase, then some modifications are necessary. The resulting equation is:

$$\mu=[(A_1+A_2)\ n\ \Omega\ V_M^2\ /NRT]\exp[-(Q_1 + Q_2 + Q_d)/R\ T] \qquad (14)$$

where A_1 and A_2 are the probabilities of successful atomic jumps across the grain boundary from the dissolving grain into the liquid (solubility factor) and from within the liquid across the boundary to the lattice of the growing grain (reprecipitation), respectively [14]. The Q_1 is the activation energy per atom to leave the dissolving grain, while Q_2 is that to join the growing grain. The Q_d is the activation energy for diffusion through the liquid. If either Q_1 or $Q_2 >> Q_d$ then the interface or phase boundary reaction is the rate controlling mechanism. However, if $Q_d >> Q_1$ or Q_2, then the grain growth process is controlled by diffusion through the liquid. It is appropriate to note here that if Q_1, Q_2 and Q_d are similar

in magnitude, then the measured Q values for grain growth during liquid phase sintering may not be those of either of the individual processes or reactions.

Diffusion controlled grain growth is frequently reported for liquid phase sintering, although there are also a number of observations of phase boundary reaction controlled grain growth. Phase boundary reaction control is typically observed in the more complicated systems involving several components. Table (II.2.1) summarizes the grain growth observations for several systems [16].

When diffusion through a grain boundary liquid layer of a thickness y is the rate controlling process, then the grain boundary velocity, V_{lld} is given by [17,18] :

$$V_{lld} = D\ S\ V_M\ f\ /y\ k\ T, \qquad (15)$$

where : D is the diffusivity of the species in the liquid phase, S is the solid solubility in the liquid, V_M is the molar volume of the diffusing species, f is the driving force, and y is the liquid layer thickness. Diffusion in liquids is normally more rapid than that in solids, so that grain growth in the presence of a liquid phase can be accelerated relative to that in the solid state.

Lay [18] has examined the grain growth of ceramics in the presence of a liquid grain boundary layer. He modified the equations that were originally derived for

Table II.2.1 - Controlling Grain Growth Mechanisms During Liquid Phase Sintering [16].

Diffusion Control	Reaction Control
Mo-Ni-Fe	PbS-NaCl-KCl
$MgO-V_2O_5$	$SmCo_5$-Sm-Co
Fe-Cu	TiC-Mo-Ni
Co-Cu	NbC-Fe-B
Cu-Ag	WC-Co
W-Ni-Cu	TiN-TiC-Ni
W-Ni-Fe	
W-Ni	
TiC-Co	
HfC-Co	
TaC-Co	
Mo_2C-Co	
NbC-Co	
$CaO-MgO-Fe_2O_3$	
Pb-Sn	
VC-Co	

the coalescence of solid particles which are widely dispersed in a liquid to account for the fact that the actual content of liquid phase which is necessary for liquid phase-influenced grain growth has been observed to be very small. The principal modification is the inclusion of a term involving the average liquid grain boundary layer thickness. Also, the particle size distribution considered in Lay's analysis is not that for widely spaced particle sizes, but rather the distribution expected for solid-state grain growth, as predicted from geometrical grain packing requirements. When diffusion through a liquid phase is the rate controlling mechanism, for the case of closely packed particles of the average grain size, G, Lay derived the following equation for grain boundary migration in the presence of a liquid layer, V_{lld}, as:

$$V_{lld} = 2\ D\ S\ V_M\ [(G/G_c)-1]\ /y\ k\ T\ G. \qquad (16)$$

In Equation (16), D is the diffusion coefficient in the liquid phase, S is the solubility in the grain boundary liquid and G_c is the critical grain size below which particles, or grains, tend to disappear rather than grow. Hillert [17] has suggested that $G_c = (8/9)\ G$. V_M is the molar volume and y is the thickness of the liquid layer, while k and T have their usual meanings.

Alternatively, if the rate controlling grain growth process is one of the phase boundary or surface reaction control, then the grain boundary velocity in the presence of a liquid layer, V_{lsr}, is expressed by :

$$V_{lsr} = K \left(V_M f / k T \right), \qquad (17)$$

where : K is the rate constant, which depends exponentially on the temperature, V_M is the molar volume, f is the driving force, and k and T have their usual meaning. It is evident from Equations (12), (16) and (17) that the grain boundary migration velocity will vary exponentially with temperature. This is because it is a function of the diffusion coefficient, both in Equations (12) and (16). In Equation (17) it also depends on the rate constant K, which varies exponentially with temperature.

For the situation where the grain growth is controlled by diffusion through the liquid layer, Equations (12) and (16) also reveal that the grain boundary velocity is inversely proportional to the grain boundary thickness, w, in the case of solid state grain growth. It is similarly inversely proportional to the thickness of the liquid grain boundary layer, y, in the case of grain growth in the presence of a liquid phase.

II.2.1.3 - Normal Grain Growth Kinetics

Very little reliable information on grain boundary migration has resulted from direct, in situ, measurements of individual grain boundary velocities. It is generally derived through an analysis of grain growth kinetics based on various mechanisms or processes that have been advanced to explain the grain growth process. These deal with the kinetics of change in the mean grain size and/or analysis of the topological requirements for space filling by the grains.

To describe normal grain growth Burke and Turnbull [19] considered the migration of a grain boundary to occur by atomic transport across the boundary, driven only by the pressure of the boundary surface curvature. They formulated a theory by considering a crystal or grain as an isolated entity and postulating that the results could be extended to represent the mean behavior of a dense array of grains. Two important simplifying assumptions which they incorporated are:

(a) - the rate of grain growth can be directly related to the average grain boundary migration velocity, and

(b) - the grain size distribution remains the same throughout the grain growth process.

On the basis of the first assumption the average grain boundary velocity, V_{av}, can be written:

$$V_{av} = 1/2 \ (dG/dt) \tag{18}$$

where G is the grain size, and (dG/dt) is the rate of grain growth. Substitution of Equation (18) into Equation (12) results in:

$$V_{av} = 1/2 \ (dG/dt) = g \ D_a \ \gamma \ /K' \ G \ w \ k \ T \tag{19}$$

Rearranging and then integrating from the initial or original grain size, G_0, to the final grain size, G, yields:

$$1/2 \int_{G_0}^{G} G \ dG = (g \ D_a \ \gamma \ /K' \ w \ k \ T) \int_{t_0}^{t} dt \tag{20}$$

where the factor (g D_a γ /K w k T) is usually not considered to be a function of either time or the grain size. Integration yields :

$$G^2 - G_0^2 = (4 \ g \ D_a \ \gamma \ /K' \ w \ k \ T \ ) \ (t - t_0) \tag{21}$$

or

$$G^2 - G_0^2 = K \ (t - t_0) \tag{22}$$

where the rate constant K is given by :

$$K = 4\ g\ D_a\ \gamma\ /K'\ w\ k\ T \qquad (23)$$

Because the diffusivity has an exponential temperature dependence, the kinetic constant, K, in this form, is very sensitive to the effects of temperature.

According to the Burke-Turnbull model expressed by Equation (22), a parabolic grain growth law is to be expected for pure, single phase systems completely free of, or with only very weak interactions that might impose any type of drag effect on the motion of grain boundaries. This model adequately describes many pure metallic systems at elevated temperatures.

C.S. Smith [20] has stated that "Grain growth results from the interaction between topological requirements for space-filling between the edges, faces and vertices of the grain ensemble and the forces driving the boundaries to migrate to reduce boundary curvature and subsequently, boundary energy." He argued that it is inadequate to treat a grain as an isolated entity and that any theory of grain growth must always account for the multiple interactions within the complete assemblage of grains, especially those including the first nearest neighbor grains.

Felthan [21], Hillert [17] and Louat [22] have independently developed mean field theories for grain growth in which the effects of the ensemble of grains is considered to be like a field in which the individual growing grain is immersed. Felthan and Hillert both assumed grain growth to occur only as a result of the driving force for the removal of the grain boundary curvature. They neglected the possibility of random changes in grain size. Louat addressed the statistical nature of grain growth, with grain boundaries excecuting random walks. These mean field theories have only considered the average effect of the environment on the grains. Each also predicts parabolic grain growth because they have not fully considered the topological constraints of the complete grain assemblage in three dimensions, 3-D.

A 2-D description of grain growth as a dislocation climb process has been presented by Hillert [17]. It has been extended to 3-D by Morral and Ashby [23]. The average grain was assumed to have 6 sides for the 2-D case and 14 sides for the 3-D situation. Dislocations were associated with grains that deviated from this average. Again parabolic grain growth kinetics resulted from these analyses.

Rhines and Craig [15], Doherty [24], Hunderi [25] and Kurtz and Carpay [26] have applied parameters called sweep constants and the concept of a structural gradient to

quantify the tendency for grain growth. Some controversy exists as to the definitions of these concepts. Hunderi supports Doherty's definition of a sweep constant as the number of grains which vanish when grain boundaries sweep through a volume equal to the mean grain volume. Kurtz and Carpay favour the Rhines and Craig definition for the structural gradient as $(M_V\ S_V\ /N_V)$; where, M_V is the curvature per unit volume, N_V is the number of grains per unit volume and, S_V is the surface area of the grain boundary per unit volume.

Rhines and Graig obtained the following expression for the mean grain volume at a time t :

$$V_g = V_0 + (\Theta \mu \gamma M_V/N_V)\ t, \qquad (24)$$

where Θ is the sweep constant as defined by Doherty, μ is the grain boundary mobility, γ is the grain boundary surface energy, V_0 is the mean grain volume at time t=0, while M_V and N_V are defined as previously. The resulting linear dependence of V_g on t which has been obtained by Rhines and Graig, is equivalent to the grain radius growing as $t^{1/3}$. This is indicative of a cubic grain growth law, for the exponent obtained by these authors is three instead of the value of two which was predicted by the preceding theories which yielded parabolic grain growth.

Computer simulations for normal grain growth have been completed in an attempt to explain deviations from parabolic grain growth kinetics. Voorhees and Glicksman [27-29] have simulated the coarsening of a multiple particle system considering the behavior of the individual grains versus time, the volume fraction of solid and the grain size distribution. They demonstrated the expected shrinkage of small grains with the simultaneous growth of large grains. They found the grain growth exponent, n, to be equal to three in all cases. Although there is a neighbor effect on the growth or shrinkage of individual grains, the overall system appears to converge to an environmentally independent form.

In some computer simulations the topological constraints are an intrinsic part of the model since the network is simulated directly. Srolovitz [30] observed that the grain sizes of the large grains tended to vary randomly with time and that small grains tend rapidly to zero. He concluded that the nature of grain growth lies somewhere between the concepts of curvature directed motion and that of a random walk in a statistical sense. This statement reflects the fact that both diffusion and the reduction of surface area (curvature) must both be considered when modeling grain growth.

Coalescence of non-interacting solid particles dispersed in a liquid phase as a mechanism of grain growth

has been considered by Wagner [31], Lifshits and Slezov [32] and Greenwood [33]. These authors have concluded that the coalescence of solid particles which are widely separated follows a cubic growth law. It is of the form:

$$G^3 - G_0^3 = K\ t, \tag{25}$$

where the rate constant K is that given by Greenwood [33] as :

$$K = 2\ D\ S\ V_M\ \gamma\ /\ k\ T, \tag{26}$$

where D, S, V_M, γ, k and T have the same meanings that were previously described. In contrast with the parabolic growth law obtained by Burke and Turnbull [19] for normal solid state grain growth, coalescence of widely separated solid particles dispersed in a liquid phase follows the cubic growth law as described by Equation (25).

Lay [18] has examined the grain growth kinetics for the case of a close packed structure where the content of the liquid phase is very small and forms only a thin layer between the particles. He assumed a dihedral angle equal to zero. For very small contents of the liquid phase the microstructure appears very similar to that which is observed when no liquid phase is present at all. However, the kinetics of grain growth is very different from that

for the solid state. This is because the material transport process for grain boundary migration is that of diffusion through the liquid phase.

For the case of close packed particles of an average size, G, Lay derived the expression previously given in Equation (16) for the velocity of grain boundary migration in the presence of a wetting grain boundary liquid phase. Considering that the diffusion distance in the liquid phase, y, is directly related to the grain size, for y increases as the average grain size increases, and also that the critical grain size G_c is (8/9)G, then the condition expressed by Equation (16) prevails, Equation (18) can be integrated as follows :

$$\int_{G_0}^{G} G^2 dG = S\ D\ V_M /\ 4\ k\ T \int_{t_0}^{t} dt \qquad (27)$$

Integration of Equation (27) yields the cubic growth law:

$$G^3 - G_0^3 = (\ 3\ D\ S\ V_M\ /4\ k\ T)\ (t - t_0) \qquad (28)$$

Equation (28) is usually written in the form:

$$G^3 - G_0^3 = K\,t. \qquad (29)$$

where the rate constant K is given by :

$$K = 3\,D\,S\,V_M / 4\,k\,T \qquad (30)$$

Because the diffusivity, D, and the solubility, S, may both have exponential temperature dependencies, the kinetic rate constant, K, can be highly sensitive to temperature. Lay concluded that grain growth controlled by diffusion through a liquid layer follows the same cubic growth law as for the coalescence of widely dispersed solid particles in a liquid phase, although the particle size distribution is that expected for solid state grain growth.

The effect of the volume fraction of solid on the rate of grain growth during liquid phase sintering has been considerd by several authors [27,29,32-42]. When the solid volume fraction is increased, then the rate of grain growth is accelerated. This is because the diffusion distance through the liquid phase, y, decreases. The basic kinetic law is the cubic one as derived by Lay, but the rate constant K is modified to account for the effect of the shorter diffusion distance as the volume fraction of the solid phase is increased [42].

If the volume fraction of the solid phase remains

constant during grain growth, then the number of grains per unit volume must decrease as the mean grain size increases. The grain-liquid phase interfacial surface area per unit volume depends on the grain size and the grain population. Accordingly, the grain surface area per unit volume, S_V, will vary according to:

$$S_V = 4 \pi G^2 N_V, \tag{31}$$

where G is the average grain size and N_V is the number of grains per unit volume.

The mean separation between the grains also increases with sintering time [16]. As the grain growth kinetics depends on the grain separation, this in turn is dependent on the grain size and volume fraction of the liquid phase. Diffusion through the liquid is the usual mechanism for grain growth. Rapid grain growth occurs for small initial grain sizes, high sintering temperatures, low dihedral angles, high volume fractions of solid and when there is a high solubility of the solid in the liquid phase.

II.2.1.4 - The Phenomenological Grain Growth Expression

Related to the previously derived grain growth laws, a general phenomenological equation has been applied to describe the phenomenon of grain growth to allow for the experimentally observed discrepancies from parabolic and

cubic growth law kinetics. It is of the form:

$$G^n - G_0^n = K_0 \, t \exp (- Q/RT), \qquad (32)$$

where n is known as the grain growth exponent, G_0 and G are the average grain sizes at times 0 and t respectively, K_0 is the rate constant and Q is the activation energy for grain growth.

Numerous experimental studies of the grain growth process have reported a variety of different values for the grain growth exponent, n. These discrepancies from the parabolic law have been attributed to several different factors, as summarized in Table (II.2.2). It can be observed in the Table (II.2.2) that the most common experimental value for n is three, a value that can be indicative of at least five different grain growth mechanisms. From these results it is evident that compositional parameters, the pore size and its distribution, the extent of solid solution, second phases, the level of dopants (additives) and their segregation and texture must all be considered when studying grain growth, each may have an influence on the grain growth process.

In nearly all studies of grain growth kinetics, the grain sizes are almost invariably obtained from analyses of 2-D sections through the microstructure. The mean grain diameter, the average grain size, is estimated from

Table II.2.2 - Summary of Exponents for Grain Growth for Various Proposed Mechanisms [75].

Proposed Mechanisms	Grain Growth Exponent (n)
Boundary Control in a Pure System	2
Boundary Control in a Impure System	
Coalescence of Second Phase by Lattice Diffusion	3
Coalescence of Second Phase by Grain Boundary Diffusion	4
Diffusion Through a Continuous Second Phase	3
Impurity Drag (Low Solubility)	3
Impurity Drag (High Solubility)	2
Diffusion Through Dislocation Pipe	5
Pore Drag Control	
Surface Diffusion	5
Lattice Diffusion	3
Vapor Transport (P=const)	4
Vapor Transport ($P=2\gamma/r$)	3

the average linear intercept. As was derived by Mendelson [43], the average grain size, $\overline{G}$, can be obtained from :

$$\overline{G} = 1.56\,\overline{L}, \tag{33}$$

where $\overline{L}$ is the average grain boundary intercept length of a series of random lines on the 2-D micrographs. Rhines and Craig [15] pointed out that the mean grain intercept is sensitive to the shape of the grains and will alter significantly if the grains are distorted, e.g. by rolling. However, the mean grain volume will not change if the grains are rolled. An important question is therefore whether or not a true 3-D grain size can be determined or estimated from mean grain intercept measurements on 2-D sections of the microstructure. Rhines and Craig [15] suggested that anisotropy could be the reason for the inconsistency between their 2-D and 3-D results. Cahn [45] and Doherty [24] have both concluded that for an isotropic structure the mean grain size from a 2-D section will approximate the 3-D mean grain size, although for a highly anisotropic structure there may exist some discrepancies. However, because of topological restraints, most researchers do not believe that the modeling or simulation of a 2-D structure can correctly predict the changes of a 3-D one.

II.2.2 - Grain Growth Inhibition

Microstructural control is a very important issue in the fabrication of advanced ceramics. For ceramic materials consolidated by liquid phase sintering, grain growth is often detrimental to the final properties. As a consequence, several techniques to inhibit grain growth during the latter stages of sintering have been developed [49-51]. One approach to control grain growth is to decrease the solid solubility or the diffusivity. Also, chemical additives can alter the interfacial energy and interfere with the interfacial dissolution and precipitation rates and thus affect the grain growth rate. Another approach to slow the grain growth rate is to reduce the grain boundary migration by means of segregation, second phase and pore drag mechanisms.

II.2.2.1 - Segregation

Even in very pure materials there is a space-charge atmosphere of lattice defects and solute segregation associated with the grain boundaries. Impurities and additive atoms will segregate to the grain boundaries if they lower the free energy of the system. The change in free energy as a result of segregation of the solute from the bulk to the grain boundary corresponds to the strain energy introduced by a solute that fits poorly into the lattice, both elastically and electronically. When the

ionic size differences are large and a considerable misfit results, it is reasonable to assume that the elastic strain energy is an important contribution to the segregation.

The phase diagram provides an initial indication of the segregation and surface energy changes due to additives and impurities. The favorable factors for solute segregation are decreasing liquidus and solidus, a wide liquidus and solidus separation, a small solid solubility of the solute and a large ionic size ratio. For extensive solid solution to occur the ionic size ratio must be about 15% or less.

The effects of these lattice defects and the impurity atmosphere is to create a drag and reduce the grain boundary velocity. The influence of this atmosphere appears to intensify as the grain size increases and the average boundary curvature decreases. Several impurity drag models have been presented in the literature [44-48]. The simplest model is that which has been presented by Cahn [45]. It predicts a parabolic grain growth law. When solutes segregate very strongly at the grain boundaries and very fine grains are involved, Brook [47] has demonstrated that a grain growth exponent of three may occur, so that a cubic grain growth law is equally possible. These models suggest that a grain growth exponent of either two or three may be expected for

solute drag controlled grain growth. Inhibition of grain growth due to solute segregation to the grain boundary has been reported for the cases of additions of K_2O to ZnO [71] and of CaO, MgO and FeO to Al_2O_3 [82,94].

II.2.2.2 - Second Phase Particles

The migration of grain boundaries can be slowed by the effects of second phase particles. These particles interact with the grain boundary by exerting a drag effect reducing the rate of grain growth. When a second-phase particle is attached to a grain boundary the grain boundary can break away leaving the particle behind, or the grain boundary can drag the particle along, in which case it remains attached to the grain boundary as it moves. The latter requires material transport across the particle, which may proceed by interface/surface or volume diffusion, by viscous flow, or by solution or evaporation. When the inclusion is dragged along by the boundary the velocities of the two are identical. For the case in which the mobility of the particle is much lower than the mobility of the boundary, the resulting grain boundary velocity is controlled by the driving force on the boundary together with the mobility of the inclusion particles and the number of inclusions per unit boundary area.

Second phase precipitate particles increase the

energy necessary for the movement of the grain boundary and inhibit grain growth. When a number of inclusions are present on a grain boundary, its normal curvature becomes insufficient for continued grain growth once some limiting size is reached. Zener [44] has predicted a limiting grain size in the presence of second phase particles given by:

$$G_l = d_p/V_{fp} \tag{34}$$

where G_l is the limiting grain size, d_p is the particle size of the inclusion and V_{fp} is the inclusion volume fraction. Although this relationship is only an approximate one, it indicates that the effectiveness of inclusions increases as the particle size is decreased and their volume fraction is increased. A more fundamental approach has been provided by Hillert [17], whereas Smith [44] predicted that the stabilizing effect varies depending on the particle location, e.g. boundary, triple points grain edges etc.

I.2.2.3 - Porosity

A second phase which is present in almost all technical ceramics prepared by sintering is the residual porosity which remains from the interparticle space present in the initial powder compact. This porosity can

occur both on the grain boundaries (intergranular) and within the grains (intragranular).

Grain boundary migration is affected by the presence of pores. During grain growth three cases are possible: (i) pores can have a high mobility and move along with the boundaries, offering little impedance to grain growth; (ii) pores can have low mobility and move along with the boundaries with the pore mobility controlling and reducing the boundary velocity; or (iii) or pores can be so immobile that the grain boundary escapes from the pores.

The motion of a pore can be accomplished by several different mechanisms, including [77]:

(a)-volume diffusion through the surrounding matrix,
(b)-mass diffusion along the pore surface, or
(c)-vapor transport within the pore.

When the pores are attached to the grain boundary, any of these mechanisms can control the mobility of the grain boundary. The effects of each of these controlling mechanisms on the rate exponent, n, were summarized in Table (II.2.2). Values from two to five appear to be possible.

Kingery and Francois [87] have suggested that for pores of a constant shape, the rate of pore migration is inversely proportional to the pore diameter because the

distance of material transport changes in proportion to the pore size. They showed that pore migration during grain growth leads to pore growth in UO_2 in which grain growth is much more rapid than pore elimination. They also suggested that in UO_2 the pores coalesce by a vacancy diffusion process, similar to the coalescence of second phase inclusions.

As with second solid phase inclusions, pores on the grain boundaries may also be left behind by the moving boundary or migrate with the boundary, gradually agglomerating at the grain corners. In the early stages of sintering, when the boundary curvature and the driving force for grain boundary migration are high, pores are frequently left behind. However, in the later stages of sintering, when the grain sizes are much larger and the driving forces for boundary migration are lower, it is common for pores to be dragged along with the grain boundaries, thus slowing grain growth. Inclusion particle and pore agglomeration at the boundaries during the latter stages of sintering is observed for many ceramic materials.

As grain growth proceeds, the driving force diminishes, and the inclusions and pores which are dragged along by the boundaries increase in size so that their mobility decreases. As a result, the exact way in which second-phase inclusions or pores inhibit grain growth not

only depends on the particular system, but can also change during the grain growth process. It is possible for several competing processes to occur simultaneously, so that discerning these effects requires a careful evaluation of the microstructural evolution in combination with the kinetics of grain growth.

II.2.2.4 - Defect Chemistry

The simplest mechanism of diffusion and that most often encountered in practice is the vacancy mechanism. It occurs in both metals and compounds of the MeX type. Defects of the vacancy type predominate over a wide range of temperatures and pressures in many crystalline structures, including oxides, sulphides, and spinels. Diffusion processes which occur according to this mechanism consist of sucessive jumps of atoms or ions from lattice sites to neighboring vacancies. Hence the condition necessary for the change of the position of an atom in the lattice is the presence of a vacancy on a lattice site adjacent to the atom.

The probability for the jump of an atom is proportional to the probability of finding a vacancy in the immediate neighborhood of the atom. This probability increases with increasing concentration of vacancies in the lattice and is equal to the fraction of lattice site vacancies. The diffusion coefficient can be expressed as:

$$D = \alpha\, a_0^2\, w\, N_b \qquad (35)$$

where α is a geometrical factor which depends on the crystal structure and the mechanism of diffusion, a_0 is the lattice parameter, and N_d is the mole fraction of defects or vacancies.

The frequency of atomic jumps and the concentration of vacancies, are both exponential functions of the temperature and therefore the general relationship for the diffusion coefficient is expressed by the Equation (36):

$$D = D_0 \exp\ (-E_d/RT) \qquad (36)$$

where E_d is the activation energy for diffusion and D_0 encompasses the temperature independent terms. D_0 is a function of the entropies of formation and migration of the defects.

As Brook [88] has pointed out, solid solution impurities in ceramic systems affect the defect chemistry and consequently may change the diffusion coeficient. For the specific case of solid solutions formed by additions of Nb_2O_5 and Al_2O_3 to the ZnO there can be a substitution of the Zn^{2+} ions by the Nb^{5+} or the Al^{3+} ions. When this occurs vacancies are formed according to Equations (37) and (38).

For charge balance the solid solution addition of Nb_2O_5 to the ZnO lattice requires that two Nb^{5+} ions replace five Zn^{2+} ions on the cation lattice sites, therefore three Zn vacancies are formed according to the reaction:

$$Nb_2O_5 \xrightarrow{ZnO} 2\ Nb^{5+}_{Zn"} + 3\ V_{Zn"} + 5\ O^{-2}_{O} \qquad (37)$$

Similarly, addition of Al_2O_3 in solid solution also creates vacancies in the ZnO lattice. In this case, to maintain the charge balance, each two Al^{3+} ions must replace three Zn^{2+} on cation sites, creating a single Zn vacancy, according to the reaction:

$$Al_2O_3 \xrightarrow{ZnO} 2\ Al^{3+}_{Zn"} + V_{Zn"} + 3\ O^{-2}_{O} \qquad (38)$$

Additions of Nb_2O_5 obviously create more cation lattice site vacancies than additions of Al_2O_3. The formation of these vacancies can enhance the Zn^{2+} diffusivity because there are more jump sites available for the diffusing Zn^{2+} ions. These changes in the diffusivity can have profound effects on the migration of the grain boundaries and on the rate of grain growth.

When an association of vacancies and solutes occurs there may be a variety of values for the observed activation energy for diffusion. In some cases the

association of the diffusing ions with vacancies can lead to very high diffusion coefficients [52].

II.2.3 - Discontinuous Grain Growth

Discontinuous or exaggerated grain growth occurs when a small number of individual grains grow to a large size, rapidly consuming the uniform finer grain-size matrix surrounding them. The resulting grain size distribution varies with the sintering time as indicated in Figure (II.2.2). In that figure, the difference between discontinuous and normal grain growth is quite evident.

Two stages have been identified as essential to discontinuous grain growth: (i) the nucleation of the abnormal grains, and (ii) the preferred growth of those grains. There often appears to be an induction or incubation period corresponding to the increased growth rate and the formation of a few grains large enough to grow at the expense of the uniform, fine grain-size matrix. The driving force for discontinuous grain growth is generally accepted to be the lower surface energy of the large grains compared with the high surface energy, or small radii of curvature of the adjacent much finer matrix grains.

Discontinuous or abnormal grain growth has been attributed to several different factors, including:

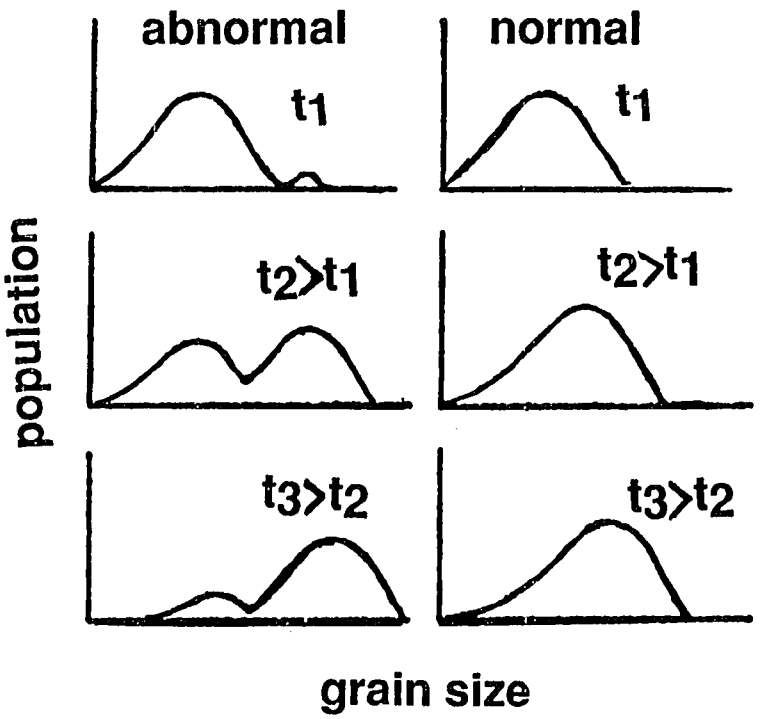

Figure II.2.2 - A Contrast Between Grain Size Distributions During Normal and Abnormal Grain Growth [16].

(a) - The presence of dense agglomerates of solid particles in the green compact. These densify more rapidly and serve as the embryos for the large grains.

(b) - The presence of impurities, non-stoichiometric grains, second phases and porosity.

(c) - A very small particle size of the starting material. Presumably the probability of finding large grains to serve as nuclei is greater for smaller initial particle size.

The occurence of discontinuous grain growth is easily caused by the presence of small dense clusters of grains in the powder compact. These agglomerates of solid particles undergo more rapid initial densification and subsequently exhibit a higher grain growth rate than the remainder of the material. This would be expected from the dependence of the grain growth rate on the volume fraction of solid. Agglomerate inhomogeneities nucleate a large grain which then eventually grows into the neighboring matrix which has a lower volume fraction of solid.

Discontinuous or abnormal grain growth is believed particularly likely to occur when uniform continuous grain growth is inhibited by the presence of impurities, second phases, porosity and off-stoichiometry grains.

Discontinuous grain growth is also sometimes observed in systems having minor concentrations of impurities which give rise to only a small amount of grain boundary phase. If the amount of grain boundary phase is increased, however, both normal and abnormal grain growth may be inhibited. In some cases the effects of impurities appear to be most detrimental when they occur inhomogeneously in the powder mix, compositional differences are also potential causes for discontinuous grain growth. Rhodes [86] studied the effects of a second phase on the sintering and grain growth of yttria. He pointed out that the key element for the occurrence of discontinuous grain growth in those systems appeared to be the nearness of the composition to the phase boundary in the phase diagram. He postulated that a few precipitates may be formed locally and retard grain growth, but that a neighboring grain may have its grain boundaries free of precipitates and is able to grow until it reaches the conditions for discontinuous grain growth with enhanced kinetics. In many cases some large, abnormal grains have boundaries that are nearly perfectly straight indicating that the grain boundary energy is highly anisotropic.

When polycrystalline ceramic bodies are made from fine powders, the extent of discontinuous grain growth may also depend on the particle size of the starting material. The reason for this is that there are almost always

present in the fine grain size matrix, a few particles of substantially larger particle size than the average. These can act as embryos for discontinuous grain growth. In contrast, as the starting particle size increases, the chances of particles being present which are much larger than the average particle size are decreased. Consequently. the nucleation of discontinuous grain growth is more difficult. In order to obtain complete densification, discontinuous grain growth must be prevented.

II.3 - Sintering

The term sintering refers to the collective phenomena that occur during the process of heating packed powders. During sintering, interparticle bonds are formed and grain boundaries develop, resulting in a reduction of the surface area and a consequent strengthening of the original powder compact. Sintering can occur in the solid state or in the presence of a liquid phase. The presence of a liquid phase often accelerates the rate of interparticle bonding during sintering. Nicholson [91] has observed that the liquid phase greatly influenced the kinetics of grain growth in MgO compacts.

At least three stages have been identified to occur

during liquid phase sintering:

(i) - liquid flow and particle rearrangement

(ii)- solution and reprecipitation

(iii)-final stage densification

These three stages are represented in Figure (II.3.1) During the particle rearrangement stage, the liquid phase forms and the capillary forces exerted by the wetting liquid on the solid particles cause particle rearrangement and rapid densification. There is pore elimination as the system minimizes its surface energy. This results in an increasing liquid phase viscosity which decreases the densification rate. Grain growth occurs during the latter two stages.

A general attribute of the second stage, that of solution-reprecipitation is grain growth. The solubility is higher for the smaller grains than for the larger grains, thus creating concentration gradients in the system and consequently material transport from the smaller grains to the larger grains, resulting in microstructural coarsening. During this stage, shape accomodation occurs, with tighter packing of the grains, pore elimination and densification.

The third stage is considered to be solid state controlled sintering. The development of a solid skeleton

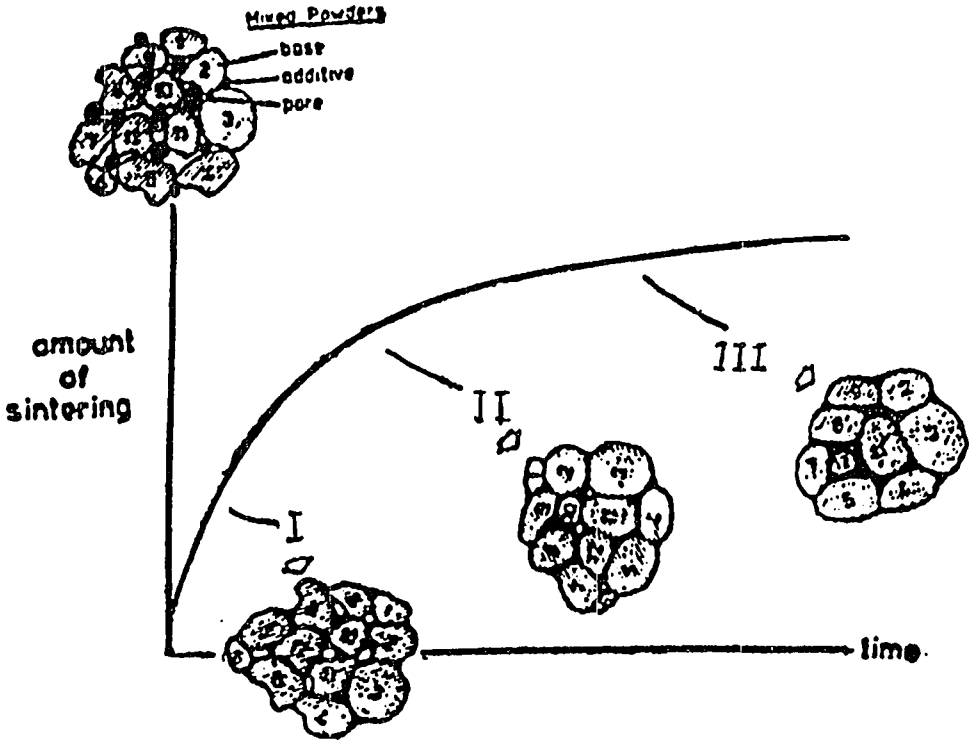

I - Rearrangement: liquid formation and spreading, repacking, rapid densification.

II - Solution -Reprecipitation: grain growth shape accomodation, neck formation.

III - Solid State: neck growth, grain growth, coalescence, pore coarsening.

Figure II.3.1 - The Classic Stages of Liquid Phase Sintering [16].

from interparticle contact reduces the rate of densification, however, diffusion results in further microstructural coarsening. Often, entrapped gases cause an enlargement of residual pores with consequent swelling. A prolonged final stage can cause degradation of the physical properties.

Capillarity is one of the most important aspects of the interfacial energies associated with liquid phase sintering. Capillary attraction is increased by a smaller capillary tube diameter or opening. During liquid phase sintering this means that a wetting liquid will preferentially penetrate those regions of the smallest pore diameters, drawing the powder particles together. As typical green compacts have inhomogeneous microstructures, differences in powder packing and pore size leads to differences in liquid penetration on a local scale.

The most beneficial aspect of capillarity is the strong surface forces exerted on the solid particles once the liquid phase forms. The attractive force between two particles with a wetting liquid, as represented in Figure (II.3.2) is given by summing the pressure and surface energy contributions. The force, F_C, on one of the particles depends on the meniscus size, X, as indicated in Equation (39) [16]:

$$F_C = (\pi X^2 P) + (2 \pi X \gamma_{LV} \cos \psi), \qquad (39)$$

where, P is the liquid pressure, X is the meniscus size, γ_{LV} is the liquid-vapor surface energy, and the angle ψ is that shown in Fig.(II.3.2.a).

The pressure P has been previously specified as:

$$P = \gamma_{LV} (1/r_1 + 1/r_2). \qquad (8)$$

For good wetting the force between the particles is an attractive one, leading to a nearly zero separation between the particles. Alternatively, for poor wetting the liquid forces a separation between the particles. These two conditions are contrasted in Figure (II.3.2.b).

Combination of Equations (9) and (39) for spheres yields:

$$F_c = (2 \pi X^2 \gamma_{LV})/r + (2 \pi X \gamma_{LV} \cos \psi). \qquad (40)$$

This shows that the attractive force between particles due to a wetting liquid varies with the radius of the particles and with the surface energy. The attractive force decreases as the liquid surface energy decreases and as the quantity of liquid increases. The contact force for a wetting liquid also decreases with particle separation. Thus, particles with a connecting meniscus of wetting liquid will be drawn together with a increasing

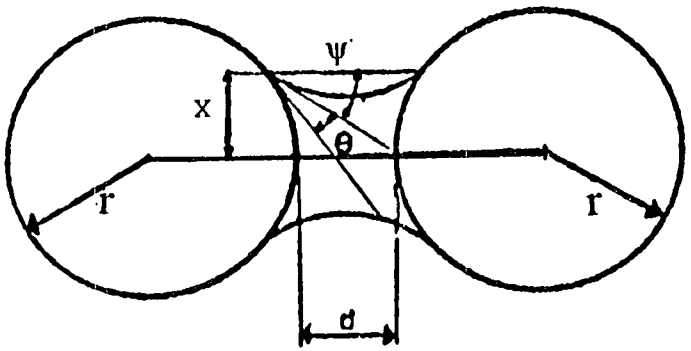

(a)

Figure II.3.2 - Capillary Forces Between Two Particles [16].
(a) - Two Spherical Particles with a Liquid Bridge and the Geometric Factors Involved in Calculating the Wetting Force.

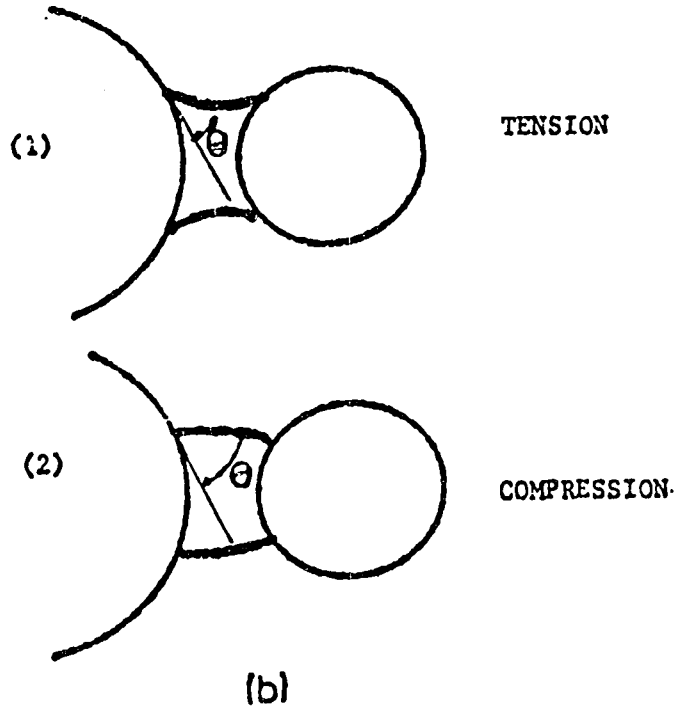

Figure II.3.2 - Capillary Forces Between Two Particles [16]. (b) - The Effect of the Two Extremes of Contact Angle (1) Good Wetting Leading to an Attractive Force, and (2) Poor Wetting Leading to a Repulsive Force.

force. Furthermore, smaller particle sizes are beneficial since the magnitude of the attractive force is inversely related to the particle size, as shown by the first term in Equation (40). For many practical systems the particle diameter must be below 10 μm for the capillary forces to give significant densification by rearrangement during liquid phase sintering.

II.3.1 - Sintering of Pure Zinc Oxide

The schematic idealized two sphere model shown in Figure (II.3.3) can be used to describe a number of proposed sintering mechanisms. In crystalline materials, the mass transport processes generally accepted to be active to some extent during sintering are bulk diffusion, surface diffusion, grain boundary diffusion, plastic flow, evaporation/condensation or some combination thereof. In all cases the themodynamic driving force is the reduction of surface energy. Studies of these mechanisms during the sintering of ZnO have been conducted by a number of workers utilizing the characterization methods of gas adsorption for surface area measurements [8,54,55], shrinkage of compacts [8,9,56], pore size distribution measurements [2-4] and grain growth [8,56-59].

Several different atmospheres i.e. vacuum [59], reducing atmospheres [60], oxygen at several different pressures [55,56,58,59,61,62], helium [9,56,62], hydrogen

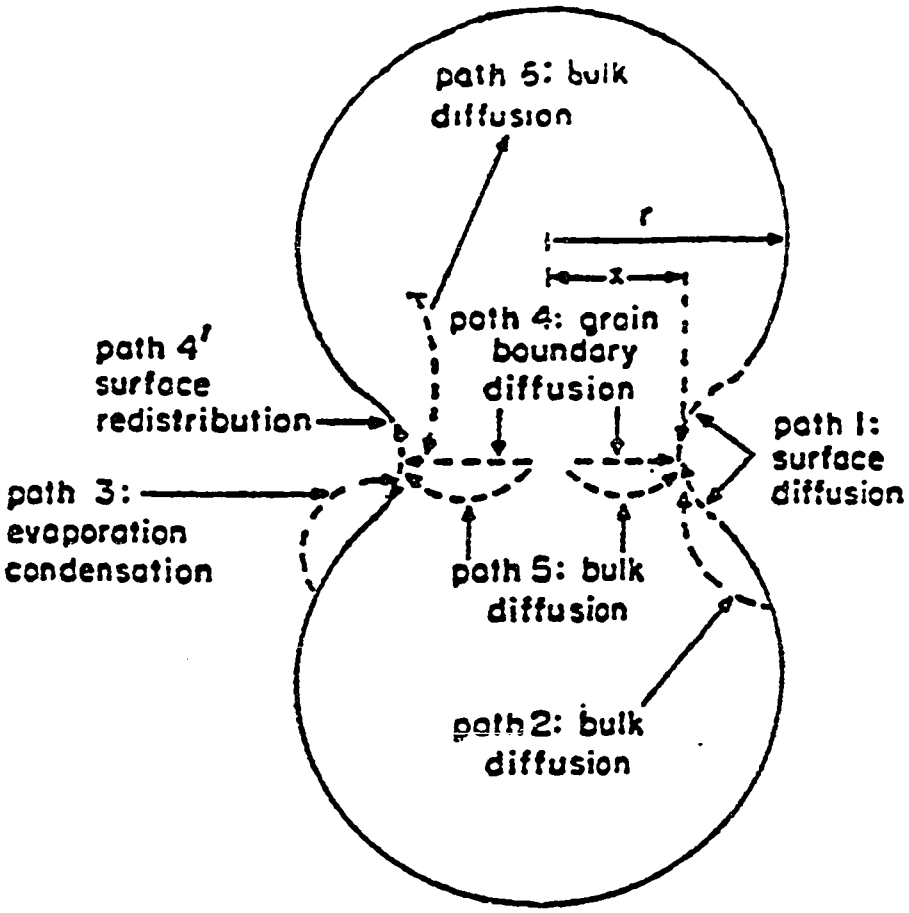

Path	Transport Path	Source	Sink
1	Surface Diffusion	Surface	Neck
2	Bulk Diffusion	Surface	Neck
3	Vapor	Surface	Neck
4	Boundary Diffusion	Boundary	Neck/Boundary
4'	Surface Diffusion	Neck/Boundary	Neck
5	Bulk Diffusion	Boundary	Neck
6	Bulk Diffusion	Dislocations	Neck

Figure II.3.3 - Mechanisms of Sintering [53]

[62], argon [61], nitrogen [8,9], and air [56,57,59,61-65] have all been employed in studies of the sintering of pure ZnO. Weyl [60] observed that sintering was promoted in a slightly reducing atmosphere. He interpreted this result in terms of the enhanced lattice diffusion resulting from the creation of lattice vacancies. Lee and Parravano [62] observed that fresh ZnO sinters rapidly in air and oxygen, but it does not sinter appreciably in helium at the same temperatures. They explained the mechanism of ZnO sintering by the diffusional transfer of a stoichiometric excess of Zn ions and postulated that the sintering of ZnO was essentially a solid state reaction controlled by the free energy change between the interior and the surface of the crystallites.

Effects of the atmosphere on ZnO grain growth have been reported by Dutta and Spriggs [59] and Gupta and Coble [56]. Dutta and Spriggs demonstrated that the grain growth rates of pure ZnO are the highest in a vacuum and the lowest in oxygen, while the grain growth rate in air is intermediate. They concluded that the different grain growth rates for ZnO in air, oxygen and vacuum may be related to the nonstoichiometric composition of ZnO in these environments.

Kinetic studies of the grain growth of pure ZnO have consistently reported a grain growth exponent,or n value of three. Activation energies for grain growth varying

from 213 to 409 kJ/mol have been reported in the literature [57-59]. Gupta and Coble [56] related the densification and grain growth rates in the intermediate and final stages of sintering to the lattice diffusivity of Zn ions. Senda and Bradt [57] have studied the kinetics of grain growth in pure ZnO and also concluded that the controlling mechanism is the diffusion of Zn^{2+} ions in the ZnO lattice. Table (II.3.1) summarizes the different studies of the sintering of pure ZnO, including initial conditions, processing, results and proposed mechanisms.

II.3.2 - The Role of Additives in the Sintering of ZnO

Commercial ZnO-varistor ceramics are extremely complex multicomponent materials that contain a number of metal oxide additives. In general the compositions of ZnO based varistor ceramics are designed to optimize the non-ohmic properties of the device. These properties are controlled by the ceramic microstructure. Asokan et al [2-5] using SEM, X-ray diffraction and electron probe microanalysis have observed and reported three types of solid phases in sintered commercial ZnO-varistor ceramics, including:

a) - The ZnO phase which may have the cations of the additive oxides in solid solution.

Table II.3.1 - Summary of ZnO Grain Growth Exponents and Activation Energies [57].

Reference	Parameter Measured	Temperature Range (°C)	Growth Exponent	Activation Energies (KJ/mol)
Norris Parravano (1963) [63]	Neck Length of Spheres	1050-1250	3	440-461
Nicholson (1965) [58]	Grain Size	900-1100	3	409
Gupta and Coble (1968) [56]	Grain Size	900-1300	3	253±42
Dutta and Spriggs (1968) [59]	Grain Size	950-1250	3	213
Moriyoshi and Komatsu (1968) [92]	Shrinkage	800-1000	-	193
Komatsu et al (1969) [8]	Shrinkage	800- 900	-	223
Gupta (1971) [71]	Grain Size	1100-1300	5	-
Whittemore Varela (1981) [64]	Surface Losses	450-550	3.6-3.8	184
Whittemore et al.(1983) [65]	Shrinkage	600-725	-	267
Wong (1980) [66]	Grain Size	1100-1400	6	243
Readey et al (1988) [7]	Grain Size	950-1200	3	326
Senda and Bradt [57]	Grain Size	900-1400	3	224±16

b) - A Bi_2O_3-rich network that developed as the liquid phase separating the individual ZnO grains.

c) - Spinel phases such as $Zn_7Sb_2O_{12}$ or $Zn_3Nb_2O_8$ that exist as distinct, faceted octahedral crystallites. These are usually present on the ZnO grain boundaries.

However, both Wong [66] and Levinson [11] have consistently reported the presence of the $Zn_7Sb_2O_{12}$ spinel phase within individual ZnO grains as well as at the ZnO-ZnO grain boundaries.

The presence of these additive oxide can affect the ZnO-varistor ceramic properties in several ways including:

(a) - Creation of lattice defects which contribute to the back-to-back Schottky barriers, thus directly affecting the electrical performance of the device.

(b) - Controlling the diffusion of interstitial Zn^{2+} ions and the other ionic species, therefore affecting the sintering, the grain growth processes and the final microstructure.

(c) - Precipitation of new phases within the material which can affect the grain boundary mobility and consequently, the grain growth kinetics and

ultimately also the final microstructure.

To control the microstructural development of ZnO during sintering it is necessary to understand the individual effects of each of the various types of oxide additions, as well as their synergistic effects at different levels on the sintering and grain growth of ZnO.

II.3.2.1 - The Role of Bi_2O_3 in the Sintering of ZnO

For the commercial Bi_2O_3-containing ZnO varistor ceramics the resulting microstructure is a consequence of the liquid phase sintering process. Bi_2O_3 is the low melting point component (825°C) and forms the initial liquid phase that dissolves some of the ZnO and the other additive oxide constituents during actual sintering. During cooling the Bi_2O_3-rich liquid phase solidifies at the multiple-grain junctions. Figures (II.1.4) and (II.1.5) show a schematic of the ZnO grain and the Bi_2O_3 at the grain junctions.

Complete surveys of the known bismuth oxide phases and their crystal structures have been presented by Medernach and Snyder [67] and by Harwig [68] and are summarized in Table (II.3.2). Cerva and Russwurm [10] have analysed the microstructure of bismuth oxide phases in ZnO varistor ceramics by means of transmission electron microscopy and X-ray diffraction. They concluded that the

majority of the multiple grain junctions are filled with the metastable tetragonal β-Bi_2O_3 phase. Individual grains of β-Bi_2O_3 were found to consist of two types of domains, having the same basic tetragonal lattice but different microdefect populations. A few of the multiple grain junctions also contained the stable monoclinic α-Bi_2O_3 phase in addition to the β-Bi_2O_3 phase. Heat treatment induces a transformation of the α and β-Bi_2O_3 phases into the cubic γ-Bi_2O_3 phase. The β-Bi_2O_3 phase has also been reported to transform into nonstoichiometric crystallites of a $Bi_2O_{2.33}$ phase.

Wong [66], Asokan et al [2-5] and Senda and Bradt [57] have all studied the effects of Bi_2O_3 on the sintering and grain growth of ZnO. They concluded that the presence of the Bi_2O_3-rich liquid phase not only enhances densification, but also promotes grain growth of the ZnO. Volatilization of Bi_2O_3 occurs during sintering and was observed to affect the microstructure of the ZnO ceramics, resulting in loss of nonlinearity [66]. Senda and Bradt [57] determined that the grain growth kinetic exponent, the n-value, increased from three for pure ZnO to five for the binary system ZnO-Bi_2O_3. Simultaneously, the apparent activation energy for grain growth decreased from 224 kJ/mol for pure ZnO to only 150 kJ/mol with additions of Bi_2O_3. This latter activation energy was independent of the Bi_2O_3 content. They concluded that the

Table II.3.2 - Crystal Structures of Some ZnO Varistor Phases.[67,68]

Phase	Crystal Structure	Lattice Parameters (A°) a	b	c
ZnO	Hexagonal	324.8	520.3	
$Zn_7Sb_2O_{12}$	Inverse Spinel			
	Cubic	855		
α-Bi_2O_3	Monoclinic	584.8	751.0	816.6
Stable at room temperature			$\beta = 113°$	
β-Bi_2O_3	Tetragonal	774.2	563.1	
Metastable at room temperature				
γ-Bi_2O_3	BCC Sillenite structure			
δ-Bi_2O_3	Cubic	525		
Stable at high	Defect CaF_2 Structure			
$Bi_2O_{2.33}$	Tetragonal			
Nonstoichometric	Superlattice	385		3510

grain growth process in $ZnO-Bi_2O_3$ ceramics is controlled by the phase boundary reaction between the solid ZnO grains and the Bi_2O_3-rich liquid phase.

II.3.2.2 - The Role of Spinel Forming Additives

The roles of the three spinel-forming additives Sb_2O_3, Nb_2O_5, and Al_2O_3 on the sintering and grain growth of ZnO ceramics have been previously investigated in only a very superficial manner [1,2-5,7], except for the study of $ZnO-Sb_2O_3$ by Senda and Bradt [70]. Additions of Sb_2O_3 result in the formation of the $Zn_7Sb_2O_{12}$ spinel and are known to drastically inhibit the grain growth of ZnO. Additions of Al_2O_3 [7] form the spinel phase $ZnAl_2O_4$ and also inhibit grain growth. Additions of Nb_2O_5 were found to induce the formation of the $Zn_3Nb_2O_8$ spinel, affect ZnO grain growth and also to improve electrical nonlinearity. The optimum Nb_2O_5 content for improved electrical properties has been reported to be 0.2 wt% [5].

Kim et al [69] have investigated the sintering effects of additions of antimony oxide through Sb_2O_3, $ZnSb_2O_6$, α-$Zn_7Sb_2O_{12}$ and Sb_2O_4 additions. They concluded that the addition of Sb_2O_3 from 0.1 to 2.0 mol% increased the densification temperature of ZnO from 600°C to nearly 1000°C regardless of the size and doping level of the Sb_2O_3. However, additions of $ZnSb_2O_6$, α-$Zn_7Sb_2O_{12}$ and Sb_2O_4 all yielded densification characteristics different

from those of Sb_2O_3-doped ZnO. Slight densification occurs at 600°C, but that densification is not completed below about 1200°C.

The effects of Sb_2O_3 on the densification characteristics of ZnO have been considered in terms of the volatile nature of Sb_2O_3. The Sb_2O_3 begins to rapidly evaporate at about 500°C and then condenses on the ZnO particle surfaces as a non-crystalline phase, causing retarded densification. Densification does not proceed until the Sb-oxide film on the ZnO particle surfaces is changed through reaction of the Sb_2O_3 and ZnO for the formation of the crystalline α-$Zn_7Sb_2O_{12}$ spinel at about 700°C or perhaps even higher temperatures.

Similar to their systematic kinetic studies of grain growth in pure ZnO and ZnO-Bi_2O_3, Senda and Bradt [70] have also systematically addressed a series of ZnO-Sb_2O_3 compositions. They reported that additions of Sb_2O_3 to ZnO reduced the grain growth of the ZnO, an effect that was dependent on the Sb_2O_3 content, as greater Sb_2O_3 contents yielded finer grain sizes. The values of the grain growth exponent and those of the activation energy both increased with additions of Sb_2O_3. Interestingly, the Sb_2O_3 also caused twinning in the ZnO as virtually every grain contained a twin, even at low Sb_2O_3 levels.

Readey et al [7] have observed that additions of Al_2O_3 inhibited grain growth of ZnO. They have attributed

this ZnO grain growth inhibition to the presence of the $ZnAl_2O_4$ spinel phase exerting a drag effect on the grain boundaries.

II.3.2.3 - Effects of Other Oxide Additives

Gupta [71] has reported that additions of K_2O to ZnO drastically inhibit the grain growth and that grain sizes of ZnO ceramics with only 0.12 wt% K_2O are much smaller by about a factor of two than those of pure ZnO. Komatsu et al [8,9] have analysed the effects of the alkali oxides Li_2O and Na_2O as well as Al_2O_3 and In_2O_3 additions on the sintering of ZnO over the temperature range from 600°C to 1200°C in air. They measured the linear shrinkage of the compacts and the surface areas. The alkali oxides Li_2O and Na_2O were found to promote the sintering of ZnO while Al_2O_3 and In_2O_3 were both observed to inhibit sintering. They interpreted these results were in terms of the diffusion of interstitial zinc ions which are controlled by the solution of these additives in the ZnO structure.

II.4 - Phase Diagrams

Figure II.4.1 depicts the ZnO-Nb_2O_5 phase diagram. It is observed that the compositions considered in this study, 0.80 wt% Nb_2O_5 and less, are in a two phase field formed by the ZnO and the spinel $Zn_3Nb_2O_8$.

Figure II.4.2 illustrates the ZnO-Al_2O_3 phase

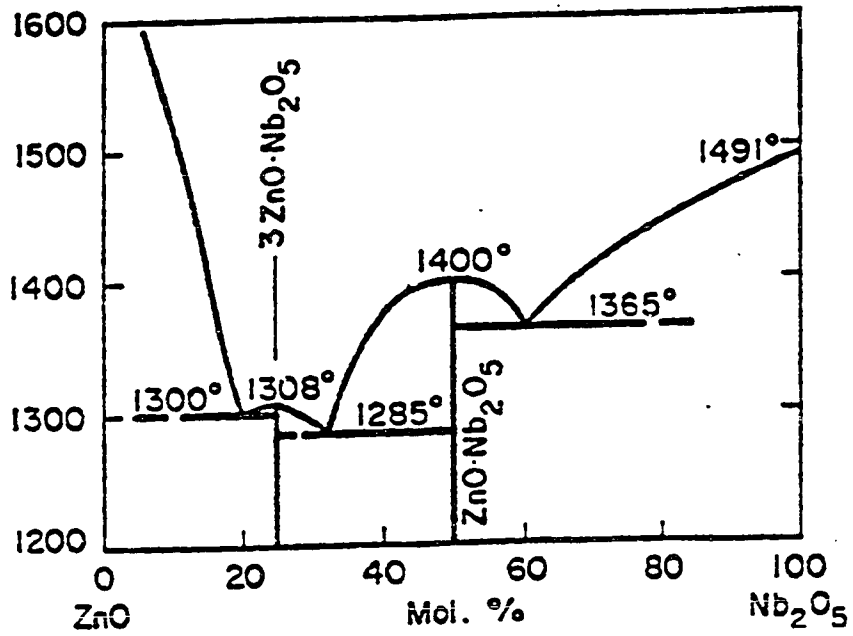

Figure II.4.1 - $ZnO-Nb_2O_5$ Phase Diagram [72]

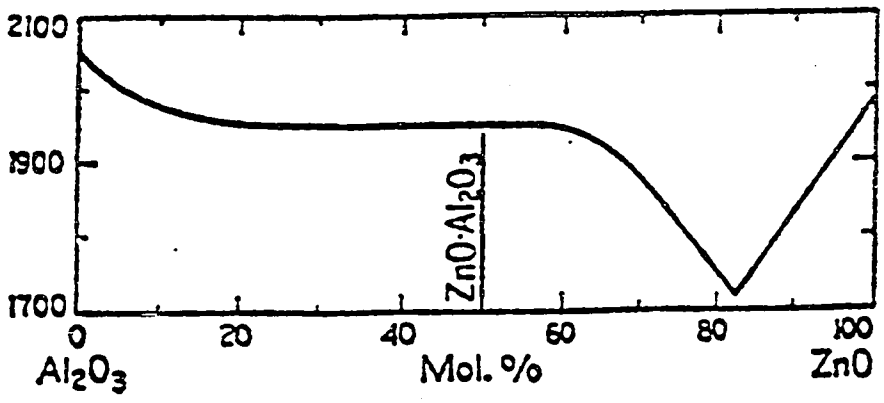

Figure II.4.2 - $ZnO-Al_2O_3$ Phase Diagram [72]

diagram. Although only the liquidus curve of the system $ZnO-Al_2O_3$ is shown in this figure, it is clear that the compositions under study which contained 0.80 wt% Al_2O_3 or less, are in a two phase field consisting of ZnO and the spinel phase $ZnAl_2O_4$.

II.5 - Crystal Structures

II.5.1 - Zinc Oxide

The ZnO crystal structure is the Wurtzite structure. It consists of hexagonal close packing of the large oxygen ions, with half of the tetrahedral interstices filled with the zinc ions. This structure is depicted in Figure (II.5.1). Both the anions and the cations have a tetrahedral configuration.

II.5.1 - Spinel

In the spinel structure the oxygen anions form a close packed cubic lattice in which the cations occupy the octahedral and the tetrahedral intersticial positions. The elementary cell of the spinel contains 32 oxygen anions and hence it has 32 octahedral and 64 tetrahedral positions. These positions can be filled by cations in different ways and as a a result two spinel structures, the normal and the inverse, are formed. In the classical normal spinel, e.g. $MgAl_2O4$, one half of the octahedral positions are filled by the trivalent aluminum ions and

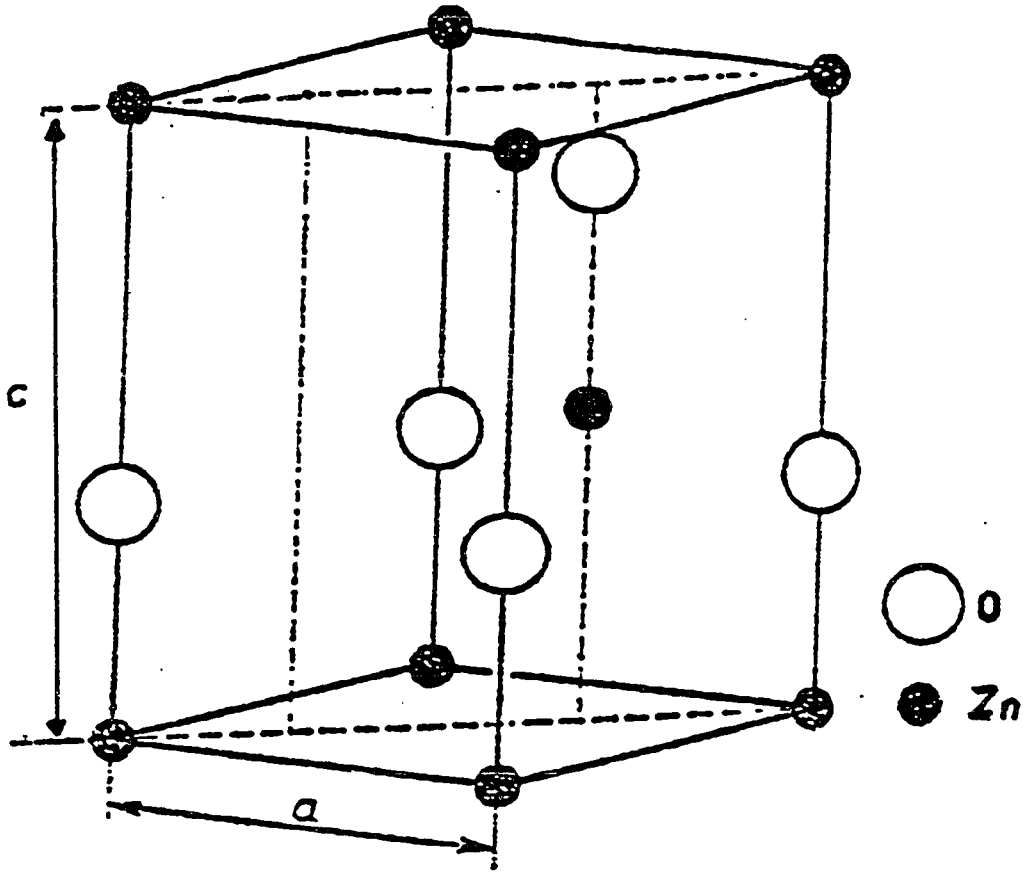

Figure II.5.1 - The ZnO Crystal Structure (Wurtzite)

1/8 of the tetrahedral positions are filled by divalent magnesium ions. In the inverse spinel 1/8 of the tetrahedral positions are filled by the trivalent cations while the rest of the trivalent cations, as well as the divalent cations, are situated in the octahedral positions. The two common spinel structure are depicted in Figure II.5.2. The $ZnAl_2O_4$ spinel is similar to the $MgAl_2O_4$, the trivalent aluminum ions occupy one half of the octahedral positions, and the divalent zinc ions occupy 1/8 of the tetrahedral positions.

The unit cell of the spinel $Zn_3Nb_2O_8$ also contains 32 oxygen atoms, 32 octahedral sites, and 64 tetrahedral sites. However, the pentavalent niobium ions occupy only 1/4 of the octahedral sites, while the divalent zinc ions fill approximately 1/3 of the tetrahedral positions. Therefore, the $Zn_3Nb_2O_8$ spinel has a defect structure, with many vacancies in the octahedral sites and an excess of zinc ions in the tetrahedral sites.

The unit cell of the $Zn_7Sb_2O_{12}$ spinel phase has 108 oxygen atoms, 108 octahedral sites and 216 tetrahedral sites. Since the stoichiometry indicates that only 1/6 of the octahedral sites are filled by the trivalent antimonium ions, while an excess of zinc ions fill approximately 1/3 of the tetrahedral sites, it is clear that the structure of the $Zn_7Sb_2O_{12}$ spinel is also a defect structure containing many octahedral-site vacancies and excess zinc ions.

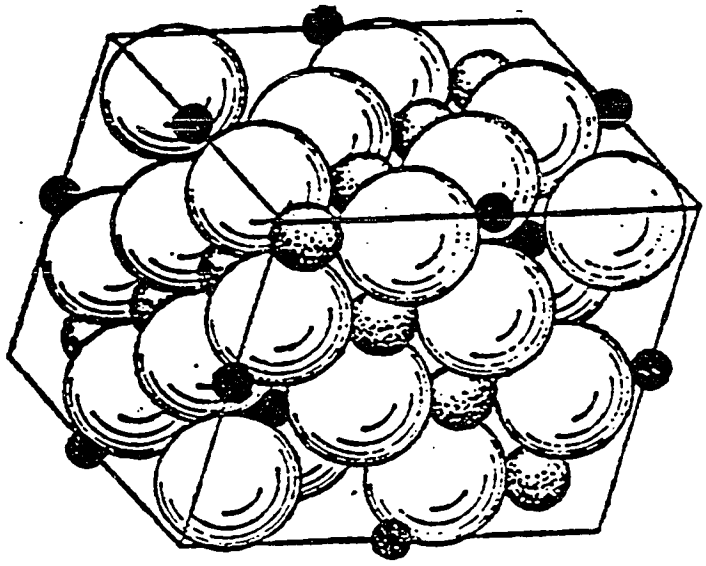

(a)

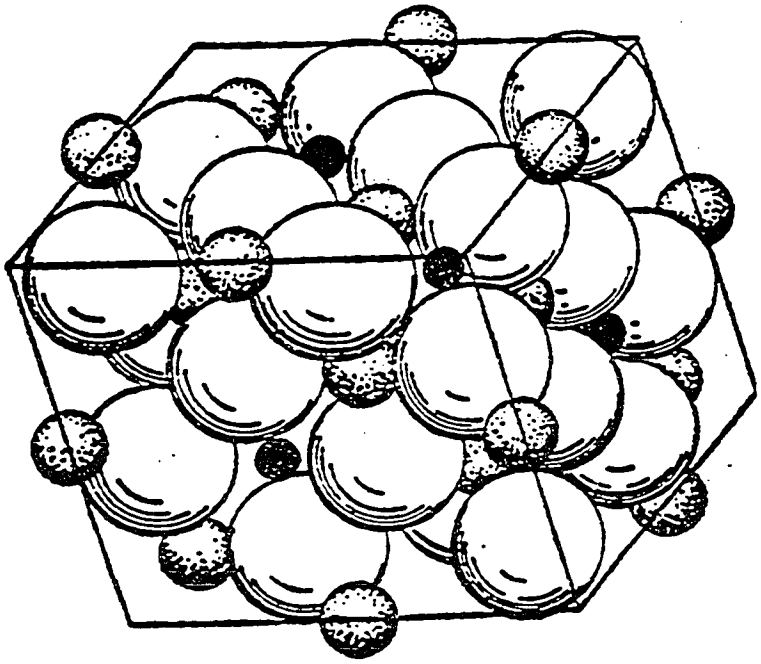

(b)

Figure II.5.2 - The Spinel Structure

(a) - Normal Spinel

(b) - Inverse Spinel

CHAPTER III - EXPERIMENTAL PROCEDURES

III.1 - Materials

The ZnO powders used in this study were all products of the French process which produces nearly spherical powders by oxidizing pure Zn metal vapor. The French process powders (Grades 911, 920, 930, and 506) of the St. Joe Zinc Co, Monaca, PA, 15061, had as principal impurities, 0.0015% Fe_2O_3; 0.0007% PbO; 0.0006% CdO; 0.0001% CuO; 0.0005% MnO; 0.0051% SiO_2. These four powder grades had average particle sizes of 0.11, 0.20, 0.30, and 2.0 μm respectively.

Reagent grade powder from Ventron Corp., Danvers, MA, 01923, was the source of Bi_2O_3. Technical grade Nb_2O_5 powder from Fansteel Corp., North Chicago, Illinois, 60064, and Al_2O_3 powder was from Alcoa, grade A16.

III.2 - Compositions

Table (III.2.1) summarizes the four different starting ZnO powders, their particle diameters, calculated surface areas, volumes and the surface area to volume ratios. The available range of particle sizes have particle surface areas (SA) and volumes (V) that vary by about 10^3. However, the (SA/V) ratio varies by only a factor of ten. After some preliminary studies from which the relevance of the initial ZnO particle size to the

Table III.2.1 - ZnO Initial Particle Sizes, Surface Areas and Volumes.

Initial ZnO Powder Particle Dimensions

Diameter d (μm)	Surface Area (SA) $\pi d^2 x 10^{-2}$ (μm^2)	Volume (V) $\pi d^3/6 x 10^{-3}$ (μm^3)	SA/V (μm^{-1})
0.11	3.80	0.70	54.30
0.20	12.57	4.19	30.0
0.30	28.27	14.14	20.0
2.00	1256.64	4188.80	3.30

final grain size (microstructure) could be clearly demonstrated, only the two extreme sizes, ie, 0.11 μm and 2.0 μm were employed for subsequent experiments to study the roles of the initial ZnO particle size on the microstructural development and grain growth.

To define the base composition(s), it was necessary to decide whether the ZnO ceramics to be considered in this thesis should contain Bi_2O_3, or to be free of Bi_2O_3. The choice was made to examine Bi_2O_3-containing ZnO ceramics. This was because a number of studies have been completed with Bi_2O_3-containing ZnO ceramics and the correlations between the microstructures and the electrical properties are generally better understood than for Bi_2O_3-free ceramics.

Once the presence of Bi_2O_3 was established, it was next necessary to decide the percentage of Bi_2O_3 to incorporate into the body. To resolve this issue, the results by Palanisany and Asokan [5], were considered. As the optimum content of Bi_2O_3 is indicated to be from 3 to 6 wt%, for the present work the highest level, i.e., 6 wt% Bi_2O_3 was chosen to achieve a substantial content of liquid phase throughout the compacts during sintering.

The basic binary ZnO-Bi_2O_3 composition used in this research was:

(a) wt%	(b) mol%	(c) vol%
94 ZnO	98.92 ZnO	96.20 ZnO
6 Bi_2O_3	1.08 Bi_2O_3	3.80 Bi_2O_3

The 6 wt% Bi_2O_3 is 1.08 mol% Bi_2O_3 and 3.8 vol% Bi_2O_3.

For the study of the effects of the two spinel forming oxide additives, Nb_2O_5 and Al_2O_3, ternary (ZnO/Bi_2O_3/additive) systems were prepared by individually adding Nb_2O_5, or Al_2O_3 powders to the basic binary composition. According to Palanisany and Asokan [5] the optimum levels of Nb_2O_5 should be about 0.2 wt%. To address that level in this study, the Nb_2O_5 contents chosen were 0.05, 0.10, 0.20, 0.40, and 0.80 wt%. This range of compositions brackets the optimum level for behavior of the varistor nonlinearity and of the grain growth kinetics.

The levels of Al_2O_3 additions which were chosen were based to a large extent on the studies of Komatsu et al [8,9]. In their research, they examined a 0.6 mol% Al_2O_3 compositions, although they also studied the effects of Li_2O in ZnO-varistor ceramics for Li_2O levels from 0.1 to 1.0 mol%. In the present study, the levels of Al_2O_3 chosen were also in this range as the actual Al_2O_3 additions were: 0.10, 0.20, 0.40 and 0.80 wt%.

The relative amounts of spinel phases that these

additions of Nb_2O_5 and Al_2O_3 would form, if fully reacted with the ZnO in the appropriate stoichiometry are summarized in Table (III.2.2). These calculations assume a density of 5.82 g/cm^3 for the $Zn_3Nb_2O_8$ spinel and 4.61 g/cm^3 for the $ZnAl_2O_4$ spinel.

III.3 - Specimen Preparation

Specimen compositions were prepared by initially mixing the ZnO powders with 6 wt% Bi_2O_3 and then subsequently adding either the Nb_2O_5, or the Al_2O_3 and 3 wt% of Carbowax-4000 as a binder. The binder was added from a solution of 0.5 g/cm^3 of Carbowax in distilled water. To obtain well homogenized mixtures, two different mixing processes were utilized for the preparation of the base binary systems ($ZnO-Bi_2O_3$). One binary mixture was prepared in a mortar and pestle and another was ball milled with distilled water (150 cc distilled water for 100 g powder) for 1/2 hour in a 1.0 liter polyethylene jar using dense alumina media, approximately 1 cm in diameter. The ball-milled mixture was then dried at 150°C, after which it was manually ground in a mortar and pestle to break up the cakes. A portion of the ball milled powder was then passed through a 50-mesh screen.

These ZnO + 6 wt% Bi_2O_3 mixtures were obtained from the different processes, including:

Table III.2.2 - Additive and Spinel Contents.

Additive	wt%	mol%	vol%	Spinel Phase	
				wt%	vol%
				$Zn_3Nb_2O_8$	
Nb_2O_5	0.05	0.02	0.06	0.10	0.097
	0.10	0.04	0.12	0.20	0.19
	0.20	0.08	0.24	0.40	0.38
	0.40	0.16	0.48	0.80	0.76
	0.80	0.32	0.96	1.60	1.56
				$ZnAl_2O_4$	
Al_2O_3	0.10	0.09	0.14	0.18	0.23
	0.20	0.18	0.28	0.36	0.46
	0.40	0.36	0.56	0.72	0.92
	0.80	0.72	1.12	1.44	1.83

a) - powders mixed only with a mortar and pestle,

b) - powders ball milled, and

c) - powders ball milled and sieved through 50 mesh.

Each was stored in an individual container for future utilization. Subsequently, appropriate amounts of the ZnO-Bi_2O_3 mixtures were weighed and mixed with the additives, either Nb_2O_5 or Al_2O_3 powders, and with the Carbowax solution in a mortar and pestle. Powders prepared in this manner were finally pressed into discs approximately 12.8 mm in diameter by 4 mm thick at 100 MPa (15,000 psi). The green densities of the as-pressed compacts were about 65 % of the theoretical density.

III.4 - Firing

For firing, specimens were first heated slowly in room air and held at 500°C for one half hour to burn off the carbowax binder. The temperature was then raised to the desired sintering temperature at a rate of 10°C/min. Series of specimens were fired at four different temperatures, (900°C, 1030°C, 1192°C, and 1400°C) for four different sintering times, (0.5, 1, 2, and 4 hours). Thus each composition had 16 time-temperature combinations. There were 80 Nb_2O_5 specimens and 64 Al_2O_3 samples.

III.5 - Polishing and Etching

For microstructural examination, which was conducted primarily by reflected light microscopy, the fired specimens were mounted in an acrylic resin. After grinding with 600-grit size SiC paper under a stream of tap water, final polishing was accomplished with 0.3 μm alumina powder in an automatic vibratory polishing machine (Syntron) with a distilled water vehicle. Ultrasonic cleaning of the specimens while immersed in distilled water was performed after each individual preparation step. To reveal the microstructure, the polished specimens were etched in a dilute acetic acid solution (10%) for approximately 30 seconds.

III.6 - Microstructural Analysis

Grain size measurements were conducted directly from 400X photomicrographs of the polished and etched specimens using a ZIDAS Image Analyser. The ZIDAS (Zeiss Interactive Digital Analysis System) is an image analysis system that derives measurements and statistics from images traced on a digitizing tablet. An electro-magnetic field is generated in the tablet. When the cursor, or stylus is positioned or moved on the tablet surface pulses are detected which relate to the location of the cursor or stylus on the tablet. An automatic closure feature

enables the user to trace the perimeter of an object without returning precisely back to the starting point. The grain sizes were measured using the Equivalent Circle Diameter Function which computes the area of an irregular shape and transforms it into an equivalent circle diameter for easier visualization of size.

The average grain sizes for a few specimens were measured by the Linear Intercept Method proposed by Mendelson and by using the Image Analyser to verify how both methods compared with each other. The values of the average grain sizes obtained with the ZIDAS Image Analyser were the same as the values obtained using the average linear intercept method derived by Mendelson [43] using Equation [33]. This showed that since both methods are equivalent either one could be used to measure the grain sizes, the choice of the Image Analyser Method was simply a question of convenience because this method is much faster.

For statistical evaluation, about 50 grains were measured on each micrograph and the STAT function was used in the Program Mode to obtain the sum, the mean, the standard deviation and the variance of the equivalent-circle-diameter (grain size) of the micrograph.

III.7 - Method of Analysis of Grain Growth Parameters

The experimental grain growth results were analysed

in terms of the previously discussed phenomenological kinetic grain growth expression, Equation (32):

$$G^n - G_o^n = K_o\ t\ \exp\ (-Q/RT) \qquad (32)$$

If it is assumed that the initial mean grain size, G_0, is relatively small compared to the final mean grain size, G, after the sintering time t, ($G>>G_0$), then Equation (32) can be simplified to yield:

$$G^n = K_o\ t\ \exp\ (-Q/RT) \qquad (41)$$

The logarithmic form of Equation (41) is:

$$n \log G = (\log K_0 - 0.434\ Q/RT) + \log t \qquad (42)$$

This form of Equation (32) was used on a (log G) versus (log t) plot to estimate the experimental kinetic grain growth exponent, n. The exponent n is determined as the inverse of the slope of the line log G versus log t.

Fluctuations in the n-value are common and can have at least two sources. One is due to the statistical error that accompanies every experimental measurement, and the other is due to variations of the grain growth rate with the firing temperature. Since the grain growth exponent is related to the grain growth rate, some variation in the

experimental value of n with the firing temperature is to be expected.

During analysis of the kinetics of grain growth, different procedures are often employed to determine the optimum value of the grain growth exponent, or n-value, in order to construct an Arrhenius plot. In one approach, for the cases in which the changes in the n-value are relatively small and fall within the limits of the statistical error an average value for n is calculated from the n values for the several different firing temperatures. The actual n-value is taken as the "nearest-integer" to this average. This "nearest-integer" n-value is then used in the Arrhenius plot.

Another procedure is used in those cases where the changes in the n-value with temperature are large, indicating that the grain growth rate is varying with the temperature. In these cases the best value(s) for n are found through trial and error estimates best fit the Arrhenius plot.

Once an appropriate grain growth exponent,or n-value has been established, the logarithmic form of Equation (41) can be rewritten in the form:

$$\log (G^n/t) = \log K_0 - 0.434 (Q/RT) \qquad (45)$$

When plotted, this form of the grain growth equation

should yield a straight line for log (G^n/t) plotted versus (1/T). The activation energy for grain growth can be determined from the slope of this line (- 0.434 Q/R) and the pre-exponential factor K_0 can be estimated as the (log K_0) intercept.

Analysis of the grain growth kinetics using Equation (32) cannot be applied directly to those cases where the grain growth is discontinuous, because for this process the grain size distribution is neither lognormal nor time invariant. However, analysis of the grain growth kinetics can still be attempted for those cases in which the grain growth process started as a discontinuous one, once the large grains have completely consumed the fine matrix grains and are colliding with one another. For those cases the term G_0^n cannot be neglected in that analysis, because the initial grain size G_0 is not much smaller than G. Then, the measured values of G_0 and G were applied to the Equation (32′) in which the initial time t_0 is that corresponding to G_0:

$$\log[(G^n - G_o^n)/(t-t_0)] = \log K_0 - 0.434\ Q/RT \qquad (32')$$

The left side of this equation is be plotted versus 1/T using the trial and error method, assuming n = 3, 4, 5, 6, etc and then choosing the n-value that gives the best fit for the line in this plot. Then the grain growth kinetic

parameters Q and K_0 can be estimated from the slopes and the intercept of the resulting line.

CHAPTER IV: RESULTS AND DISCUSSIONS

IV.1 - Effects of the Initial ZnO Particle Size

IV.1.1 - Preliminary Studies

It was previously noted that for investigation of the effect of the initial ZnO particle size on the grain growth, four different ZnO powders were chosen for the study. The initial ZnO particle sizes were 0.11 μm, 0.20 μm, 0.30 μm, and 2.0 μm. Scanning electron micrographs of these four powders are presented in Figures IV.1 (a to d). A preliminary study was performed to decide if the differences in these four particle sizes were sufficiently great to result in significant differences on the final ZnO microstructures after firing.

In the preliminary studies the four particle size powders were first employed to prepare specimens containing ZnO + 6 wt% Bi_2O_3 and then fired in air at 1192 °C for 1 hour. The resulting microstructures are illustrated in Figures IV.2 (a to d) for the initial powder particle sizes increasing from 0.11 μm to 2.0 μm, respectively. Figure IV.2.(a) depicts the ZnO + 6 wt% Bi_2O_3 consolidated with the 0.11 μm ZnO, and has an average grain size of (39 ± 2) μm. Note that some very elongated grains are present. Figure IV.2.(b) is for the specimen consolidated from the 0.20 μm ZnO powder, which yielded an average grain size of (33 ± 2) μm. Figure

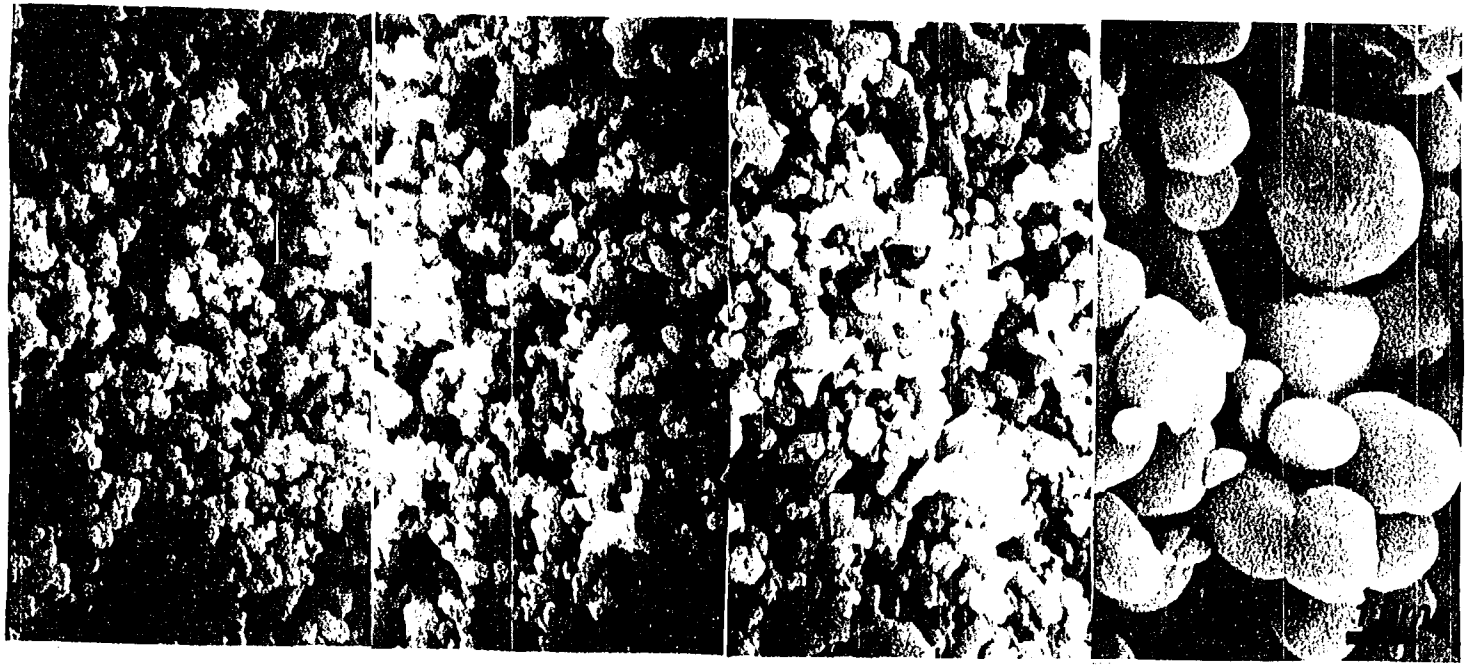

IV.1-(a)	IV.1-(b)	IV.1-(c)	IV.1-(d)
0.11μm ZnO	0.20μm ZnO	0.30μm ZnO	2.0μm ZnO

Figure IV.1 (a to d) - Scanning Electron Micrographs of the ZnO Powders with Different Initial Powder Particle Size - Magnification 10^4 X

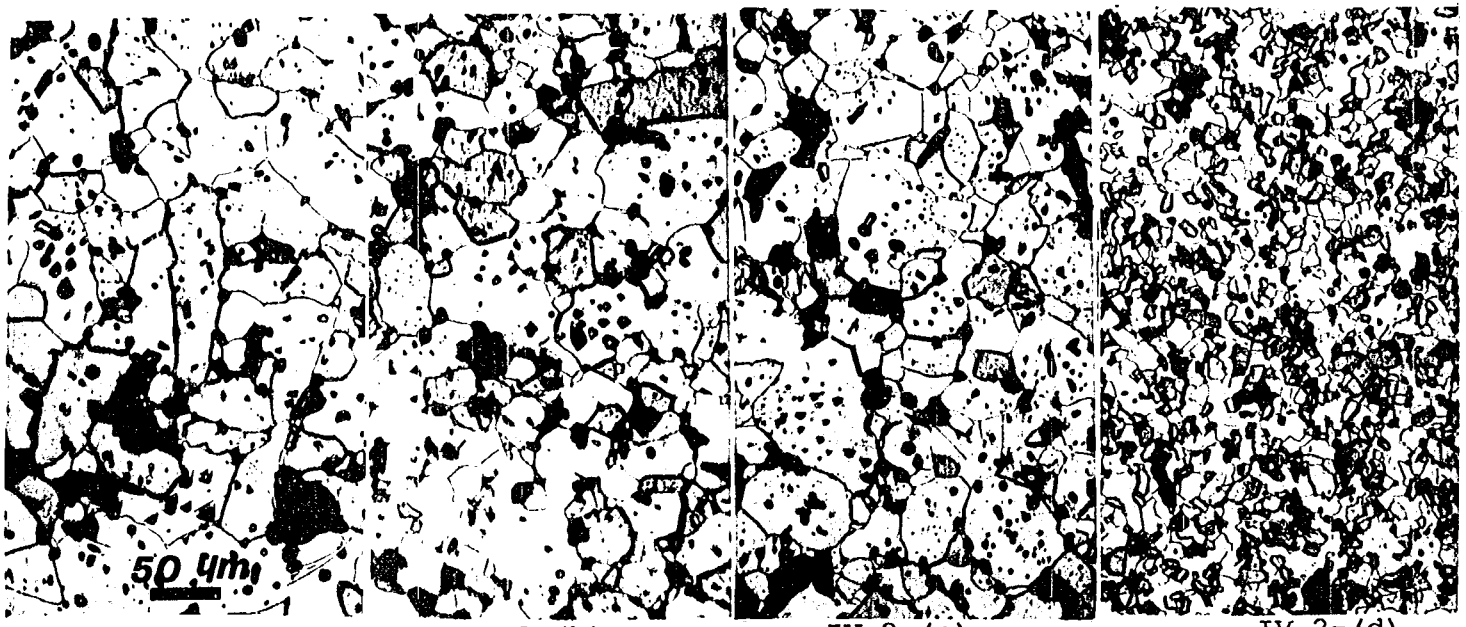

IV.2-(a)	IV.2-(b)	IV.2-(c)	IV.2-(d)
0.11µm ZnO	0.20µm ZnO	0.30µm ZnO	2.0µm ZnO
G=(39±2)µm	G=(33±2)µm	G=(29±2)µm	G=(11±3)µm

Figure IV.2 (a to d) - Optical Micrographs of the ZnO + 6 wt% Bi_2O_3 for ZnO Powders of Different Initial Particle Size. Fired at 1192°C for 1 Hour. Magnification 200 X

IV.2.(c) is for the specimen consolidated with the 0.30 μm ZnO and Figure IV.2.(d) is for the specimen with the 2.0 μm ZnO. Their average grain sizes are (29 ±2) μm and (11 ±3) μm, respectively. It is evident that the microstructures of those specimens prepared with the three finer powder particle sizes are very similar, as there is a wide range of grain sizes and all three also contain numerous elongated grains. However, a substantial difference of the final grain size is observed for the ZnO powder particle size of 2.0 μm. It is much finer and a nearly equiaxed microstructure, one that appears to have developed by normal grain growth processes.

On the basis of these experimental results, since the three powder particle sizes of 0.11 μm, 0.20 μm, and 0.30 μm all yielded very similar microstructures, the two intermediate particle sizes of 0.20 μm and 0.30 μm were abandoned. Subsequent comparisons of the effect of the initial powder particle size were carried out by employing only the two extreme powder particle sizes, 0.11 μm and 2.0 μm.

Having established which initial ZnO powder particle sizes to further study, the particle-size-effect study proceeded by investigating the following two different systems i.e.:

a) - The solid state system consisting of the "pure"

ZnO powders.

b) - A system containing substantial liquid phase at the firing temperature, consisting of ZnO + 6 wt% Bi_2O_3.

The results for each of these two situations are presented and discussed in the following sections.

IV.1.2 - The Solid State System

Figures IV.3 and IV.4 illustrate the microstructures resulting from the firing of the two "pure" zinc oxides, the finest (0.11 μm) and the coarsest (2.0 μm), both at 1400 °C for 1 hour in air. The microstructures which result from the solid state sintering of these two "pure" ZnO powders both have grains with a very regular geometrical shape, as the angles of most of the grain junctions are essentially 120°. These grain shape characteristics are usually associated with normal grain growth processes. The finer initial powder particle size yielded the larger final grain size, (40 ± 2) μm for the 0.11 μm ZnO, but only (10 ± 4) μm for the 2.0 μm ZnO, a difference of a factor of about four.

The average grain sizes for "pure" ZnO which have been reported in the literature by Gupta and Coble [56], Dutta and Spriggs [59], and Senda and Bradt [57], are all in close agreement with the average grain size observed in

Figure IV.3 - Optical Micrograph of the "Pure" ZnO
Fired at 1400°C for 1 Hour.
Initial ZnO Particle Size 0.11μm.
Average Grain Size G=(40±2)μm. Magnification 200 X.

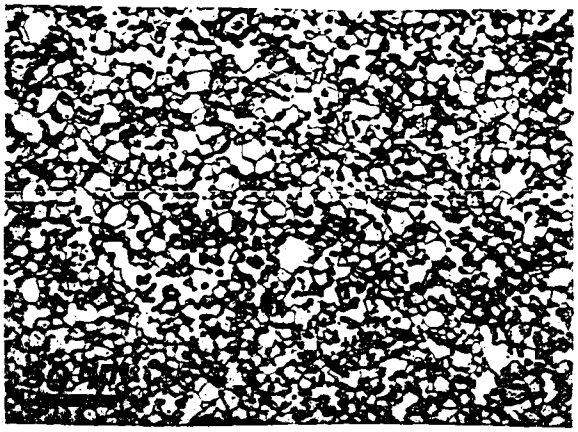

Figure IV.4 - Optical Micrograph of the "Pure" ZnO
Fired at 1400°C for 1 Hour.
Initial ZnO Particle Size 2.0μm.
Average Grain Size G=(10±4)μm. Magnification 200 X.

this study for the 0.11 μm ZnO. However, the average grain sizes reported by Nicholson [58], Wong [66], and Asokan et al [3] are all somewhat smaller and appear to correlate more closely with those reported in this study for the 2.0 μm ZnO. Wong [66] and Asokan et al [3] did not report the initial particle sizes which they employed in their studies, therefore, their results cannot be attributed to the effects of the initial particle size with absolute certainty. Nicholson used ZnO powders of the smallest size (0.10 μm) and he also obtained very small final grain sizes, an apparent contradiction when the results obtained by the other authors [56,57,59] and in this study are considered. However, Nicholson's results may have been related to atmospheric effects, since his specimens were sintered in oxygen instead of air. As Dutta and Spriggs [59] have proposed, the rate of grain growth for ZnO sintered in oxygen may be much lower than that for firing in air.

Figures IV.3 and IV.4 illustrate that during the solid state sintering of these ZnO powders, the smaller initial powder particle size results in the larger final average grain size. Also, since smaller initial particle size results in a higher rearrangement and densification rates, the specimens consolidated with the smaller initial particle size have a lower volume fraction of pores and a higher fired density, 97%, while under the same firing

conditions, the specimens consolidated with the larger initial particle size have a fired density of only 85%.

Since the driving force for grain growth is the reduction in the surface free energy, the system consolidated with the smaller initial particle size, having a larger surface energy per unit volume, is expected to have a higher driving force for grain growth in the initial stages. During the initial stage of grain growth on a porous body, when the effective force acting on the grain boundaries is large and exceeds the force binding the pores to the boundary, the boundaries become detached from the pores and consequently have a high mobility.

For a normal grain growth process, the grain growth rate, dG/dt, can be related to the driving force, f, and to the grain boundary mobility, μ ,by the equation:

$$(dG/dt) = 2\ g\ \mu\ f \qquad (44),$$

where g is a geometrical factor. It is evident from Equation (44) that the system consolidated with the 0.11 μm ZnO will have a higher grain growth rate at all stages of the grain growth process. At the initial stages, the grain growth rate is larger due to the contribution of the driving force factor, and at the later stages due to higher grain boundary mobilities. This might explain why

the system with the smaller initial particle size results in the larger grain size microstructure as observed experimentally and illustrated in Plates IV.9 and IV.10.

The effect of the initial particle size on the final microstructure has been explained in terms of the driving force that enables the grain boundaries to leave many pores behind. Since this driving force decreases as the initial particle size increases it is reasonable to expect the existence of a critical particle size above which the driving force is not sufficiently high to exceed the force binding the pores to the boundary. In those cases, the grain boundaries will remain attached to the pores and the effect of the initial particle size will be observed only during the very early stages of the grain growth process when the effects of the driving forces are relevant.

No further investigation of the "pure" ZnO solid state system was pursued. The remainder of this thesis addresses only those systems that contain a Bi_2O_3 liquid phase during sintering.

IV.1.3 - Effects of ZnO Particle Size During Bi_2O_3 Liquid Phase Sintering

The effect of the initial ZnO powder particle size on the fired density of the ZnO + 6 wt% Bi_2O_3 composition was studied by firing specimens with both the 0.11 μm and 2.0 μm ZnO, and then determining the densities from the

weights and the dimensions of the specimens. The theoretical density of the specimens containing a mixture of ZnO + 6 wt% Bi_2O_3 is 5.74 g/cm^3.

Figure IV.5 illustrates the final densities for the ZnO + 6 wt% Bi_2O_3, with the 0.11 μm ZnO powder, fired at the four different temperatures. At 900 °C the density increased rapidly and reached a value of about 98 % of the theoretical density after 1 h. It is also evident in this figure that as the sintering temperature increases the density decreases. This is a result of the evaporative loss of a portion of the Bi_2O_3 during firing.

Figure IV.6 illustrates the effect of the sintering temperature on the fired density of the ZnO + 6 wt% Bi_2O_3 specimens with the 2.0 μm ZnO powder. Contrary to the 0.11 μm ZnO powder specimen for which the density was a maximum at 900 °C, for the 2.0 μm ZnO powder specimen the density is the lowest for firing at 900 °C. For these specimens the density increases with the sintering temperature and reaches a maximum of 92 % of the theoretical density for firing at 1192 °C. However, for a further increase in the sintering temperature, to 1400 °C, the density decreases. The lower density at 1400 °C is probably a consequence of extensive Bi_2O_3 evaporation during firing.

By comparing Figures IV.5 and IV.6 it is seen that for the ZnO + 6 wt% Bi_2O_3 system with the 0.11 μm ZnO the

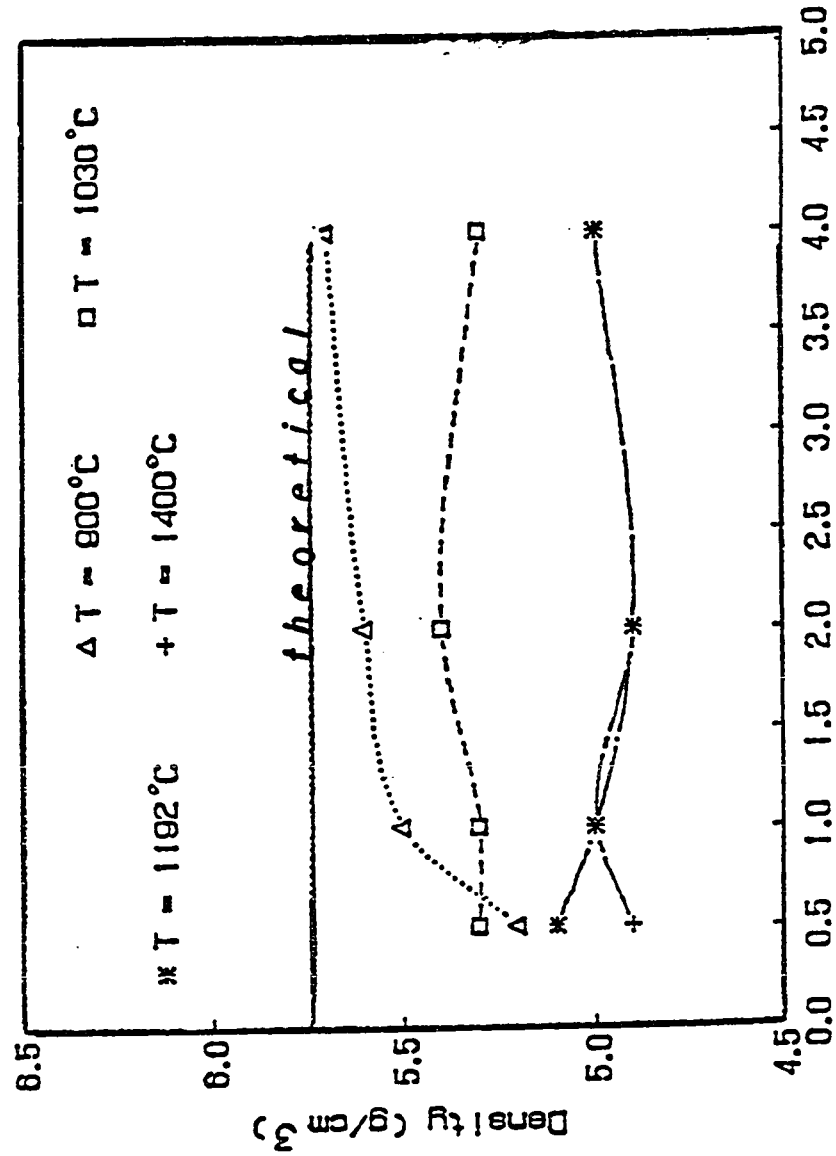

Figure IV.5 - Plots of the Density versus Firing Time for the 0.11 μm ZnO + 6 wt% Bi_2O_3.

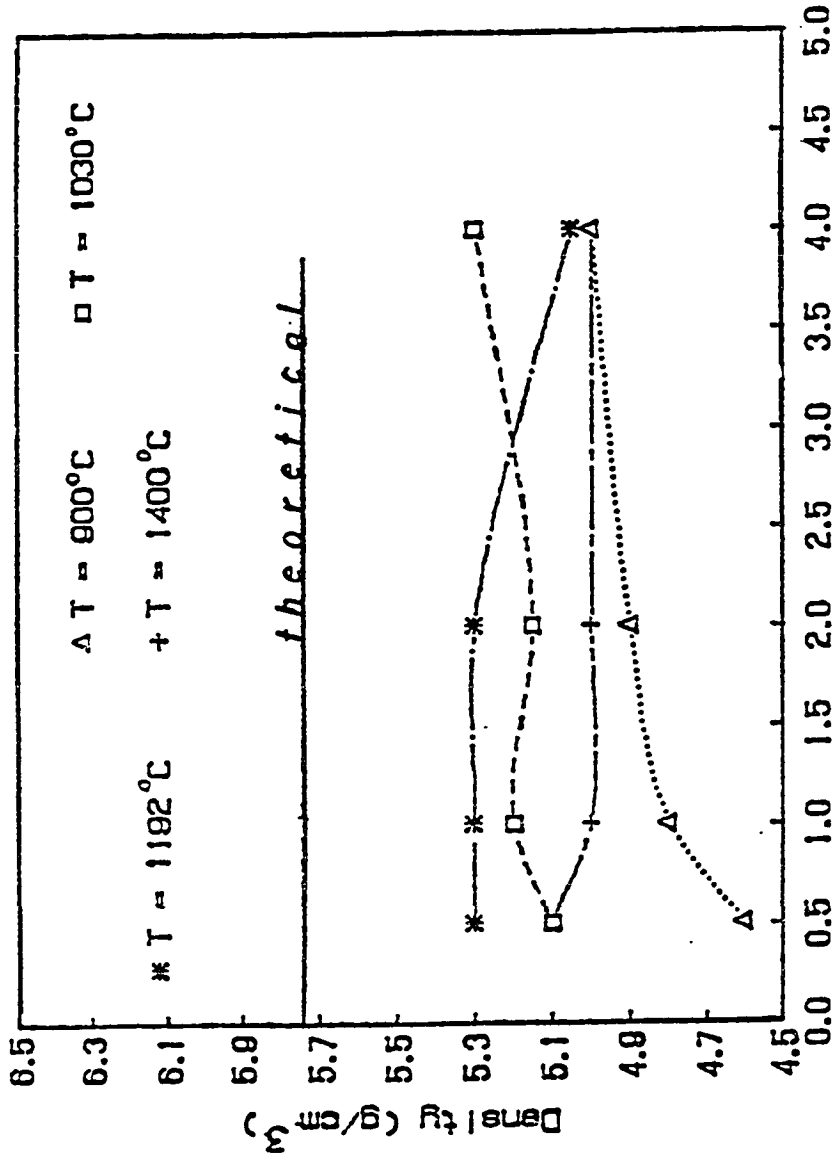

Figure IV.6 - Plots of the Density versus Firing Time for the 2.0 µm ZnO + 6 wt% Bi_2O_3

densification process appears to be complete after 1h at 900 °C, when the specimen density reached 98 % of its theoretical value of 5.74 g/cm^3. However, for the 2.0 μm powder particle size a higher sintering temperature is needed to complete the densification process, the density reached the maximum value of 92 % of its theoretical density only for firing at 1192 °C. These results demonstrate that the smaller initial powder particle size enhances densification. This may be due to better packing of the particles during the rearrangement stage of sintering when the initial powder particles are smaller.

Figure IV.7 depicts the 4 h weight losses as a function of the firing temperature for the specimens of ZnO + 6 wt% Bi_2O_3 for the finest (0.11 μm) and the coarsest (2.0 μm) initial ZnO powder particle sizes. In both cases, the highest weight losses occurred after firing at 1400 °C, but the greatest change occurred between 1030 °C and 1192 °C. Maximum weight losses of 9 % to 11 % are observed at 1400 °C. The burn off of the carbowax binder accounts for only 3 % of the total, evaporation of the Bi_2O_3 probably accounts for the major portion of this weight loss, however some ZnO must evaporate too.

When the low melting Bi_2O_3 , is added to "pure" ZnO, leading to the formation of a liquid phase during sintering, discontinuous grain growth is consistently

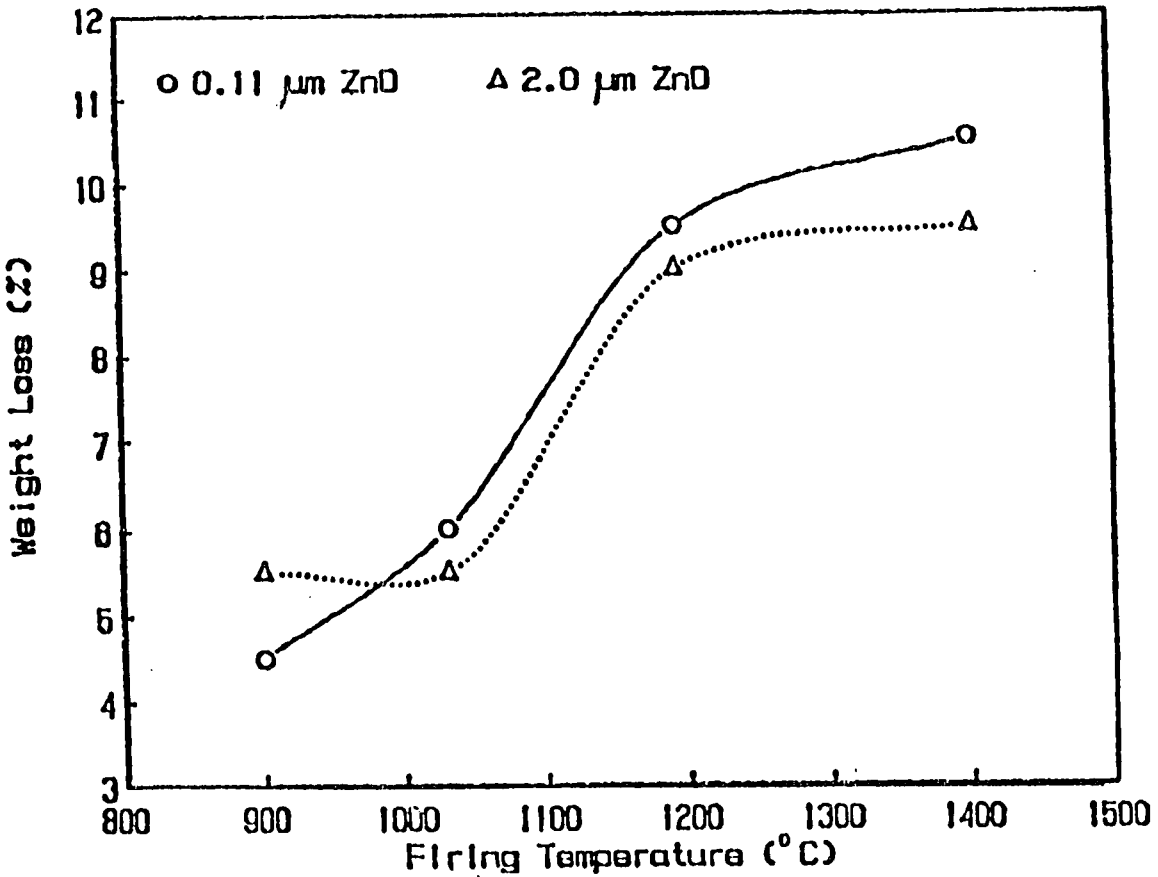

Figure IV.7 - Plots of the Weight Loss versus Firing Temperature for the (0.11 μm and 2.0 μm) ZnO + 6 wt% Bi_2O_3 Firing Time - 4 Hours.

observed for the initial 0.11 μm ZnO powder particle size.[107] This was observed independent of the experimental procedures that were followed during sample preparation, i.e. discontinuous grain growth was observed for all of the specimens prepared by the mortar and pestle method, as well as those prepared by ball milling, and also for those specimens ball milled and sieved for the 0.11 μm ZnO initial particle size. Since characteristics of discontinuous grain growth were never observed in the "pure" ZnO system free of Bi_2O_3, this suggests that the occurrence of discontinuous grain growth in this system is related to the presence of the Bi_2O_3 liquid phase during sintering.

Figure IV.8 illustrates a typical microstructure for the ZnO + 6 wt% Bi_2O_3 composition consolidated with the 0.11 μm ZnO powder that has been sintered at 900 °C for 1/2 hour . This micrograph illustrates the very early stages of the discontinuous grain growth process where an individual large grain or perhaps an aggregate of several large grains are rapidly growing into the matrix of very small grains. The average grain size of the matrix is only (2.2 ± 0.4)μm but the size of the grains in the dense aggregate are about 30 μm.

The boundaries between the very large grains and the matrix fine grains also appear exceptionally straight, indicating that the boundary of the larger grain moves

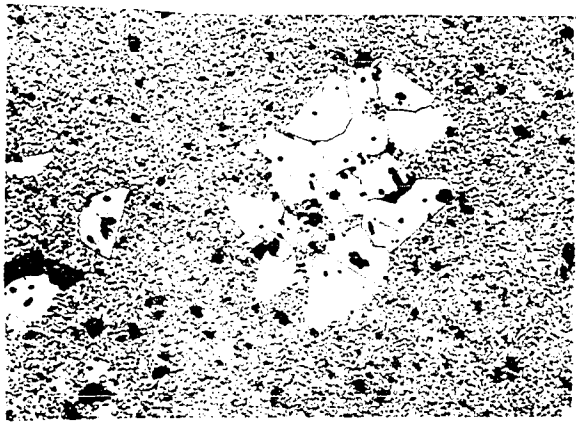

Figure IV.8 - Optical Micrograph of the ZnO + 6 wt% Bi_2O_3
Fired at 900°C for 1/2 Hour.
Initial ZnO Particle Size 0.11μm.
Average Matrix Grain Size G_{matrix}=(2.2±0.4)μm.
Average Crain Size in the Clusters $G_{cluster}$=(30±2)μm.
Magnification 200 X.

Figure IV.9 - Optical Micrograph of the ZnO + 6 wt% Bi_2O_3
Initial ZnO Particle Size 0.11 μm.
Fired at 1192°C for 1/2 Hour.
Average Grain Size G=(37±3)μm. Magnification 200 X.

through the matrix as a planar front, assimilating many of the fine matrix grains simultaneously. This may be explained by the driving force for the boundary migration of the large grain as determined by the pressure difference between the large grain and the much finer matrix grains. Since the matrix grains are small and nearly uniform in size, the pressure difference and consequently also the driving force, will be nearly uniform along the length of the boundary. All of the boundary will be subjected to nearly the same conditions and will migrate at the same rate, resulting in the straight (planar) grain boundaries observed on these micrographs. However, if pores or second phase particles become attached to the grain boundaries, then significant curvature may develop, as segments of the boundaries are slowed or perhaps arrested by drag effects. Some curved grain boundaries are evident within the cluster, or aggregate of larger grains.

Figure IV.9 shows the microstructure for the same composition (a 6 wt% Bi_2O_3 addition to the 0.11 μm ZnO) but sintered at a higher temperature (1192 °C) for the same length of time (1/2 h). The grains are an average size of (37 ± 3) μm, but are irregular in shape and with many pores located at the grain boundaries, as well as within the individual grains. This microstructure is a product of discontinuous grain growth. An important

feature of the ZnO ceramic structure observed in this micrograph is the presence of the Bi_2O_3-rich phase along many grain boundaries and at the multigrain junctions. It is evident that some of the grains do not appear to be wetted by the Bi_2O_3-rich phase, nor is this phase present at all of the multigrain junctions, as has been reported [73] for some slowly cooled sintered specimens.

Figures IV.8 and IV.9 conclusively prove that it is the presence of the Bi_2O_3 liquid phase during the sintering of ZnO which promotes discontinuous grain growth when the initial ZnO particle size is small (0.11 μm). However, the effect of the Bi_2O_3-rich liquid phase to create a system that is susceptible to discontinuous grain growth appears to be suppressed when the initial ZnO particle size is larger (2.0 μm). This is evident in Figure IV.10 and IV.11 for specimens containing the 2.0 μm ZnO + 6 wt% Bi_2O_3 fired for 1/2 h at 900 °C and 1192 °C respectively. The average grain size is only (5 ± 2) μm for the first specimen and (10 ± 3) μm for the second. No evidence of discontinuous grain growth was observed in the specimens consolidated from the coarse ZnO (2.0 μm) powder.

IV.1.3.1 - The Effect the Bi_2O_3 Liquid Phase Content

The results presented in the previous section on the effects of particle size during liquid phase sintering

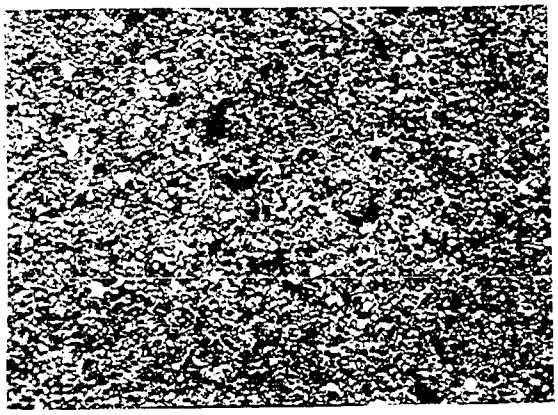

Figure IV.10 - Optical Micrograph of the ZnO + 6 wt% Bi_2O_3
Initial ZnO Particle Size 2.0μm.
Fired at 900°C for 1/2 Hour.
Average Grain Size G=(5±2)μm. Magnification 200 X.

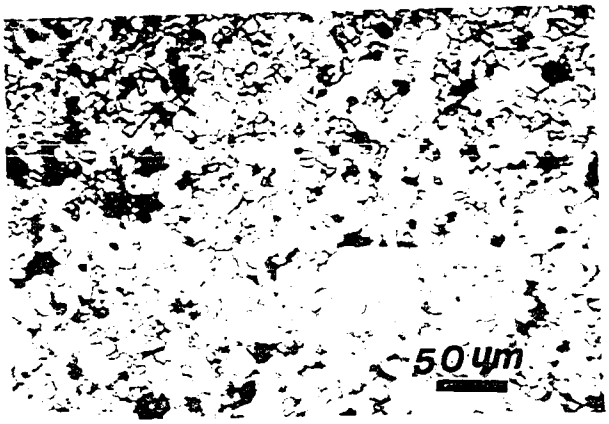

Figure IV.11 - Optical Micrograph of the ZnO + 6 wt% Bi_2O_3
Initial ZnO Particle Size 2.0μm.
Fired at 1192°C for 1/2 Hour.
Average Grain Size G=(10±3)μm. Magnification 200 X.

were obtained from ZnO specimens that contained 6 wt% Bi_2O_3. For these specimens it has been shown that if the initial ZnO powder particle size is increased from 0.11 μm to 2.0 μm then the grain growth process changes from an abnormal discontinuous one to a normal one. The final microstructures are also substantially different. An important question arises concerning whether the amount of liquid phase has significant influence on this behavior. To address that concern, the amount of liquid phase was reduced to 3 %. Accordingly, again both the 0.11 μm and the 2.0 μm ZnO powders were used to prepare specimens containing only 3 wt% Bi_2O_3. These specimens were fired at 1192 °C for 1 h.

Microstructures of the specimens are shown in Figures IV.12 and IV.13. These should be compared with the microstructures of specimens containing 6 wt% Bi_2O_3 shown in Figures IV.14 and IV.15. Figure IV.12 represents the microstructure for the ZnO + 3 wt% Bi_2O_3 with the 0.11 μm ZnO. The average grain size is (18 ± 2) μm. This micrograph reveals that some grains that are very large and irregular in shape, a clear indication that discontinuous grain growth has occurred. Figure IV.13 is for the specimen of ZnO + 3 wt% Bi_2O_3 with the 2.0 μm ZnO powder. The average grain size is (11 ± 5) μm, but the microstructure has the general characteristics of normal grain growth.

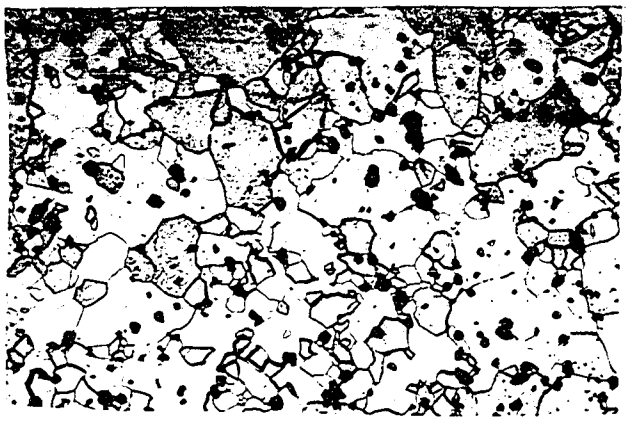

Figure IV.12 - Optical Micrograph of the ZnO + 3 wt% Bi_2O_3
Initial ZnO Particle Size 0.11μm.
Fired at 1192°C for 1 Hour.
Average Grain Size G=(18±2)μm. Magnification 200 X.

Figure IV.13 - Optical Micrograph of the ZnO + 3 wt% Bi_2O_3
Initial ZnO Particle Size 2.0 μm.
Fired at 1192°C for 1 Hour.
Average Grain Size G=(11±5)μm. Magnification 200 X.

For comparison, the microstructures of specimens containing 6 wt% Bi_2O_3, also sintered at 1192 °C for 1 h, are illustrated in Figures IV.14 and IV.15. Figure IV.14 is for the specimen consolidated with the 0.11 μm ZnO powder. It has an average grain size of (39 ± 3) μm and the grains are very irregular. Figure IV.15 is for the specimen consolidated with the 2.0 μm ZnO powder. Its average grain size is (11 ± 2) μm, and the grains are much more regular in shape and size. Even when the content of the Bi_2O_3 liquid phase is reduced to only 3 wt% the discontinuous grain growth process still occurs for the finer ZnO powder. It also remains suppressed by increasing the initial ZnO particle size to 2.0 μm.

These results demonstrate that the presence of the Bi_2O_3 liquid phase is a critical nucleating factor for the occurrence of discontinous grain growth in the ZnO-Bi_2O_3 system. The content of the Bi_2O_3 liquid phase over the range of 3 wt% to 6 wt% does not seem to alter the role of the initial ZnO particle size in the discontinuous grain growth processes. This Bi_2O_3 content range may be much more extensive, for Wong [66] has reported exaggerated grain growth in ZnO + Bi_2O_3 compositions for sintering temperatures above 1100 °C in mixtures containing as low as 0.05 mol% Bi_2O_3. In combination, all of these results emphasize the point that the presence of the Bi_2O_3 liquid phase is the critical factor in the determination of the

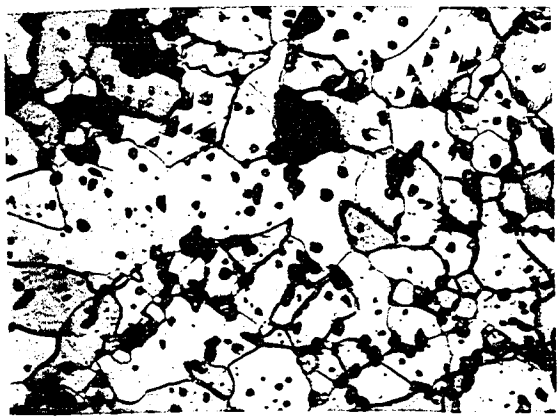

Figure IV.14 - Optical Micrograph of the ZnO + 6 wt% Bi_2O_3
Fired at 1192°C for 1 Hour.
Initial ZnO Particle Size 0.11μm.
Average Grain Size G=(39±3)μm. Magnification 200 X.

Figure IV.15 - Optical Micrograph of the ZnO + 6 wt% Bi_2O_3
Fired at 1192°C for 1 Hour.
Initial ZnO Particle Size 2.0μm.
Average Grain Size G=(11±2)μm. Magnification 200 X.

type of ZnO grain growth process, discontinuous or normal.

The effect of the initial ZnO particle size on the grain growth is further emphazised by Figures IV-12 to IV-15. In these plates all the specimens were fired at 1192 °C for 1 h. The initial ZnO particle size is 0.11 μm for Figures IV.12 and IV.14, but 2.0 μm for Figures IV.13 and IV.15. The occurrence of discontinuous grain growth in the specimens with the 0.11 μm ZnO leads to the large irregularly shaped grains, as compared to the smaller, more equiaxed grains for those specimens prepared with the 2.0 μm ZnO powder.

To observe the effects of the addition of Bi_2O_3 on the grain growth and on the final grain size, compare the microstructures depicted on Figures IV.12 and IV.14 for the specimens with the 0.11 μm ZnO. For the specimen containing 3 wt% Bi_2O_3 the average grain size is only (18 ± 2) μm, however for the specimen containing 6 wt% Bi_2O_3 the average grain size is (39 ± 3) μm. It is an increase in grain size of a factor of about two when the Bi_2O_3 content is increased from 3 wt% to 6 wt%. This increase in the grain size with the increased addition of Bi_2O_3 can also be observed for higher sintering temperatures by comparing Figures IV.3 and IV.16. Figure IV.3 is for the "pure" 0.11 μm ZnO sintered at 1400 °C for 1 hour, the average grain size is (40 ± 2) μm. Figure IV.16 is for the 0.11 μm ZnO containing 6 wt% Bi_2O_3

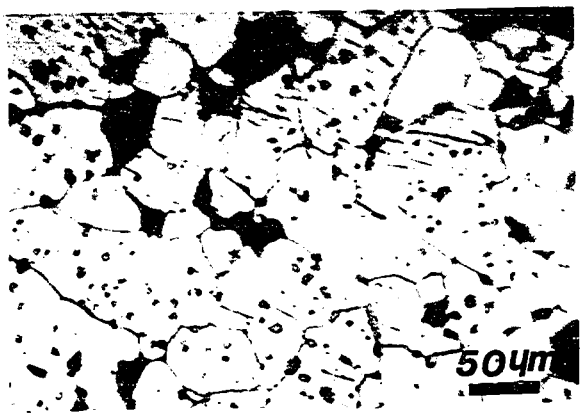

Figure IV.16 - Optical Micrograph of the ZnO + 6 wt% Bi_2O_3
Fired at 1400°C for 1 Hour.
Initial ZnO Particle Size 0.11 μm.
Average Grain Size G=(45±5)μm. Magnification 200 X.

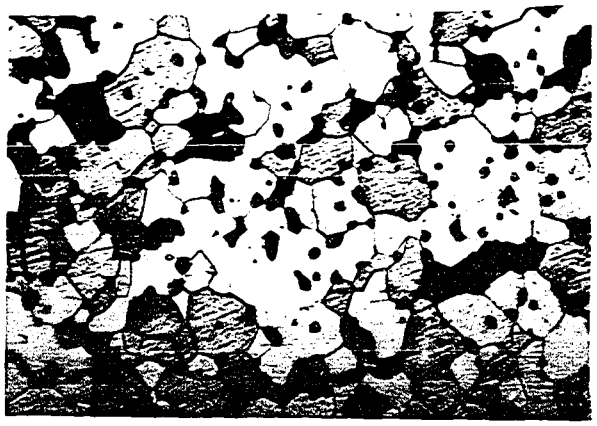

Figure IV.17 - Optical Micrograph of the ZnO + 6 wt% Bi_2O_3
Fired at 1400°C for 1 Hour.
Initial ZnO Particle Size 2.0 μm.
Average Grain Size G=(30±4)μm. Magnification 200 X.

sintered under the same conditions. The average grain size is (45 ± 5) μm.

For specimens with the 2.0 μm ZnO, sintered at 1192 °C, the grain size does not seem to change very much within the range of Bi_2O_3 content of 3 wt% to 6 wt%, for the average grain size is about 11 μm for both, as observed in Figures IV.13 and IV.15. However, at a higher sintering temperature, the addition of 6 wt% Bi_2O_3 to the "pure" 2.0 μm ZnO is observed to increase the average grain size. This is evident when comparing the microstructures depicted in Figures IV.4 and IV.17. Figure IV.4 is for "pure" ZnO and Figure IV.17 is for a specimen containing ZnO + 6 wt% Bi_2O_3. The 2.0 μm ZnO was used in both specimens. The sintering temperatures (1400 °C) and the sintering times (1 h) were also identical. The addition of 6 wt% Bi_2O_3 increases the final average grain size from (10 ± 4)μm to (30 ± 4)μm. This enhancement of ZnO grain growth by the addition of Bi_2O_3 has been previously well documented by Wong [66], Asokan et al [3], and Senda and Bradt [57].

IV.1.4. - Capillary Forces in Liquid Phase Sintering

It has been established that the presence of the Bi_2O_3 liquid phase in the ZnO + Bi_2O_3 system is a critical factor for promoting discontinuous grain growth when the initial ZnO particle size is small. This is related to

the action of capillary forces in the system. When the Bi_2O_3-rich liquid phase forms during the initial stages of liquid phase sintering, strong capillary forces are exerted by the liquid on the solid particles and this pulls the particles together. This fact has been well documented during the particle rearrangement portion of the liquid phase sintering process.

With a liquid that wets the solid, the force is an attractive one and the two particles with a connecting meniscus of the wetting liquid are drawn together by a strong attractive force. The presence of the Bi_2O_3-rich liquid phase creates strong attractive capillary forces between the fine ZnO solid particles, which are then drawn together to form aggregates. One of these aggregates is clearly evident in Figure IV.8 for the composition 0.11 μm ZnO + 6 wt% Bi_2O_3. This large aggregate formed during the early stages of sintering. These aggregates experience a much higher rate of densification and grain growth than the remainder of the matrix. This is probably related to the fact that the volume fraction of solid is initially higher within the aggregates than in the matrix. These higher density aggregates then serve as the nuclei which lead to the onset of discontinuous grain growth.

The capillary forces exerted by a wetting liquid of a meniscus size, X, connecting two particles of radius r is given by Equation (40), which was previously presented in

Section II.3:

$$F_C = (2 \pi X^2 \gamma_{LV} / r) + (2 \pi X \gamma_{LV} \cos \psi) \qquad (40)$$

The first term in Equation (40) explains why there is an effect of the initial ZnO powder particle size on the discontinuous grain growth process. The attractive capillary force between particles decreases as the size of the particles (r) increases, until the capillary forces between the particles are no longer strong enough to form the aggregates.

As an additional point it is important to note that when the liquid phase is non-wetting, as is the case for Sb_2O_3, then discontinuous grain growth is not expected and it is not observed. This is also consistent with Equation (36) as the capillary force, F_C, is a repulsive one for a non-wetting liquid.(See Fig. II.3.2).

In order to estimate the magnitude of the capillary effects involved, the stress generated by the interparticle forces in the area of contact between the liquid and solid can be calculated. Assuming that the contact area is (πX^2) the stress σ_C is obtained by dividing the capillary force, F_C, by the area as:

$$\sigma_C = F_C/\pi X^2 = (2 \gamma_{LV}/r) + (2 \gamma_{LV} \cos \psi/X) \qquad (41).$$

If X = 0.5 r, the resultant stress is:

$$\sigma_C = (2\ \gamma_{LV} / r) \quad x \quad (1 + 2 \cos \psi) \qquad (42).$$

Then the stress resulting from capillary effects increases with increasing γ_{LV} and decreasing particle size and the angle ψ. The minimum value of this stress obtained when $\cos \psi = 0$ is:

$$\sigma_C = (2\ \gamma_{LV})/r \qquad (43).$$

For γ_{LV} = 1000 erg/cm^2 and r = 0.05 μm (0.11 μm ZnO particles) the stress is $\sigma = 4 \times 10^8$ dy/cm^2 which is equal to (6,000 psi). If the larger initial particles (the 2.0 μm ZnO) are used the stress is 0.21×10^8 dy/cm^2 (300 psi), about 20 times smaller as expected since it is inversely proportional to the particle size. These stresses caused by capillary effects are very large and are comparable to the compressive yield stress of many materials. The decrease by a factor of 20 in the capillary stresses when the initial ZnO particle size is increased from 0.11 μm to 2.0 μm has been shown experimentally in this study to be sufficiently large to supress the discontinuous grain growth process.

IV.1.5 - The Grain Growth Kinetics

When analysing the effects of the initial ZnO particle size on the grain growth kinetics, it must be noted that the classical grain growth law:

$$G^n - G_0^n = K_0 \, t \exp (- Q/RT) \qquad (32)$$

was derived to describe the normal grain growth process. It assumes that the grain size distribution is a lognormal one that is time invariant. Therefore, this familiar phenomenological equation cannot be directly applied to the discontinuous grain growth process where the grain size distributon is neither lognormal, nor time invariant.

The kinetics of discontinuous grain growth is not very well understood. In studies of the phenomenon it has usually been assumed that the grain boundary mobility is proportional to the average grain size [74], or that the grain growth rate is inversely proportional to the average grain size of the matrix [52]. However, for the present results there does not exist a well established model or equation to describe the kinetics of discontinuous grain growth. For these reasons, the quantitative analysis of the grain growth kinetics by directly applying Equation (32) can only be carried out for those specimens consolidated with the 2.0 μm ZnO powder, because those specimens were the only ones for which the grain growth process was a normal one.

IV.1.5.1 - The Grain Growth Exponent

The grain growth exponent, or n-value, can be determined as the inverse of the slope of the lines of the plots of the logarithm of grain size versus the logarithm of time as previously illustrated in Equation (42). Figure IV.18 is a plot of log G versus log t for those specimens consisting of ZnO + 6 wt% Bi_2O_3 with the 2.0 μm ZnO initial particle size sintered at the four different temperatures. The average grain size consistently increases with increasing firing temperature and for longer firing times as predicted by Equation (32).

The slopes of the lines are (0.176 ± 0.045) at 900 °C, (0.177 ± 0.056) at 1030 °C, (0.247 ± 0.100) at 1192 °C, and (0.276 ± 0.220) at 1400 °C. The kinetic exponents are (5.69 ± 1.48) at 900 °C, (5.65 ± 1.85) at 1030 °C, (3.65 ± 1.38) at 1192 °C and (3.62 ± 1.49) at 1400 °C. Previous studies [3,57] of the kinetics of grain growth in the ZnO + Bi_2O_3 system have also reported large grain growth exponents, usually equal to five. Grain growth exponents equal to three for "pure" ZnO have been observed by Gupta and Coble [56], Dutta and Spriggs [59], Readey et al [7] and Senda and Bradt [57]. Increases of the grain growth exponent from three to five has been observed by several authors who have studied the effects of the additives, Bi_2O_3 [57], Sb_2O_3 [3,70], and K_2O [71] on the grain growth

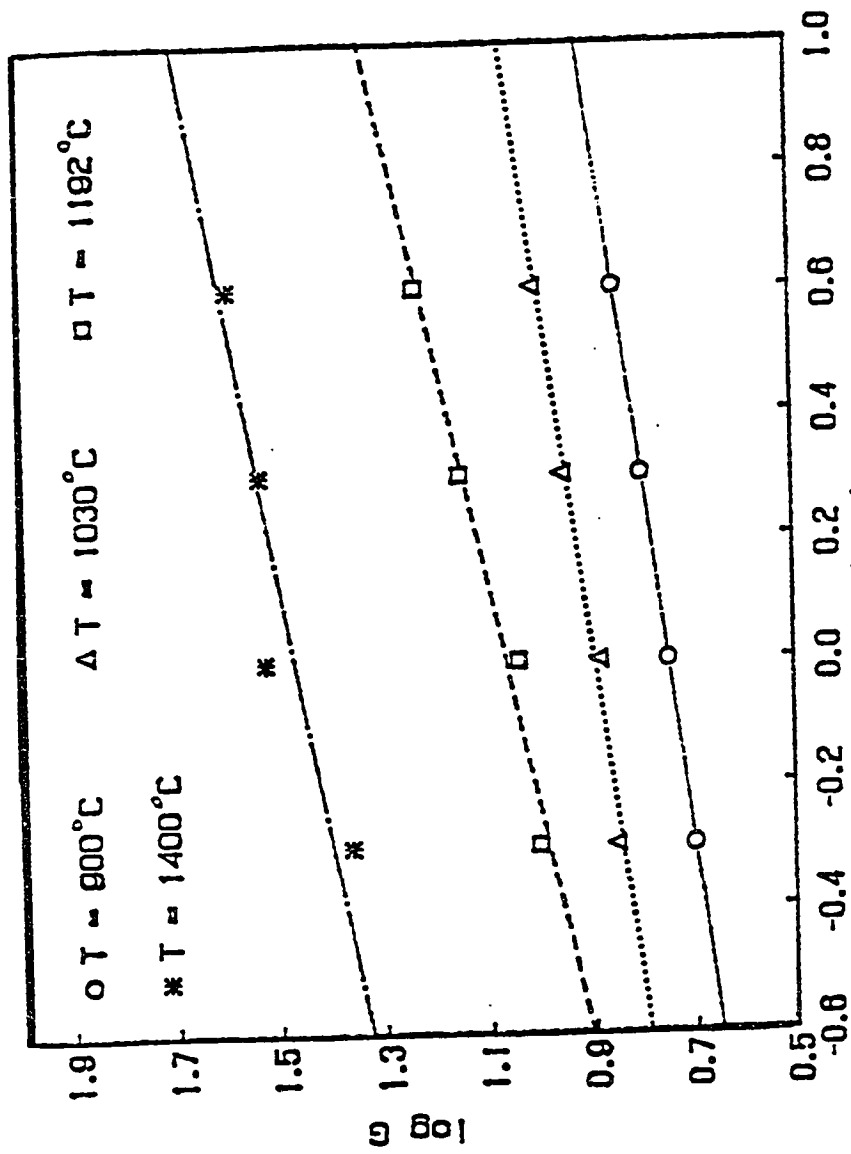

Figure IV.18 - Plots of Log (Grain Size) versus Log (Time) for the 2.0 µm ZnO + 6 wt% Bi_2O_3

kinetics of ZnO.

These Bi_2O_3-containing specimens also contain high porosity, either at the grain boundaries or within the grains. Grain growth exponents of three, four, and five have each been theoretically predicted for situations involving pore controlled mechanisms in which the material is transferred either through the vapor phase within pores, yielding n-values of three or four, or by diffusion on the pore surfaces, which results in a grain growth exponent of five as previously summarized in Table (II.2.2). Thus, grain growth exponents of four or five are reasonable and are to be expected.

An effect of the firing temperature on the grain growth exponent is evident in Figure IV.18 The grain growth exponent decreases from nearly six at 900 °C and 1030 °C to approximately four at 1192 °C and 1400 °C. Large or high grain growth exponents have been reported by previous authors, usually either at low firing temperatures or during the initial stages of sintering. From the Wong [66] data the grain growth exponent for specimens fired at 1100 °C (calculated by Senda and Bradt [57]) is about ten. Komatzu et al [8,9] also reported values of n larger than ten for ZnO in the initial stages of sintering. Norris and Parravano [63] have observed lower rates of neck growth at lower temperatures. Senda and Bradt [57] also reported an increase in the grain

growth exponent of "pure" ZnO at low firing temperatures such as 900 °C. For the case of the liquid phase sintering of MgO, Nicholson [91] observed that very little grain growth occurred below 1300 °C. He attributed this to the high viscosity and surface tension and low wetting properties of the liquid phase at low temperatures (just above the melting point).

Large grain growth exponents are indicative of a slow rate of grain growth, as apparent from Figure IV.18. This also follows from Equation (42):

$$n \log G = \log K_0 - Q/0.434RT + \log t, \qquad (42)$$

from which the grain growth rate, (dG/dt) may be obtained by differentiation with respect to time, yielding:

$$(dG/dt) = (1/n)\ (G/t). \qquad (45)$$

Equation (41) illustrates that for larger grain growth exponents, the rate of grain growth is lower. The high apparent values for the grain growth exponent which are observed in Figure IV.18 at the temperatures of 900 °C and 1030 °C is probably related to the lower fired density (85%) of the specimens fired at these temperatures as compared to the higher fired densities (92%) for the specimens fired at 1192 °C and 1400 °C.

IV.1.5.2 - The Activation Energy

The activation energy for grain growth, Q, can be estimated by plotting log (G^n/t) versus 1/T to obtain the slope of the line, which is (- Q/ 0.434 R). Since there is a large scattering of the values of the kinetic exponent at different firing temperatures, the activation energy was determined using only the data for the higher firing temperatures, 1192°C and 1400°C, for which the final density is higher.

Using an average n-value of four the Arrhenius plot is presented in Figure IV.19. The activation energy derived from the slope of the Arrhenius plot is (360 ± 12) kJ/mol.

The activation energy for the grain growth of "pure" ZnO sintered in air has been determined by a number of previous authors. Those values are summarized in Table II.3.1 and vary from 213 kJ/mol to 284 kJ/mol. They correlate well with the Gupta and Coble [56] conclusion that the mechanism of grain growth in "pure" ZnO is related to the diffusion of the zinc ions in the ZnO lattice. However, for the case of the binary ZnO + Bi_2O_3 system, Senda and Bradt [57] observed that the activation energy for grain growth decreased from that of "pure" ZnO and was independent of the Bi_2O_3 liquid phase content. They concluded that the phase boundary reaction was

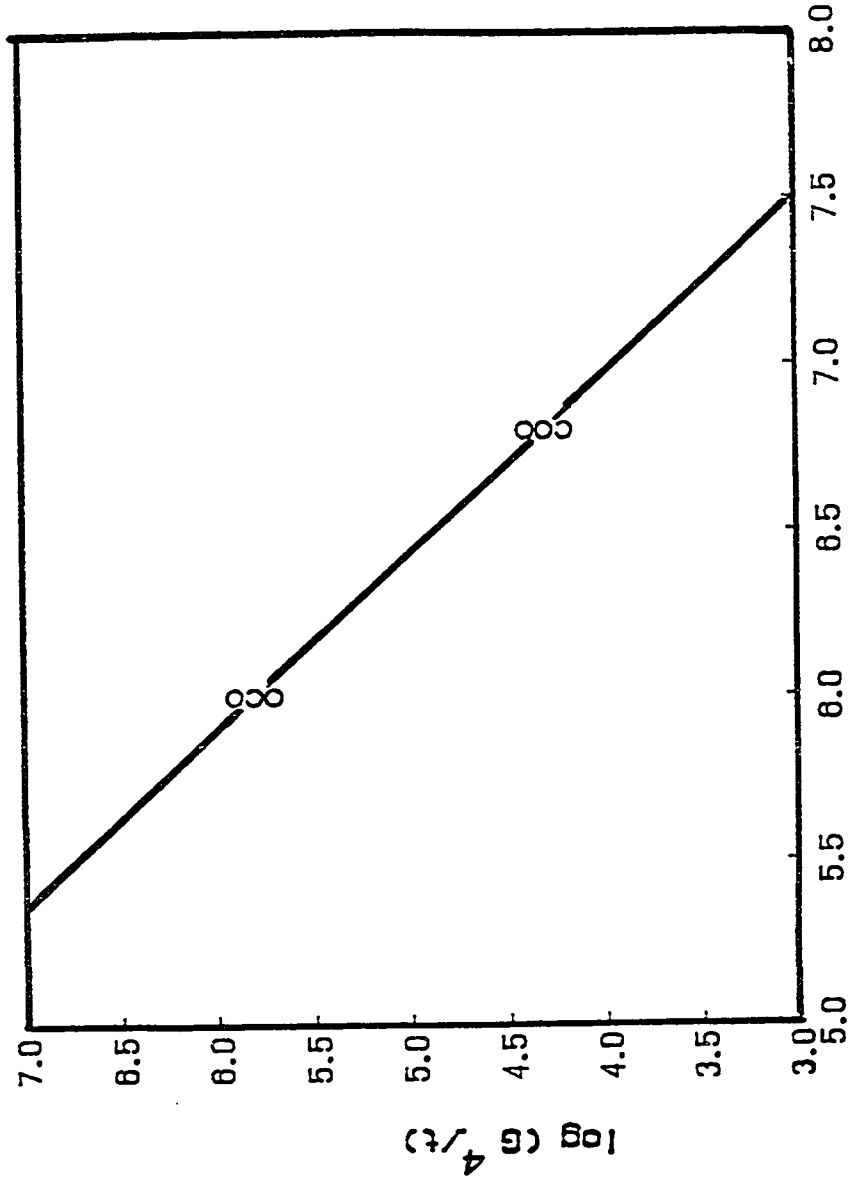

Figura IV.19 - Arrhenius Plot Log (G^4/t) versus 1/T for the 2.0 µm ZnO + 6 wt% Bi_2O_3.

probably the rate controlling mechanism for the grain growth of the ZnO-Bi_2O_3 ceramics.

For the ZnO + 6 wt% Bi_2O_3 composition consolidated with the 2.0 μm ZnO powder the high value of the activation energy, 360 kJ/mol, suggests that the grain growth process is probably controlled by pore drag mechanisms. The presence of pores at the grain boundaries, which is clearly revealed in Figure IV.17 for the 2.0 μm ZnO + 6 wt% Bi_2O_3 fired at 1400 °C for 1 hour, can reduce the grain boundary velocity, resulting in a sluggish grain growth process controlled by pore drag effects.

IV.1.5.3 - The Preexponential Factor K_0

The preexponential factor, K_0, can be determined from the intercept of log K_0, in Figure IV.19. The value of K_0 is (17 ± 3) and K_0 is 1.93×10^{17} $\mu m^4/h$. The values of the parameters for the kinetics of grain growth determined in this study are summarized in Table IV.1.1.

IV.1.5.4 - Grain Growth Kinetics for Cases that Start as a Discontinuous Grain Growth Process

The ZnO + 6 wt% Bi_2O_3 composition consolidated with the 0.11 μm ZnO powder presented a situation indicative of a discontinuous grain growth process in the initial stages of sintering. At the lower firing temperatures, 900 °C

Table IV.1.1 - Grain Growth Parameters for the 2.0μm ZnO + 6 wt% Bi_2O_3.

Slopes	(0.18 ±0.05) at 900°C
	(0.18 ±0.06) at 1030°C
	(0.27 ±0.10) at 1192°C
	(0.28 ±0.22) at 1400°C
Grain Growth Exponent (n-value)	(5.7 ±1.5) at 900°C
	(5.7 ±1.9) at 1030°C
	(3.7 ±1.4) at 1192°C
	(3.6 ±1.5) at 1400°C
Activation Energy	Q = (360 ±12) kJ/mol
Intersept	$\log K_0$ = (17 ±3)
Preexponential Factor	$K_0 = 1.93 \times 10^{17}\ \mu m^4/h$

and 1030 °C, these specimens have a distinct bimodal grain size distribution with a few very large grains surrounded by a matrix of numerous fine grains, as evidenced for example in Figure IV.8. At the higher firing temperatures, 1192 °C and 1400 °C, the large grains have consumed all of the matrix and have collided with each other as evidenced in Figures IV.9 and IV.16. It is assumed in this analysis that once the grains have collided the grain growth process presents the same mechanistic characteristics of a normal one and therefore can be analysed by the modified form of Equation (32):

$$\log (G^n - G_0^n)/(t-t_0) = \log K_0 - 0.434\ Q/RT \qquad (32')$$

As discussed previously, in this case the initial grain size G_0 can not be considered much smaller than the average grain size G, so that the factor G_0^n cannot be neglected.

To analyse the grain growth kinetics for this situation the left side of this equation was ploted versus (1/T) for different values of the grain growth exponent. Tentative n-values of three to six were tried. The best fit of the Arrhenius plot was obtained for an n-value of five. Figure IV.20 is that Arrhenius plot for the system 0.11 μm ZnO + 6 wt% Bi_2O_3. The activation energy determined from the slope of the line in this Arrhenius

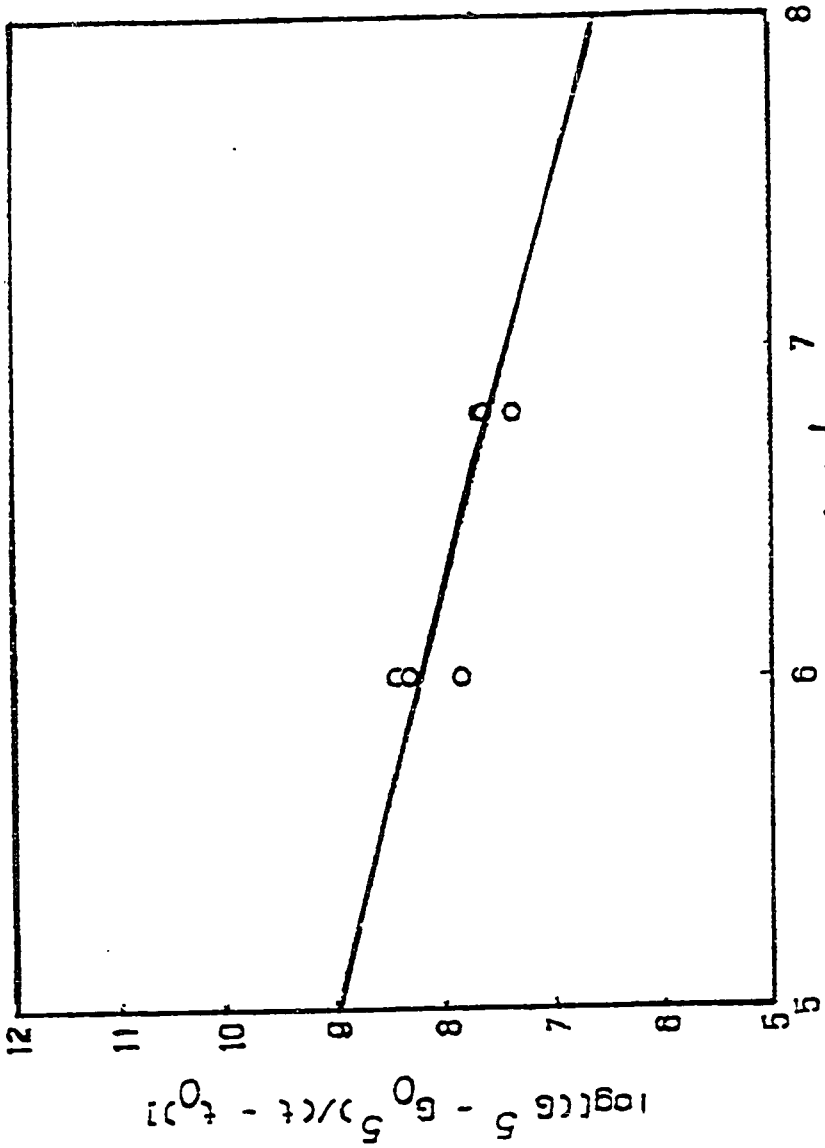

Figure IV.20 - Arrhenius Plot Log $[(G^5 - G_0^5) / (t - t_0)]$ versus 1/T for the 0.11 µm ZnO + 6 wt% Bi_2O_3

plot is Q = (154.5 ± 12.6) kJ/mol, the preexponential term was determined from the intersept of the line which is log K_0 = (13.02 ± 4.19), as $K_0 = 1.04 \times 10^{13}$ $\mu m^5/h$. These values are summarized in Table IV.1.2.

Table IV.1.2 indicates that the initial ZnO particle size affects the kinetics of grain growth in the ZnO + 6 wt% Bi_2O_3. For the cases that started as a discontinuous grain growth (0.11 μm ZnO), many pores are left behind by the highly mobile grain boundaries during the earlier stages of the grain growth process. This reduces the effect of the pore drag mechanism on the grain boundary motion and reduces the activation energy for grain growth. For the specimen consolidated with the larger initial particle size (2.0 mm), the grain growth process is normal and most of the pores are located at the grain boundaries or grain corners leading to very pronounced contribution of the pore drag mechanisms. This increases the activation energy for grain growth.

I.V.6 - Summary of the Effects of the Initial ZnO Particle Size

The study of the effects of the initial ZnO particle size on the final microstructure and on the ZnO grain growth kinetics revealed that for the solid state sintering of the two initial ZnO particle sizes (0.11 μm and 2.0 μm) the grain growth process is one of normal

Table IV.1.2 - Grain Growth Parameters for the ZnO + 6 wt% Bi_2O_3 Determined in This Study

ZnO Initial Particle Size	n	Q(kJ/mol)	log K_0	K_0
0.11μm ZnO	5	(154 ±12)	(13 ±4)	1.04×10^{13} $\mu m^5/h$
2.0 μm ZnO	4	(360 ±12)	(17 ±3)	1.93×10^{17} $\mu m^4/h$

grain growth. The normal grain growth process results in a final microstructure with uniform grain sizes and shapes. The smaller initial ZnO particle size resulted in a microstructure with larger grains. This was explained in terms of the Equation (44) which relates the rate of grain growth to the driving force for grain growth and to the grain boundary mobility. It shows that the system consolidated with the smaller initial particle sizes has a higher grain growth rate at all stages. At the earlier stages, the grain growth rate is higher due to a larger driving force and at the later stages because the grain boundaries have higher mobilities since they were able to detach themselves from many pores. It is suggested that a critical initial particle size exists, above which the driving force acting on the grain boundaries cannot exceed the force binding the pores to the boundaries and the effects of the initial particle size will be greatly reduced.

The presence of the Bi_2O_3 liquid phase promotes discontinuous grain growth when the initial ZnO particle size is small. Discontinuous grain growth results in a final microstructure with irregularly shaped grains with numerous pores located within the grains as well as at the grain boundaries. It was also observed that in the presence of the Bi_2O_3-rich liquid phase, increasing the initial ZnO particle size from 0.11 μm to 2.0 μm suppresses the tendency for discontinuous grain growth.

The onset of the discontinuous grain growth process seems to be satisfactorily explained through Equation (40) which relates the capillary forces to the particle sizes and surface energy. The attractive capillary force F_c, between two particles connected by a wetting liquid meniscus, is obtained by summing the pressure and surface energy contributions.

Clustering occurs in liquid phase sintering as a consequence of local melt formation. These clusters of wetted particles with closer packing and a higher volume fraction of solid have a higher rate of grain growth than the rest of the matrix and thus nucleate or originate the discontinuous grain growth process.

Equation (40) also satisfactorily explains the experimental observation that as the initial ZnO particle size increases the discontinuous grain growth process is suppressed. According to Equation (40) the capillary force F_c decreases as the radius of the solid particles increases and for sufficiently large initial powder particle sizes the capillary forces are not strong enough to create the clusters and the discontinuous grain growth process does not occur.

It was observed that for the solid state sintering as well as in the presence of the Bi_2O_3-rich liquid phase, that increasing the initial ZnO particle size from 0.11 μm to 2.0 μm results in a finer scale final microstructure,

and that additions of Bi_2O_3 enhance the grain growth. Study of the grain growth kinetics has revealed that for the specimens of ZnO + 6 wt% Bi_2O_3 consolidated with the 2.0 μm ZnO powder, the grain growth exponent, n, is four; that the activation energy is approximately 360 kJ/mol and that the preexponential factor, K_0, is 1.93×10^{17} $\mu m^4/h$. Grain growth exponents of four have been associated in the literature with pore controlled mechanisms. The high values of the kinetic parameters of grain growth, Q and log K_0, have been attributed in this thesis to a grain growth process controlled by pore drag mechanisms.

The grain growth kinetics for the composition ZnO + 6 wt% Bi_2O_3 which was consolidated with the 0.11 μm ZnO powder presented a discontinuous grain growth process in the initial stages. However the grain growth was analysed using Equation (32'), which does not neglect G_0^n. The grain growth kinetic exponent n was determined to be five, and the activation energy for grain growth, Q, was (154.5 ±12.6) kJ/mol. The preexponential factor was $K_0 = 1.04 \times 10^{13}$ $\mu m^5/h$. The lower values of the grain growth kinetic parameters, Q and log K_0, for the cases that started as a discontinuous grain growth are explained by the fact that many pores are left behind by the highly mobile grain boundaries at the earlier stages of the grain growth. It is concluded that the grain growth in the ZnO + Bi_2O_3 is controlled by pore drag mechanisms.

IV.2 - Effects of Nb_2O_5 Additions on the Grain Growth of ZnO

To study the effects of Nb_2O_5 additions on the microstructural development of ZnO, Nb_2O_5 was added at the 0.05 wt%, 0.10 wt%, 0.20 wt%, 0.40 wt%, and 0.80 wt% levels to the 0.11 μm ZnO + 6 wt% Bi_2O_3 composition. Figure IV.21 illustrates the effects of the Nb_2O_5 content on the density of specimens fired for one hour at the different firing temperatures. The density achieves a maximum at about 96 % of the theoretical density (5.74 g/cm^3) for firing at 900°C and then decreases as the firing temperature is increased through 1400°C.

There is some decrease in the fired density for the 0.10 wt% Nb_2O_5 composition, but as the Nb_2O_5 content is further increased, the density only gradually decreases at all firing temperatures. For example, at 900°C the density is 96% of the theoretical value for the 0.05 wt% Nb_2O_5 specimen, but only 92% of the theoretical value for the 0.80 wt% Nb_2O_5 specimen. At 1400°C the fired density decreases from 87% to only 75% of the theoretical value as the content of Nb_2O_5 is increased from 0.05 wt% to 0.80 wt%.

Figure IV.22 illustrates the weight loss as percent of $[(W_g-W_f)/W_g]$ versus the Nb_2O_5 content where W_g and W_f are the weights of the green and the fired specimens, respectively. The sharp increase for the weight loss at

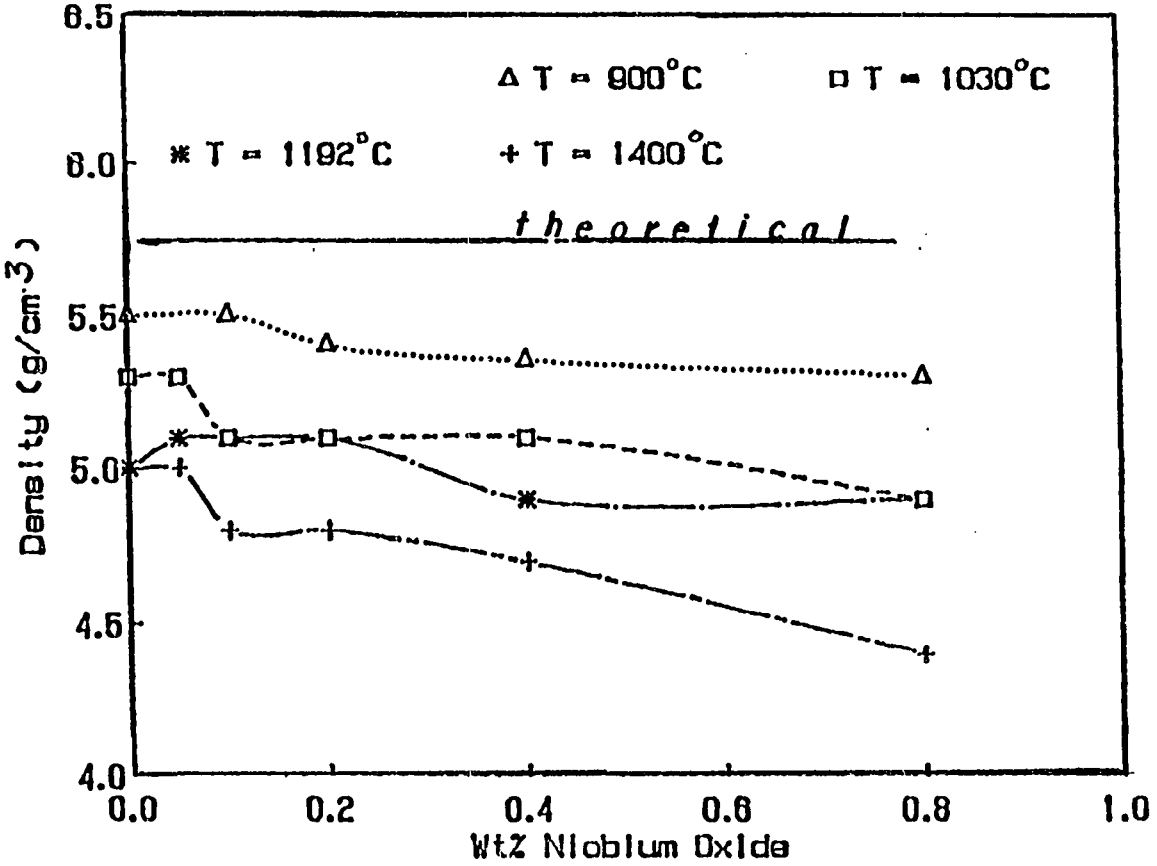

Figure IV.21 - Plots of Density versus wt% Nb_2O_5 for the 0.11 µm ZnO + 6 wt% Bi_2O_3 + Nb_2O_5 Firing Time - 1 Hour.

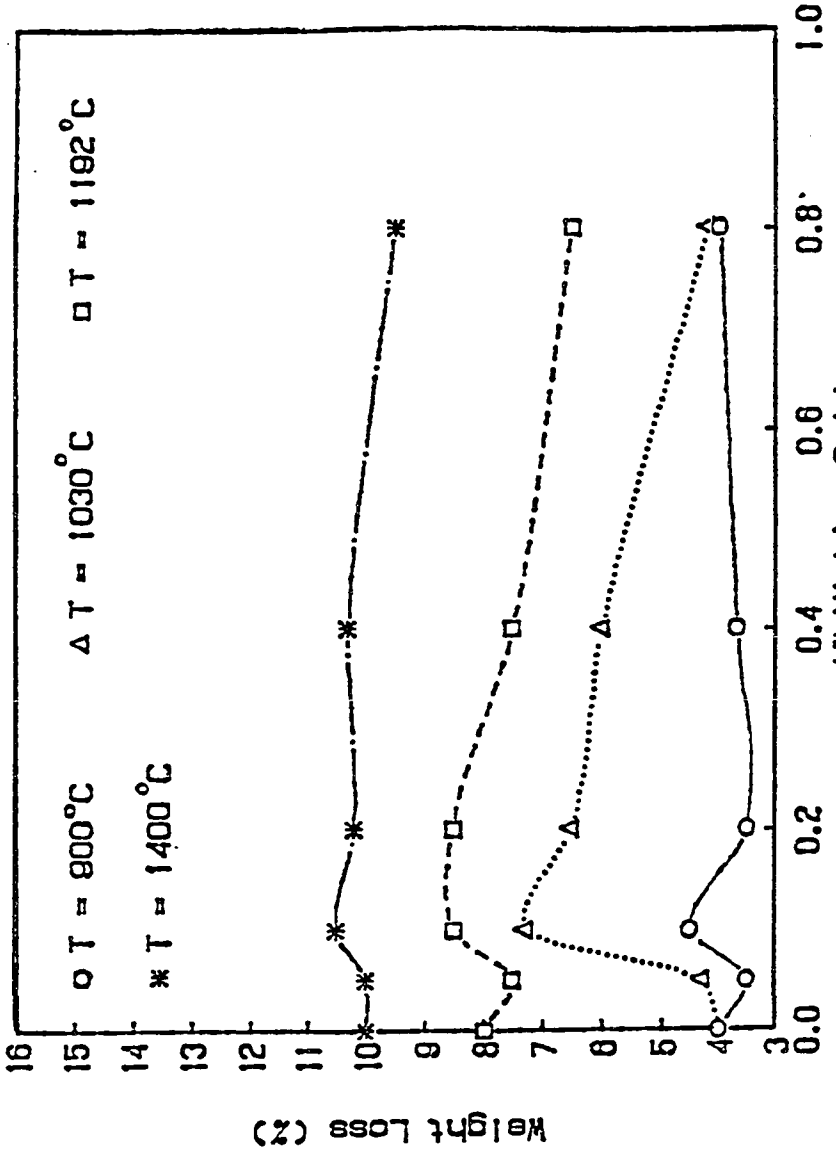

Figure IV.22 - Plots of the Weight Loss versus wt% Nb_2O_5 for the 0.11 µm ZnO + 6 wt% Bi_2O_3 + Nb_2O_5. Firing Time 1 Hour.

the 0.10 wt% Nb_2O_5 composition corresponds to the noted decrease in density for the same composition shown in Figure IV.21. It is well known that many ceramic materials lose weight during sintering, implying a significant vapor pressure of some of the constituents. An important side effect of vapor transport is that it may affect both the rate of particle coarsening and also that of densification.

IV.2.1 - Microstructural Evolution of the Nb_2O_5-Containing Specimens

Figures IV.23 (a to e) illustrate the effects of increasing additions of Nb_2O_5 on the microstructural development of a series of specimens fired at 900 °C for 2 h. Aggregates of large grains or individual large grains immersed in a matrix of very fine grains is a common characteristic of these microstructures. Another distinctive feature of this series of microstructural development is provided by Figure IV.23 (b). Even though the large grains have grown to consume most of the matrix, there remain some regions of finer matrix grains that have not yet been consumed by the discontinuous grain growth process.

Figure IV.23 (a) for the specimen containing 0.05 wt% Nb_2O_5 illustrates the initial stages of the discontinuous grain growth process for this series of Nb_2O_5 containing

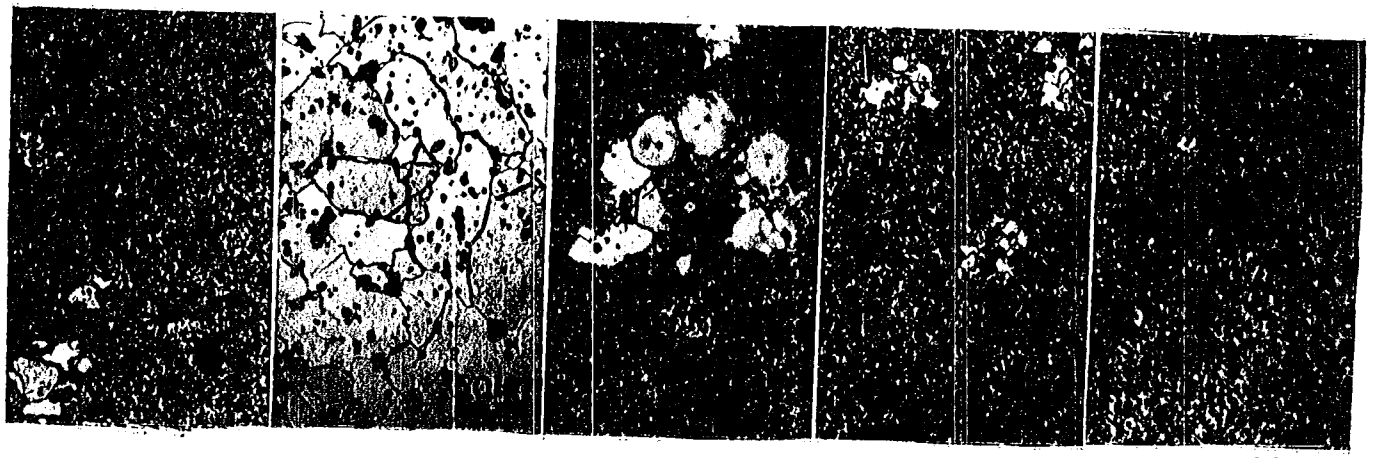

IV.23-(a)	IV.23-(b)	IV.23-(c)	IV.23-(d)	IV.23-(e)
X=0.05	X=0.10	X=0.20	X=0.40	X=0.80
	G=(37±2)μm			

Figure IV.23 (a to e) - Optical Micrograph of the ZnO + 6 wt% Bi_2O_3 + X wt% Nb_2O_5. Fired at 900°C for 2 Hours. Initial ZnO Particle Size 0.11 μm. Magnification 200 X.

specimens. A few individual large grains, or aggregates of several large grains have nucleated within the matrix of very fine grains. As the level of Nb_2O_5 addition is increased to 0.10 wt%, the discontinuous grain growth process is substantially enhanced, resulting in a microstructure that formed by the large-grain-containing aggregates rapidly growing to consume most of the fine grain size matrix and eventually contacting one another. Also evident in Figure IV.23 (b) is the presence of the Bi_2O_3-rich, previously-liquid phase at many multiple grain junctions and also along some of the grain boundaries.

Figure IV.23 (c) depicting the specimen containing 0.20 wt% Nb_2O_5, shows a microstructure that is similar to that of the specimen containing only 0.05 wt% Nb_2O_5. It exhibits only a few individual large grains and agglomerates growing into a fine grain size matrix. These aggregates appear to be somewhat larger for the specimen containing 0.20 wt% Nb_2O_5. Although discontinuous grain growth was enhanced at the 0.10 wt% Nb_2O_5 level, as the Nb_2O_5 content is further increased to 0.20 wt%, the discontinuous grain growth rate appears to be considerably reduced. Figure IV.23 (d) illustrates the microstructure for the specimen containing 0.40 wt% Nb_2O_5 and Figure IV.23 (e) that of the 0.80 wt% Nb_2O_5 specimen. These two microstructures confirm that the higher level additions of Nb_2O_5 severely inhibit the grain growth of ZnO.

As the Nb_2O_5 is added to the ZnO + 6 wt% Bi_2O_3 and fired at 900 °C for 2 hours, it is observed that the grain growth process experiences a discontinuous to normal transition. Increasing the Nb_2O_5 content suppresses the discontinuous grain growth process. However, a distinctive behavior is observed when the composition is changed from 0.05 wt% to 0.10 wt% Nb_2O_5. The grain growth rate is dramatically enhanced and the fine grain size matrix is almost totally consumed.

Figures IV.24 (a to e) illustrate the effects of Nb_2O_5 additions for those specimens fired at 1030 °C for 2 hours. These ZnO grain sizes are much larger than for the same compositions fired at 900 °C. Figure IV.24 (a), which is for the specimen containing just 0.05 wt%, Nb_2O_5 reveals that some of the ZnO grains have grown to very large sizes, nearly 50 μm. Most of the fine grain size matrix has been consumed. It is interesting to note that portions of the grain boundaries of some of the larger grains are pinned by pores at several points. However, at the same time, there are numerous pores within the grains, which indicates that many pores are not able to either pin or move along with the migrating grain boundaries. This suggests that these grain boundaries have sufficiently high mobilities to be able to break away from many of the pores which they encounter during growth.

Figure IV.24 (b) is of the 0.10 wt% Nb_2O_5 specimen,

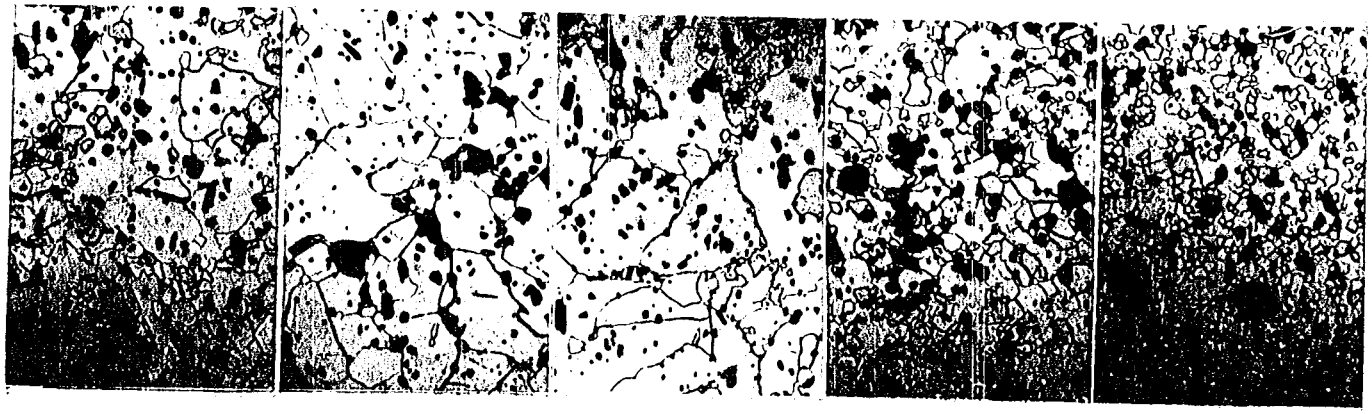

IV.24-(a)	IV.24-(b)	IV.24-(c)	IV.24-(d)	IV.24-(e)
X=0.05	X=0.10	X=0.20	X=0.40	X=0.80
G=(44±3)μm	G=(36±2)μm	G=(40±2)μm	G=(23±2)μm	G=(9±3)μm

Figure IV.24 (a to e) - Optical Micrograph of the

ZnO + 6 wt% Bi_2O_3 + X wt% Nb_2O_5

Fired at 1030°C for 2 Hours. Initial Particle Size 0.11 μm.

Magnification 200 X

with an average grain size of (36 ± 2) μm. Figure IV.24 (c) is of the specimen containing 0.20 wt% Nb_2O_5, with an average grain size of (40 ± 2) μm. The microstructures depicted by the initial three plates of low Nb_2O_5 contents are very similar. All reveal a structure dominated by large grains, but with a small content of fine matrix grains of an average grain size of only about (6 ± 2) μm remaining. The Bi_2O_3-rich phase is evident at some individual grain boundaries and multiple grain junctions.

Figure IV.24 (d) is for the specimen containing 0.40 wt% Nb_2O_5. The interesting feature of this microstructure is that even though a number of larger individual grains are present, a generally much finer microstructure results than for the three lower Nb_2O_5 content compositions fired under the same conditions. The average grain size, (23 ± 2) μm is only about one half of the average grain size of the previous three specimens. This indicates that even though the ZnO grain growth process may still be a partially discontinuous one at the 0.40 wt% Nb_2O_5 level, grain growth is becoming increasingly more inhibited by the Nb_2O_5 additions. The presence of the Bi_2O_3-rich phase at the grain boundaries is also apparent in this micrograph.

Figure IV.24 (e) is of the composition containing the 0.80 wt% Nb_2O_5 addition. The average ZnO grain size for this composition is considerably finer than the others,

less than 10 μm. The ZnO grains generally appear to be very regular in shape with a narrow grain size distribution. These two characteristcs are usually associated with a normal grain growth process. It is evident that there exists a transition from discontinuous to normal ZnO grain growth with increasing Nb_2O_5 additions in this system.

The same effects of the Nb_2O_5 additions which were observed for firing at 900 °C were also present for the firing temperature 1030 °C, i.e., discontinuous grain growth is enhanced when the levels of the Nb_2O_5 additions are low, 0.10 wt% and 0.20 wt%. Increasing the Nb_2O_5 level to 0.40 wt% appears to inhibit some of the ZnO grain growth, while at the 0.80 wt% Nb_2O_5 level the ZnO grain growth is substantially reduced and appears to be completely normal.

For the specimens sintered at 1192 °C for 2 hours, the effects of the Nb_2O_5 additions on the microstructures are shown in Figures IV.25 (a to e). Figure IV.25 (a) illustrates the specimen containing only 0.05 wt% Nb_2O_5. The average grain size is large (30 ± 3)μm. Figure IV.25 (b) depicts the specimen containing 0.10 wt% Nb_2O_5 and the average grain size is even larger (46 ± 2)μm. Figure IV.25 (c) represents the microstructure of the 0.20 wt% Nb_2O_5 specimens which has an average grain size of (43 ± 2)μm. The specimen with 0.40 wt% Nb_2O_5 in Figure IV.25

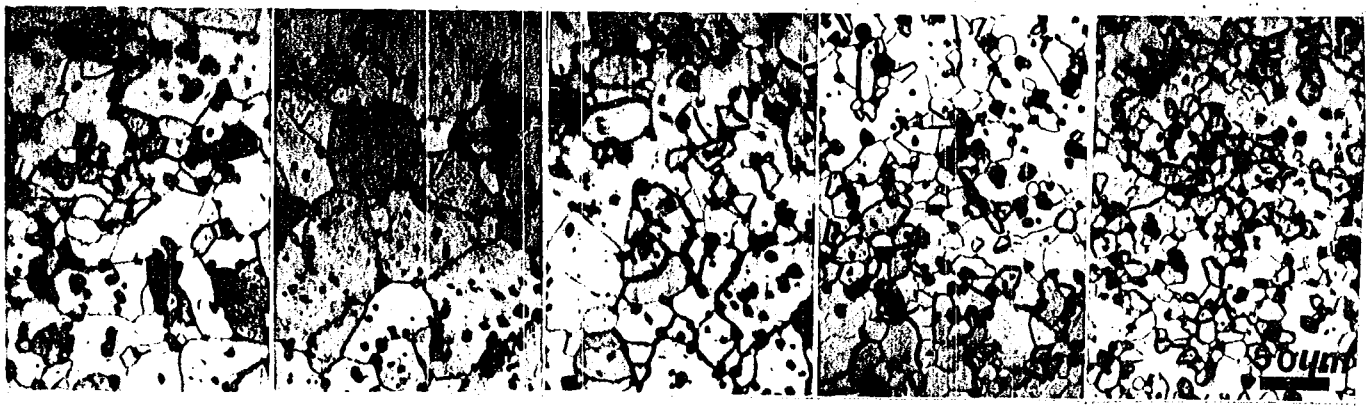

IV.25-(a)	IV.25-(b)	IV.25-(c)	IV.25-(d)	IV.25-(e)
X=0.05	X=0.10	X=0.20	X=0.40	X=0.80
G=(30±3)µm	G=(46±2)µm	G=(43±2)µm	G=(26±2)µm	G=(13±5)µm

Figure IV.25 (a to e) - Optical Micrograph of the

$ZnO + 6$ wt% $Bi_2O_3 + X$ wt% Nb_2O_5

Fired at 1192°C for 2 Hours. Initial Particle Size 0.11 µm.

Magnification 200 X

(d), however, has a finer average grain size, only (28 ± 2)μm. Figure IV.25 (e) illustrates the 0.80 wt% Nb_2O_5 composition which has a much finer grain size, only (13 ± 5) μm, and grains that are very regular in size and shape. The same Nb_2O_5 addition effects that were observed at the lower firing temperatures are again prevalent at 1192 °C, i.e., the ZnO grain growth is enhanced at the lower levels of Nb_2O_5, 0.10 wt% and 0.20 wt%, and then inhibited at higher Nb_2O_5 additions. At the 0.80 wt% Nb_2O_5 level the grain growth process appears to be a normal one.

Figures IV.26 (a to e) illustrate the microstructures of the specimens fired at 1400 °C for 2 hours. Figure IV.26 (a) is for the 0.05 wt% Nb_2O_5 specimen, and has an average grain size of (50 ± 3)μm. Many large pores are located within the grains as well as at the grain boundaries and the multi-grain junctions. Some of these pores may have been created by the vaporization of some of the Bi_2O_3. Figure IV.26 (b) is for the specimen containing 0.10 wt% Nb_2O_5. The average grain size is similar to the previous one, (47 ± 2)μm. Some of the grains have a distinct elongated shape, indicative of previous discontinuous grain growth.

Figure IV.26 (c) is for the 0.20 wt% Nb_2O_5 sample. Its average grain size is (44 ± 2)μm. This microstructure is very similar to the two lower Nb_2O_5 compositions, with some elongated grains and with many

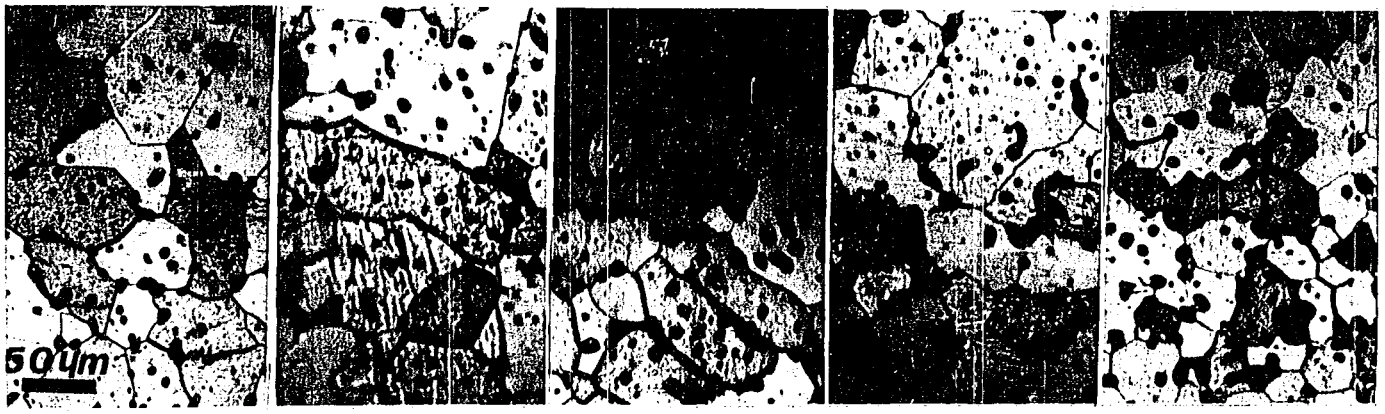

IV.26-(a)	IV.26-(b)	IV.26-(c)	IV.26-(d)	IV.26-(e)
X=0.05	X=0.10	X=0.20	X=0.40	X=0.80
G=(46±3)µm	G=(47±2)µm	G=(44±2)µm	G=(52±2)µm	G=(34±3)µm

Figure IV.26 (a to e) - Optical Micrograph of the

ZnO + 6 wt% Bi_2O_3 + X wt% Nb_2O_5

Fired at 1400°C for 2 Hours. Initial Particle Size 0.11 µm.

Magnification 200 X

pores that are located within the grains, as well as at the grain boundaries and at the grain junctions. Figure IV.26 (d) is of the specimen containing 0.40 wt% Nb_2O_5. At this composition the average grain size is (52 ± 2)μm, much larger than the average grain size for the three specimens with less Nb_2O_5. This microstructure is similar to the previous ones for the specimens fired at 1400 °C, although it appears to contain fewer elongated grains.

Figure IV.26 (e) illustrates the microstructure of the specimen containing 0.80 wt% Nb_2O_5. The average grain size is only (34 ± 3)μm. The grains are also much more uniform in size and shape. It is interesting to note that for firing at 1400 °C, all of these microstructures have very similar grain sizes except for the 0.80 wt% Nb_2O_5. This suggests that a limiting grain size of approximately 50 μm may exist for these systems. The reasons for the existence of this limiting grain size may be one or more of the following. One is the mechanism proposed by Zener [44] for grain growth in the presence of second phase inclusions, the second is the general reduction of the driving force, for as the grains grow the grain curvature and the total surface area are reduced, and the third is the mechanism proposed by Hillert [17] which relates to the topological constraints that the large grains exert on one another.

From the microstructures presented for the four

firing temperatures, it is evident that the ZnO grain growth process in the ZnO + 6 wt% Bi_2O_3 + Nb_2O_5 system is a discontinuous one at the lower levels of Nb_2O_5 additions, and then as the Nb_2O_5 level is increased, the process of discontinuous grain growth is gradually inhibited until at the 0.80 wt% Nb_2O_5 level the grain growth appears to be completely normal.

Figure IV.27 illustrates the average grain size versus the Nb_2O_5 content for the specimens sintered at 1192 °C for times varying from 0.5 h to 4 h. The tables in the Appendices summarize the experimental data for the values of the average grain sizes as a function of sintering times and temperatures. Figure IV.27 reveals that, at 1192 °C for all of the firing times, the additions of Nb_2O_5 have an initial effect of inhibiting the grain growth of ZnO. For example, the addition of only 0.05 wt% Nb_2O_5 is sufficient to reduce the average grain size from 39 μm to 27 μm. However, as the level of Nb_2O_5 is further increased to 0.10 wt% the average ZnO grain size also increases to a maximum. For higher level additions of Nb_2O_5, the average grain size consistently decreases.

Asokan et al [5] have reported the effects of Nb_2O_5 additions to the 0.50 wt% level in Bi_2O_3-free specimens consisting of ZnO + Nb_2O_5 fired at temperatures from 900 °C to 1300 °C for 2 h. They have reported for a sintering

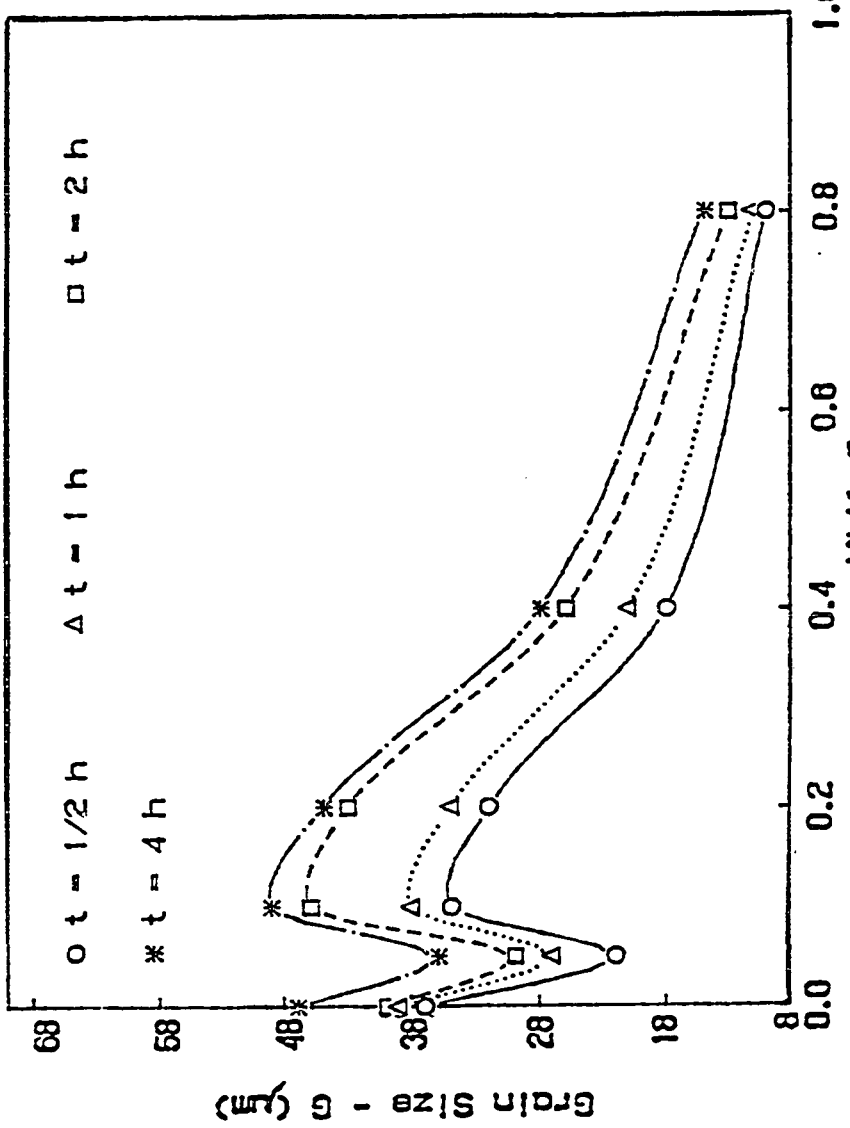

Figure IV.27 - Plots of Average Grain Size versus wt% Nb_2O_5 for the 0.11 μm ZnO + 6 wt% Bi_2O_3 + Nb_2O_5. Firing Temperature - T=1192°C.

temperature of 1100 °C that the average grain size achieved a maximum when the level of Nb_2O_5 was 0.20 wt%. These studies by Asokan et al [5] substantiate that a maximum of the average ZnO grain size is achieved during solid state sintering of ZnO at 1100 °C for samples containing about 0.20 wt% Nb_2O_5. In this study, in the presence of the Bi_2O_3-rich liquid phase, it is observed for sintering at 1192 °C that a maximum of the average grain size is attained at about 0.10 wt% Nb_2O_5. A ZnO grain size maximum occurs for Nb_2O_5 additions, independent of the presence or the absence of a Bi_2O_3-rich liquid phase.

The importance of these observations to commercial ZnO varistor ceramics, as Asokan et al [5] have pointed out, is that the nonlinearity coefficient alpha (α), also achieves a maximum value for additions of 0.20 wt% Nb_2O_5 at 1100 °C. Asokan et al [5] have observed that alpha (α) follows the same trend as the ZnO grain size for Nb_2O_5 additions.

The effect of Nb_2O_5 content on the average grain size after firing at 1400 °C is depicted in Figure IV.28. The average grain size is plotted versus the Nb_2O_5 content for specimens sintered for times varying from 0.5 h to 4 h. Similar to sintering at 1192 °C, these average grain sizes also vary with composition. There also occurs a maximum in the average grain size at an intermediate Nb_2O_5

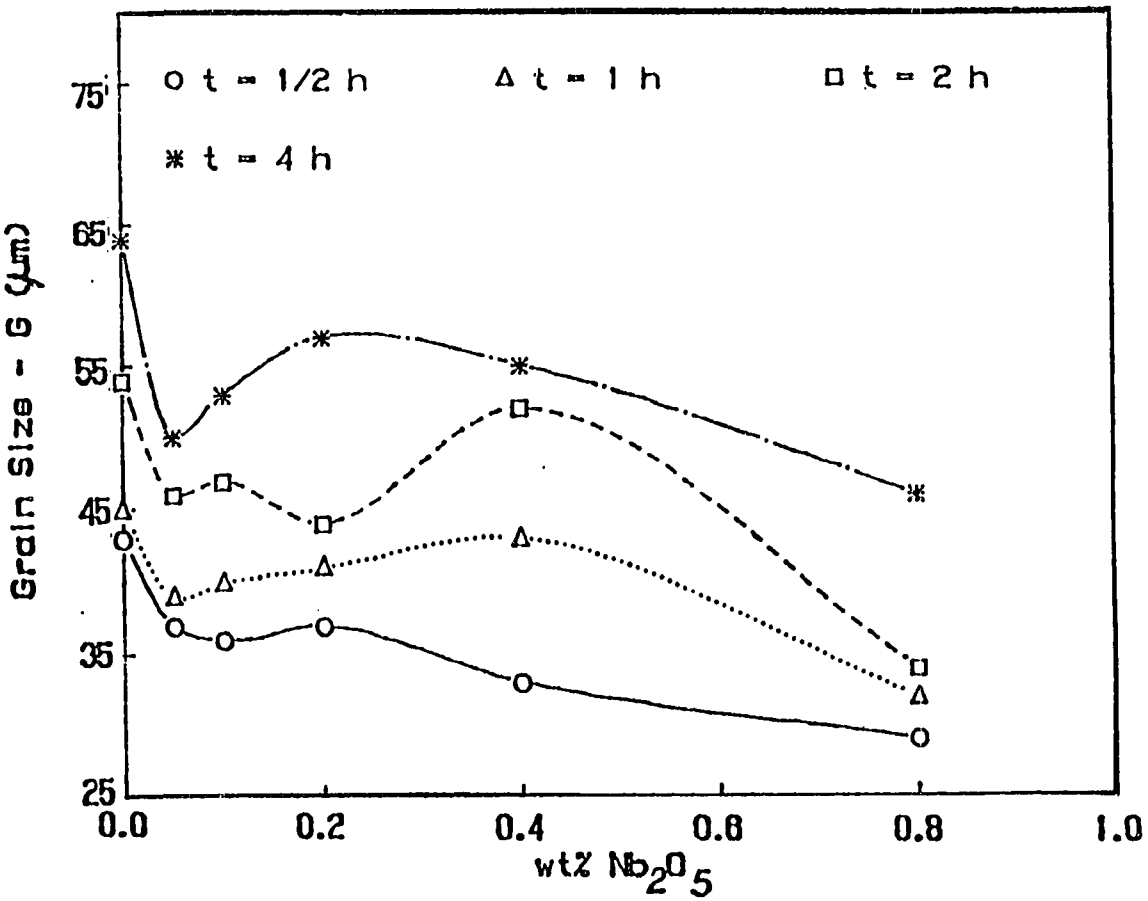

Figure IV.28 - Plots of Average Grain Size versus wt% Nb_2O_5 for the 0.11 μm ZnO + 6 wt% Bi_2O_3 + Nb_2O_5. Firing Temperature - T=1400°C.

content.

Unfortunately, for the lower firing temperatures of 900 °C and 1030 °C, many of the lower-Nb_2O_5-content microstructures possessed a distinct bimodal grain size distribution with large grains existing in aggregates dispersed within a very fine grain size matrix. This was a consequence of the discontinous grain growth process. Therefore, similar curves of the average grain size versus the Nb_2O_5 content could not constructed for the two lower firing temperatures.

The system studied by Asokan et al [5] was the simple binary solid state system consisting only of ZnO + Nb_2O_5, without any Bi_2O_3. However, the system in this study was a ternary one consisting of ZnO + 6 wt% Bi_2O_3 + Nb_2O_5, in which the Bi_2O_3 forms a liquid phase during sintering. The fact that a maximum in the average grain size exists for the intermidiate Nb_2O_5 levels whether during solid state sintering or for firing in the presence of the Bi_2O_3-rich liquid phase indicates that the existence of the grain size maximum is a consequence of an effect of the Nb_2O_5 on the ZnO. The grain size maximum with Nb_2O_5 additions does not specifically depend on the presence of the Bi_2O_3-rich liquid phase.

When Nb_2O_5 is added to ZnO during processing, a number of different processes occur, including:

a) - The Nb^{5+} ions segregate to the grain boundaries.

b) - The Nb_2O_5 creates a solid solution in the ZnO lattice as previously presented in Equation [37]. For charge balance two Nb^{5+} ions must replace five Zn^{2+} ions, leaving three vacant Zn^{2+} lattice sites.

It is well known that the presence of other oxides introduces crystalline defects into the structure of ZnO. Chiang and Kingery [74] have considered the grain boundary mobility as a function of the stoichiometry and have suggested that lattice defects which readily accomodate the stoichiometry might be the rate controlling species. For that situation the grain boundary mobilities might be expected to change with the lattice defect concentration.

c) - At higher levels, the Nb_2O_5 and ZnO react to form the defect spinel phase, $Zn_3Nb_2O_8$. This has been established to occur as the diffraction patterns of the 0.80 wt% Nb_2O_5 in Figure IV.29 clearly reveal the presence of this spinel phase.

This study of the effect of Nb_2O_5 additions to the ZnO + 6 wt% Bi_2O_3 system reveals that at the higher sintering temperatures, 1192 °C and 1400 °C, the average ZnO grain size varies in a consistent manner with the Nb_2O_5 content. That variation is described by the general

diagram represented in Figure IV.30. For purposes of discussion and analysis this schematic diagram can be separated into three different regions. These regions may be described as follows:

i) Region I - At low Nb_2O_5 contents, less than about 0.05 wt% Nb_2O_5, grain growth inhibition occurs. As the Nb_2O_5 addition level is increased in this region the average ZnO grain size decreases.

ii) Region II - At intermediate Nb_2O_5 additions, between about 0.10 wt% and 0.20 wt Nb_2O_5, distinct ZnO grain growth enhancement occurs. As the Nb_2O_5 content is increased in this region the resulting ZnO grain size also increases.

iii) Region III - At Nb_2O_5 additions of 0.20 wt% and higher, the Nb_2O_5 effect is a distinct one of ZnO grain growth inhibition. For every set of firing conditions the 0.80 wt% Nb_2O_5 specimens had the finest grain sizes.

The grain growth inhibition that is observed in Region I may be attributed to solute segregation of the Nb^{5+} cations at the grain boundaries. This also has been suggested by Gupta [71] for the case of ZnO grain growth inhibition for small additions of K_2O and also by Johnson and Stein [82] for the case of minute additions of CaO to

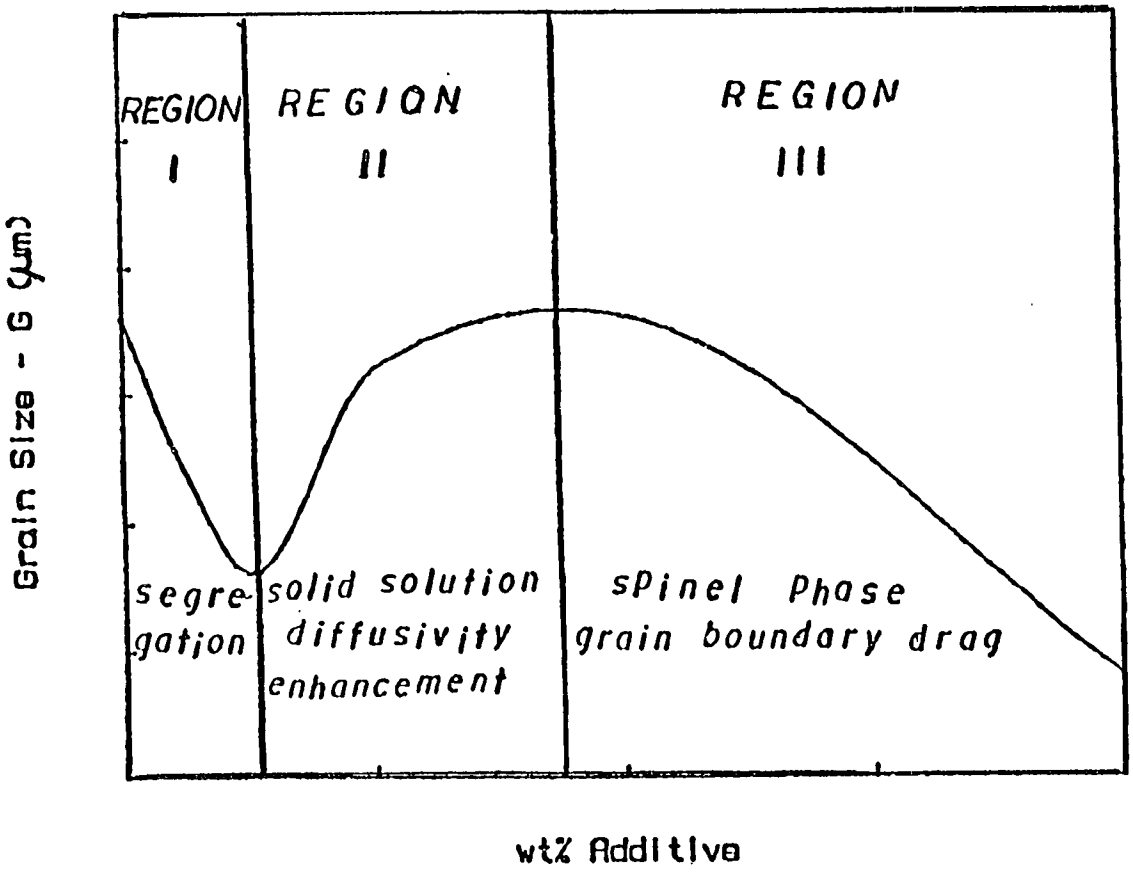

Figure IV.30 - General Curve for the Plot of the Average Grain Size versus wt% Nb_2O_5 for ZnO + 6 wt% Bi_2O_3 + Nb_2O_5

Al_2O_3. As pointed out by Johnson and Stein [82] the size misfit of the Ca^{2+} ions in the Al_2O_3 lattice is large and it is reasonable to assume that the elastic strain energy is an important contribution to segregation. Some segregation might be expected to occur when a solute fits poorly in the lattice, either elastically or electronically. The radius of the Zn^{2+} ion is 0.74 A° and the radius of the Nb^{5+} ion is 0.69 A°, which is an ionic size ratio of only 7%. This indicates that the elastic misfit of the Nb^{5+} ions in the ZnO lattice is not very large and therefore the solid solution of Nb_2O_5 into ZnO may be favored, at least from size considerations on the elastic strain energy alone. However, from a charge perspective, the Nb^{5+} ions fit very poorly into the ZnO lattice, since every Nb^{5+} ion that replaces a Zn^{2+} and enters the lattice requires the formation of three cation vacancies. Therefore, segregation of the Nb^{5+} ions to the ZnO grain boundaries is expected to occur.

Substantial grain growth enhancement occurs in Region II. This may be related to an increased rate of diffusion of Zn^{2+} in the ZnO lattice caused by the formation of the solid solution of Nb_2O_5 in ZnO. Some solid solution of Nb_2O_5 in ZnO must occur even though the ZnO-Nb_2O_5 phase diagram shown in Figure II.4.3 does not indicate the presence of an extensive solid solution. Diffusion of the Zn^{2+} in the ZnO lattice, has been reported by previous

authors [56,57] to be the rate controlling mechanism of ZnO grain growth. Therefore, any mechanism that enhances the diffusivity of the Zn^{2+} ions in the ZnO lattice may be expected to cause an increase in the rate of grain growth.

The diffusion coefficient of Zn^{2+} in ZnO is directly proportional to the Zn^{2+} atomic (ionic) mobility as expressed by Equation (11). The mobility and consequently the diffusion coefficient of the Zn^{2+} in ZnO will increase if the concentration of the Zn^{2+} cation lattice site vacancies is increased, because there are more available sites for atomic or ionic transfer. The formation of the Nb_2O_5-ZnO solid solution substantially increases the concentration of cation lattice site vacancies, therefore the Zn^{2+} diffusion coefficient is expected to similarly increase. It is believed that this results in the enhancement of the grain growth observed in Region II.

The reduction of pore drag effects is another important factor that contributes to the enhancement of grain growth in Region II. The grain boundaries have very high mobilities due to the increase of vacancy concentration and many pores are left behind in the earlier stages of grain growth. This reduces the number of pores at the grain boundaries and the effects of pore drag mechanisms and contributes to enhance the grain growth.

Additions of Nb_2O_5 to the ZnO-Bi_2O_3 system may also

inhibit the ZnO grain growth by a second phase drag mechanism. The ZnO-Nb_2O_5 phase diagram shown in Figure II.4.3 indicates that for the temperatures under consideration in this study, compositions are in a two phase field consisting of ZnO and the spinel phase, $Zn_3Nb_2O_8$. The presence of this spinel phase has been confirmed by x-ray diffraction. Figure IV.29 shows the x-ray diffraction patterns for the ZnO + 6 wt% Bi_2O_3 + 0.80 wt% Nb_2O_5 composition sintered at 1400 °C for 2 h. Positions of the peaks corresponding to the $Zn_3Nb_2O_8$ spinel phase are indicated. Some of the more intense diffraction peaks of the spinel phase are not distinguishable because they coincide with either strong ZnO or strong Bi_2O_3 peaks. However, the $Zn_3Nb_2O_8$ spinel phase is still readily identified. The grain growth inhibition observed in Region III is probably a result of the second phase-particle drag mechanism, where spinel particles which are located on the grain boundaries increase the energy necessary for grain boundary migration and thus inhibit grain growth.

The effectiveness of the second phase spinel particles in inhibiting the ZnO grain growth is a function of their size and volume fraction, as described by Equation (34) [44]. It is evident that the grain growth inhibition mechanism is more efficient when the second phase particles are small and their volume fraction is

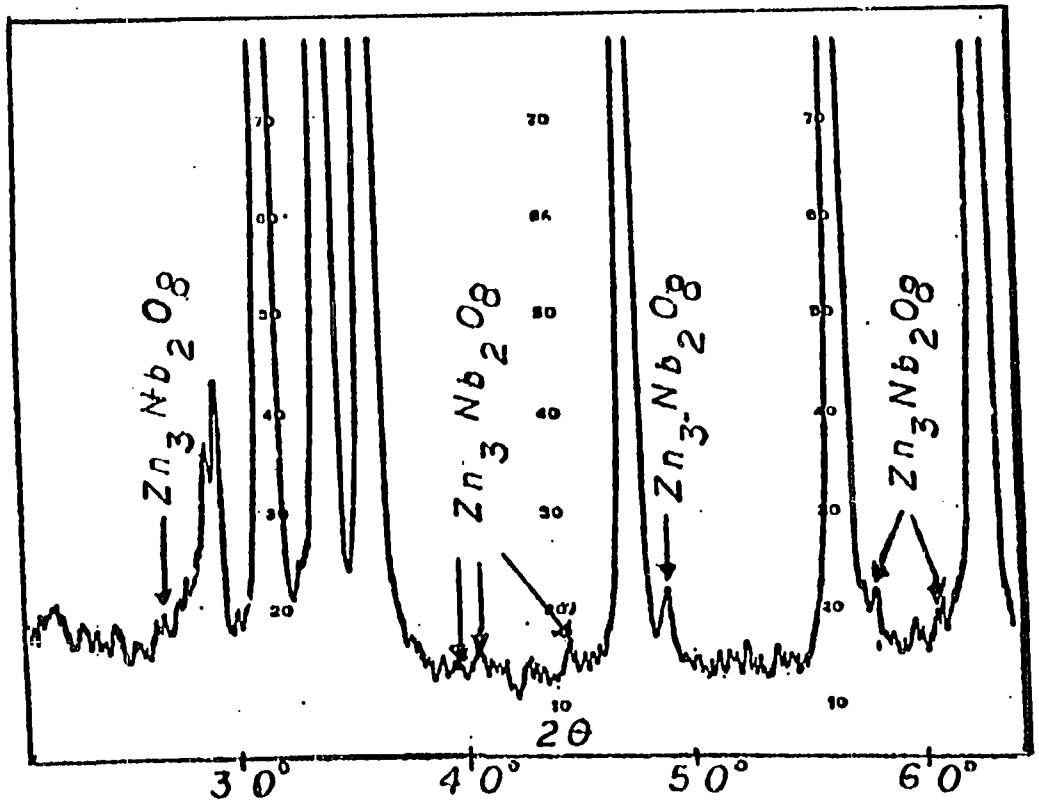

Figure IV.29 - Peaks Corresponding to the Spinel Phase $Zn_3Nb_2O_8$ on the X-ray Diffraction Pattern of the 0.11 μm ZnO + 6 wt% Bi_2O_3 + 0.80 wt% Nb_2O_5 Fired at 1400°C for 2 Hours

high. Therefore, as the volume fraction of the spinel phase is increased by increasing the Nb_2O_5 content of the system, the second phase-drag mechanism becomes more effective and prevails over the effect of the enhancement of the diffusivity by vacancy formation. The overall result is one of grain growth inhibition in Region III of Figure IV.30.

Therefore, the general behavior represented by Figure IV.30, which describes the effect of Nb_2O_5 additions on the ZnO grain growth, results from three different mechanisms. Dominant in Region I is grain growth inhibition due to solute segregation at the grain boundaries. Prevalent in Region II is grain growth enhancement by solid solution formation, creating lattice vacancies and enhancing Zn^{2+} diffusion. Finally a mechanism of grain growth inhibition due to spinel formation and a drag effect on the grain boundaries is rate controlling in Region III.

IV.2.2 - The Grain Growth Kinetics

Because the ZnO + 6 wt% Bi_2O_3 specimens with Nb_2O_5 additions often experienced discontinuous grain growth of the ZnO when the levels of Nb_2O_5 were 0.40 wt% or less, it was not possible to directly analyse those results by application of the phenomenological kinetic expression for grain growth. For the 0.80 wt% Nb_2O_5 specimens, however,

discontinuous grain growth was not observed and the grain growth exhibited the usual characteristics of a normal grain growth process.

IV.2.2.1 - The Grain Growth Exponent (n-value)

The grain growth of the ternary ZnO + 6 wt% Bi_2O_3 + 0.80 wt% Nb_2O_5 composition is represented in Figure IV.31 in the form of a log (grain size) versus log (time) plot. The slopes of the four lines are (0.20 ± 0.18) at 900 °C, (0.21 ± 0.07) at 1030 °C, (0.21 ± 0.06) at 1192 °C, and (0.23 ± 0.17) at 1400 °C. The kinetic exponents are determined from the inverse of these slopes, yielding (5.00 ± 1.60) at 900 °C, (4.72 ± 1.01) at 1030 °C, (4.85 ± 1.31) at 1192 °C and (4.27 ± 1.32) at 1400 °C. These suggest that a grain growth exponent of five is appropriate in this system.

Grain growth exponents equal to three for "pure" ZnO have been reported by Gupta and Coble [56], Dutta and Spriggs [59], Readey et al [7] and Senda and Bradt [57]. An increase of the grain growth exponent from three to five or more for ZnO with oxide additives has been reported by several authors who have studied the effects of different additives including Bi_2O_3 [57], Sb_2O_3 [3,70], and K_2O [71]. As higher grain growth exponents are indicative of a slower grain growth rate, this means that the grain boundary motion is being slowed in the presence

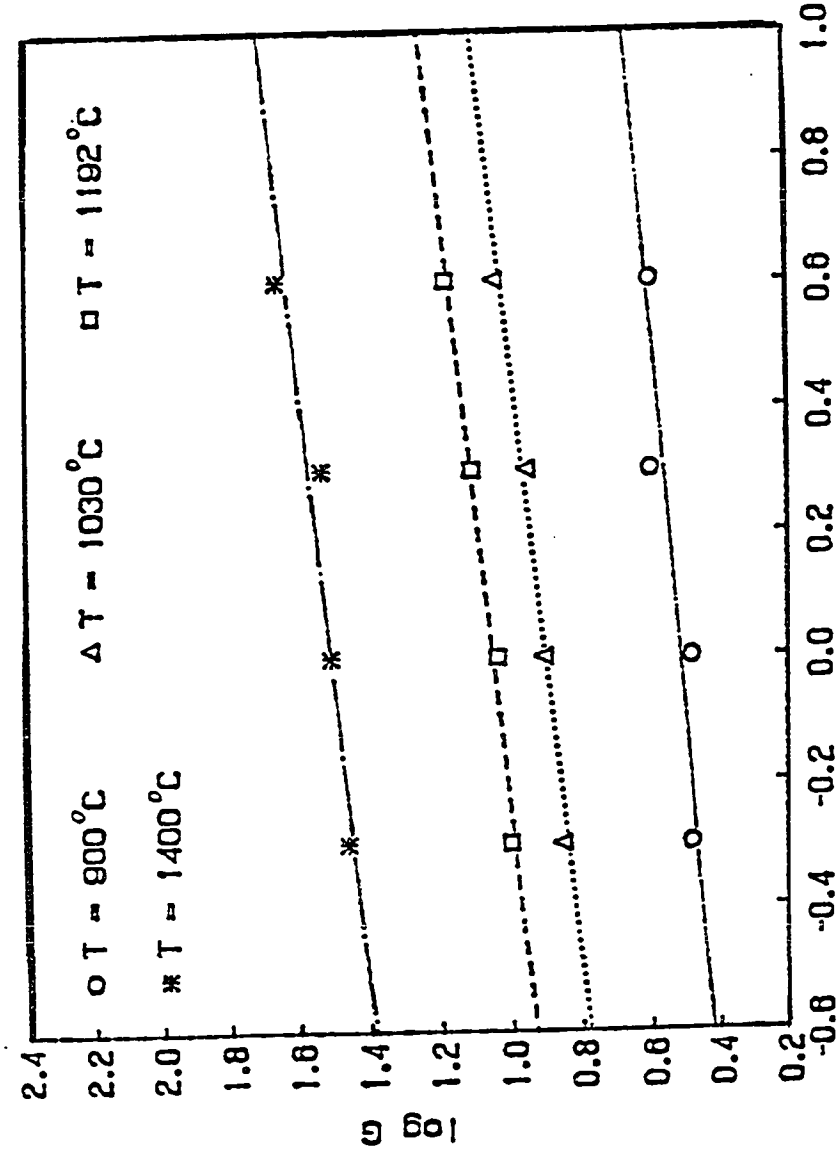

Figure IV.31 - Plots of Log (Grain Size) versus Log (Time) for the 0.11 µm ZnO + 6 wt% Bi_2O_3 + 0.80 wt% Nb_2O_5

of additives when an increase of n-value occurs.

Among the various mechanisms that can inhibit the migration of grain boundaries and are of relevance for these specimens (ZnO + 6 wt% $Bi2O_3$ + 0.80 wt% $Nb2O_5$) are:

a) - solute segregation at the grain boundaries,
b) - pore drag mechanisms, and
c) - second phase particle drag mechanims.

Impurities or additive atoms may segregate to a surface if they lower the free energy. Such segregation is a function of several variables. The relative magnitude of this segregation varies with the inverse of the solid solubility, and the equilibrium segregation increases with decreasing temperature. This segregation may have a large effect on grain growth during liquid phase sintering. One very important effect of the segregation of additive atoms to the grain boundaries is grain growth inhibition.

The pore drag mechanism proposed by Nichols [77] is certainly of relevance to these Nb_2O_5-containing ZnO microstructures. Nearly all these microstructures contain porosity at the grain boundaries, as well as some entrapment of pores within the grains. In the earlier stages of sintering, pores are usually left behind and the entrapment of pores within the grains is commonly observed

during discontinuous grain growth. In the later stages of sintering, however, it is more common for pores to be dragged along with the migrating grain boundaries. The motion of the pores can be accomplished by several different mechanisms [77], any of which can control the grain boundary motion. The effects of each of these controlling mechanisms on the rate exponent, the n-value, are reported in the literature and are summarized in Table (II.2.2). Values for the grain growth exponent from two to five have been suggested.

The second phase particle drag mechanism is of primary importance in this case because of the formation of the spinel phase, $Zn_3Nb_2O_8$. This second phase spinel can reduce the grain boundary motion and inhibit grain growth as has been reported by previous authors [3,70]. The effectiveness of the second phase particles on the grain growth inhibition [44] depends on the size and the volume fraction of the second phase particles according to Equation (34).

IV.2.2.2 - The Activation Energy

The activation energy for grain growth, similar to the grain growth exponent, could only be estimated for those specimens containing 0.80 wt% Nb_2O_5. The Arrhenius plot was constructed using a n-value of five and is presented in Figure IV.32. The activation energy derived

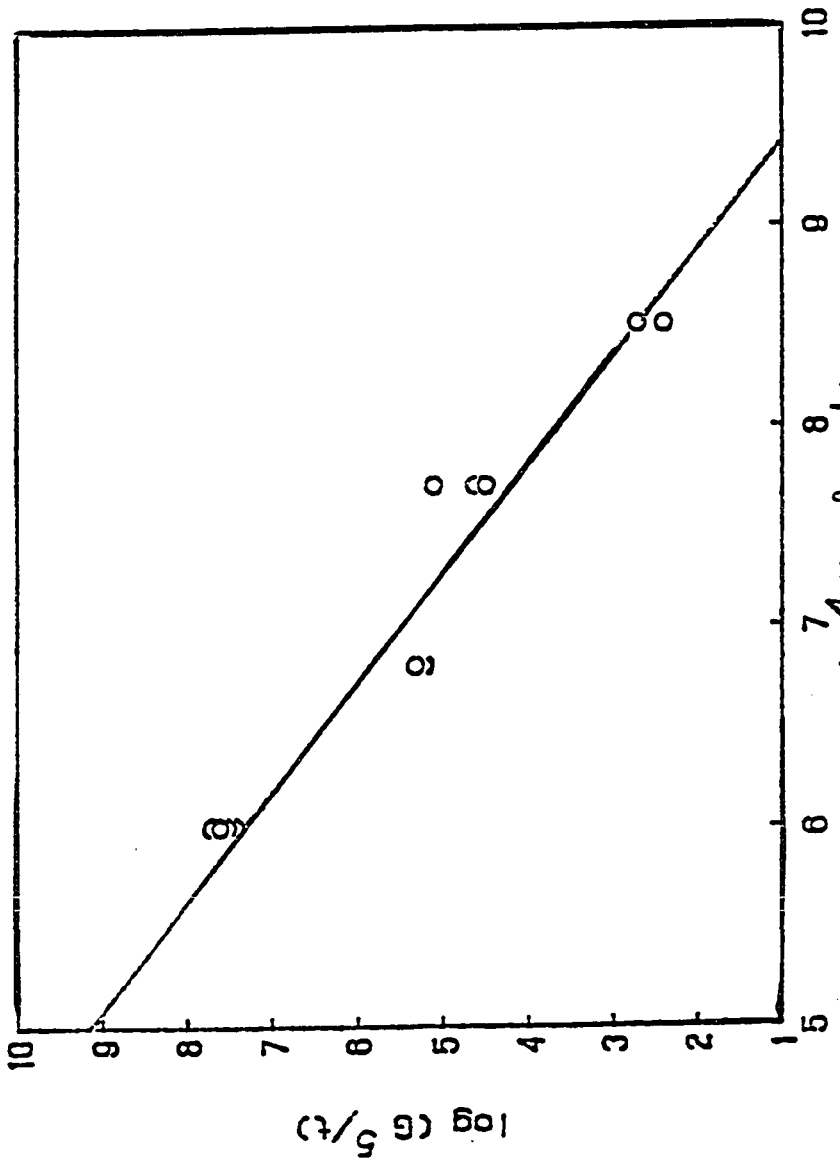

Figure IV.32 - Arrhenius Plots Log (G^5/t) versus 1/T for the 0.11 µm ZnO + 6 wt% Bi_2O_3 + 0.80 wt% Nb_2O_5

from the slope of this Arrhenius plot is (355 ± 50) kJ/mol. The activation energy for the grain growth of "pure" ZnO sintered in air has been determined by several previous authors, the results of which are summarized in Table II.3.1. These vary from 213 kJ/mol to 284 kJ/mol. It is evident that the 0.80 wt% Nb_2O_5 material has a higher activation energy for grain growth than pure ZnO, or ZnO with Bi_2O_3 additions, which has a value of about 150 kJ/mol.

When other oxides are added to ZnO the activation energy for the grain growth of ZnO may change, dependent on the mechanism of grain boundary migration. Additions of Bi_2O_3 have been observed [57] to enhance grain growth and to decrease the activation energy from 224 kJ/mol to about 150 kJ/mol. This is related to the change of the mechanism from one of Zn^{2+} lattice diffusion to that of phase boundary reaction. Additions of Sb_2O_3 [70] and K_2O [71] have both been observed to inhibit ZnO grain growth. These two additives also increase the activation energy for ZnO grain growth to 600 kJ/mol and 560 kJ/mol, respectively. The activation energy for ZnO grain growth in a complex multicomponent commercial ZnO system containing additions of (Bi_2O_3 + Sb_2O_3 + CoO + MnO_2 + SnO_3 + Al_2O_3) has been reported [78] to be 346.5 kJ/mol.

Gupta [71] has concluded that the mechanism of ZnO grain growth inhibition by K_2O additions is one of a drag

process from solute segregation at the grain boundaries. The value of 560 kJ/mol for the ZnO grain growth activation energy in the presence of K_2O suggests that the drag effect of the segregation of solute to the grain boundaries increases the activation energy for grain boundary migration of ZnO.

The effect of the spinel forming additive Sb_2O_3 on the grain growth of ZnO has also been studied by numerous authors [79,2,11,69,70]. It has been confirmed that sufficient Sb_2O_3 additions cause formation of the $Zn_7Sb_2O_{12}$ spinel phase, and also creates crystallographic twins in every grain. The Sb_2O_3 inhibits the grain growth of ZnO. Senda and Bradt [70] have systematically studied the kinetics of grain growth in the binary ZnO-Sb_2O_3 and they have concluded that the grain growth inhibition mechanism is related to the formation of the second phase spinel particles, although perhaps there may be some effects of the formation of twins in the ZnO grains. The activation energy for ZnO grain growth in the presence of Sb_2O_3 was determined to be 600 kJ/mol, a value which is of a comparable magnitude to the activation energy determined by Gupta [71] for the ZnO with K_2O additions. These results suggest that the presence of the spinel phases at the grain boundaries, similar to the presence of solute atoms, increases the activation energy necessary for grain boundary migration.

It is evident from previous experimental results that oxide additives which inhibit ZnO grain growth also usually increase the activation energy for grain growth and that those oxide additives which enhance ZnO grain growth generally decrease the activation energy. The value of 355 kJ/mol for the activation energy of the composition of ZnO + 6 wt% Bi_2O_3 + 0.80 wt% Nb_2O_5 is consistent with previous results. When 0.80 wt% Nb_2O_5 is added to the ZnO + Bi_2O_3 binary system, the grain growth of ZnO is inhibited and the activation energy for ZnO grain growth increases from 150 kJ/mol for the Nb_2O_5-free ZnO + Bi_2O_3 system to 355 kJ/mol. The presence of considerable porosity and the $Zn_3Nb_2O_8$ spinel phase in the 0.80 wt% Nb_2O_5 composition strongly suggests a grain boundary migration controlled grain growth process that is dominated by porosity and second phase drag mechanisms.

IV.2.2.3 - The Preexponential Factor K_0

The preexponential factor K_0 is readily determined from the intercept of the log (G^n/t) versus (1/T) plot. For those specimens containing 0.80 wt % Nb_2O_5, the intercept from Figure IV.32 is log K_0 = (18.4 $\pm$1.91) and $K_0 = 2.5 \times 10^{18} \mu m^5/h$. The value of the preexponetial factor, K_0, for the system ZnO + Bi_2O_3 without Nb_2O_5 additions has been reported to be $1.35 \times 10^{13} \mu m^5/h$ [57]. Therefore, the addition of 0.80 wt% Nb_2O_5 to the ZnO +

Bi_2O_3 system increases the prexponential factor K_0 from about 10^{13} $\mu m^5/h$ to approximately 10^{18} $\mu m^5/h$, about five orders of magnitude. In a different ceramic system, Nicholson [91] has reported that the value of K_0 increases with the concentration of vacancies in MgO, however, he did not explained his result.

The preexponential factor, K_0 is described by Equation (30). It is a direct function of the diffusion coefficient, the solubility of the solid species in the liquid phase and the molar volume of the diffusing species. However, K_0 is also a function of the grain boundary migration and the increase of K_0 by a factor of 10^5 with additions of Nb_2O_5 is highly significant. It is probably also related to grain boundary drag mechanisms. Values of the grain growth exponents, the activation energy and the preexponential factor determined in this study are summarized in Table (IV.2.1) for comparison with values of the kinetic parameters previously reported in this research and summarized in Table (IV.1.2).

IV.2.2.4 - Analysis of those Cases which Started as a Discontinous Grain Growth Process

The ZnO + 6 wt% Bi_2O_3 compositions containing 0.05 wt% to 0.40 wt% Bi_2O_3 exhibited discontinuous grain growth when fired at 900 °C and 1030 °C. The microstructures of those specimens have a bimodal grain size distribution as

Table IV.2.1 - Grain Growth Parameters for the

ZnO + 6 wt% Bi_2O_3 + 0.80 wt% Nb_2O_5

Slopes	(0.20 ± 0.18) at 900° C
	(0.21 ± 0.07) at 1030° C
	(0.21 ± 0.06) at 1192°C
	(0.23 ± 0.17) at 1400°C
Grain Growth Exponent (n-value)	(5.00 ± 1.60) at 900°C
	(4.72 ± 1.01) at 1030°C
	(4.85 ± 1.31) at 1192°C
	(4.27 ± 1.32) at 1400°C
Activation Energy	Q = (355 ± 50) kJ/mol
Intercept	$\log K_0$ = (18.4 ± 1.91)
Preexponential Factor	$K_0 = 2.5 \times 10^{18}\ \mu m^5/h$

evidenced in Figures IV.23 and IV.24. However, at the higher firing temperatures of 1192 °C and 1400 °C, the large grains consume all of the matrix and then collided with one another as can be observed in Figures IV.25 and IV.26.

Similar to the previous case of the composition ZnO + 6 wt% Bi_2O_3, the grain growth kinetics of the specimens containing 0.05 wt% to 0.40 wt% Nb_2O_5 can be analysed through Equation (32').

$$\log (G^n - G_0^n)/(t-t_0) = \log K_0 - 0.434\ Q/RT \qquad (32').$$

The left side of this equation was plotted versus 1/T using tentative n-values equal to three, four, five, and six. The n-value of five offered the best fit for the Arrhenius plot in every instance and thus was used to determine the activation energy, Q, and the preexponential factor, K_0 for each of the compositions.

Figures IV.33 (a to d) are the Arrhenius plots for the compositions ZnO + 6 wt% Bi_2O_3 + Nb_2O_5. Figure IV.33 (a) is for the composition with 0.05 wt% Nb_2O_5. The activation energy determined from the slope of this line is Q = (149.6 ± 6.6) kJ/mol. The intercept of the line is $\log K_0$ = (12.49 ± 2.21) which yields a preexponential factor of $K_0 = 3.05 \times 10^{12}$ $\mu m^5/h$. Figure IV.33 (b) is the Arrhenius plot for the 0.10 wt% Nb_2O_5 composition. The

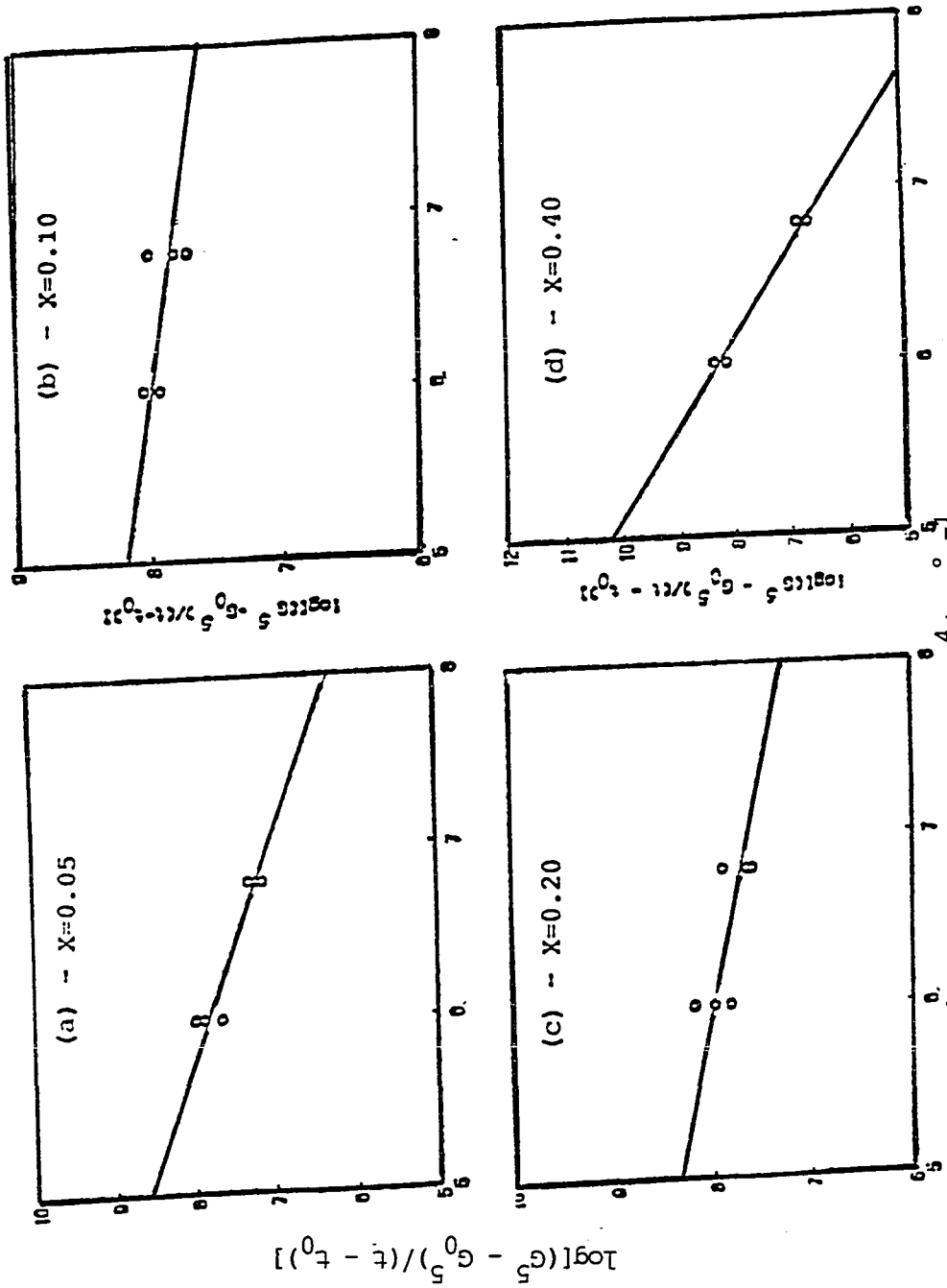

Figure IV.53 (a to d) - Arrhenius Plots - log $[(G^5 - G_0^5)/(t - t_0)]$ versus 1/T for the 0.11 um ZnO + 6 wt% Bi_2O_3 + X wt% Nb_2O_5

activation energy is only (35.2 ±5.68) kJ/mol, while the intercept is log K_0 = (9.10 ±1.90) and the preexponetial factor is $K_0 = 1.25 \times 10^9 \mu m^5/h$.

Figure IV.33 (c) is the Arrhenius plot for the 0.20 wt% Nb_2O_5 composition. The activation energy is (70.4 ± 8.83) kJ/mol, log K_0 = (10.19 ±2.95) and $K_0 = 1.54 \times 10^{10}$ $\mu m^5/h$. In Figure IV.33 (d), the Arrhenius plot for the 0.40 wt% Nb_2O_5 composition is showed. The activation energy is (376.8 ±5.95) kJ/mol, the intercept is log K_0 = (20.7 ±1.99) and $K_0 = 5.01 \times 10^{20}$ $\mu m^5/h$. These values of the grain growth parameters are summarized in Table (IV.2.2).

When the activation energies for ZnO grain growth in the different compositions containing Nb_2O_5 are compared, it is observed that the activation energy for ZnO grain growth in the system ZnO + 6 wt% Bi_2O_3 is a strong function of the Nb_2O_5 content. Figure IV.34 is a plot of the activation energy as a function of the Nb_2O_5 content. At 0.05 wt% Nb_2O_5 the activation energy is about the same as for the Nb_2O_5-free composition. But, for those compositions containing 0.10 wt% and 0.20 wt% Nb_2O_5 the activation energy is decreased. As the level of Nb_2O_5 increases to 0.40 wt% and 0.80 wt% the activation energy increases.

The preexponential factor K_0 is also a function of the level of the Nb_2O_5 addition as can be observed in

Table IV.2.2 - Grain Growth Parameters for the

$ZnO + 6\ wt\%\ Bi_2O_3 + Nb_2O_5$

Composition (wt% Nb_2O_5)	n	Q (kJ/mol)	log K_0	K_0 ($\mu m^5/h$)
0.0	5	(154±12)	(13.0±4.2)	1.04×10^{12}
0.05	5	(149±66)	(12.5±2.2)	3.05×10^{12}
0.10	5	(35±6)	(9.1± 1.9)	1.25×10^{9}
0.20	5	(70±9)	(10.2± 2.3)	1.54×10^{10}
0.40	5	(377±65)	(20.7± 2.0)	5.01×10^{20}
0.80	5	(355±50)	(18.4± 1.9)	2.5×10^{18}

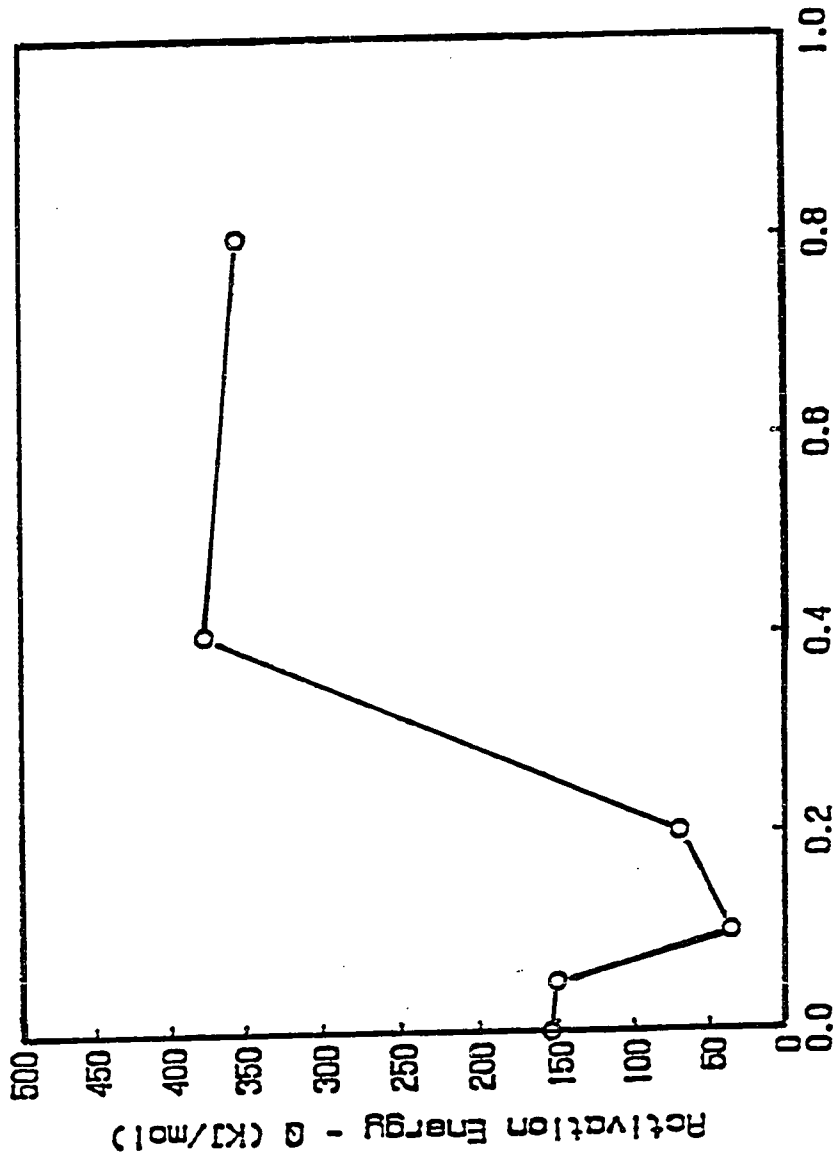

Figure IV.34 - Plot of the Activation Energy for Grain Growth versus the wt% Nb_2O_5 for the 0.11 µm ZnO + 6 wt% Bi_2O_3 + Nb_2O_5

Figure IV.35 which is a plot of log K_0 versus the level of Nb_2O_5. When Figures IV.34 and IV.35 are compared it is seen that the activation energy and the preexponential factor exhibit the same variation with respect to the Nb_2O_5 content. The minimum value of the activation energy and the preexponential factor occurs for the compositions containing 0.10 wt% and 0.20 wt% Nb_2O_5. This corresponds to the maximum in the average grain sizes depicted in Figures IV.27 and IV.28. These, minima for the activation energy and the preexponential factor correspond to Region II in Figure IV.30. In this region there is grain growth enhancement, probably from the increase in the cation vacancy concentration due to Nb_2O_5 in solid solution in ZnO. The decrease in the grain growth kinetic parameters, Q and K_0 in this region corresponds to an enhancement of the diffusivity due to solid solution effects.

Senda and Bradt [57] have reported that the activation energy of the composition ZnO + Bi_2O_3 is 150 kJ/mol and is independent of the Bi_2O_3 content. These authors concluded that the grain growth rate controlling mechanism was that of the phase boundary reaction. In this study it is observed that the addition of 0.05 wt% Nb_2O_5 decreases the rate of particle coarsening without appreciably changing the activation energy. It was concluded that the grain growth inhibition in Region I is due to the segregation of the Nb^{5+} ion to the grain

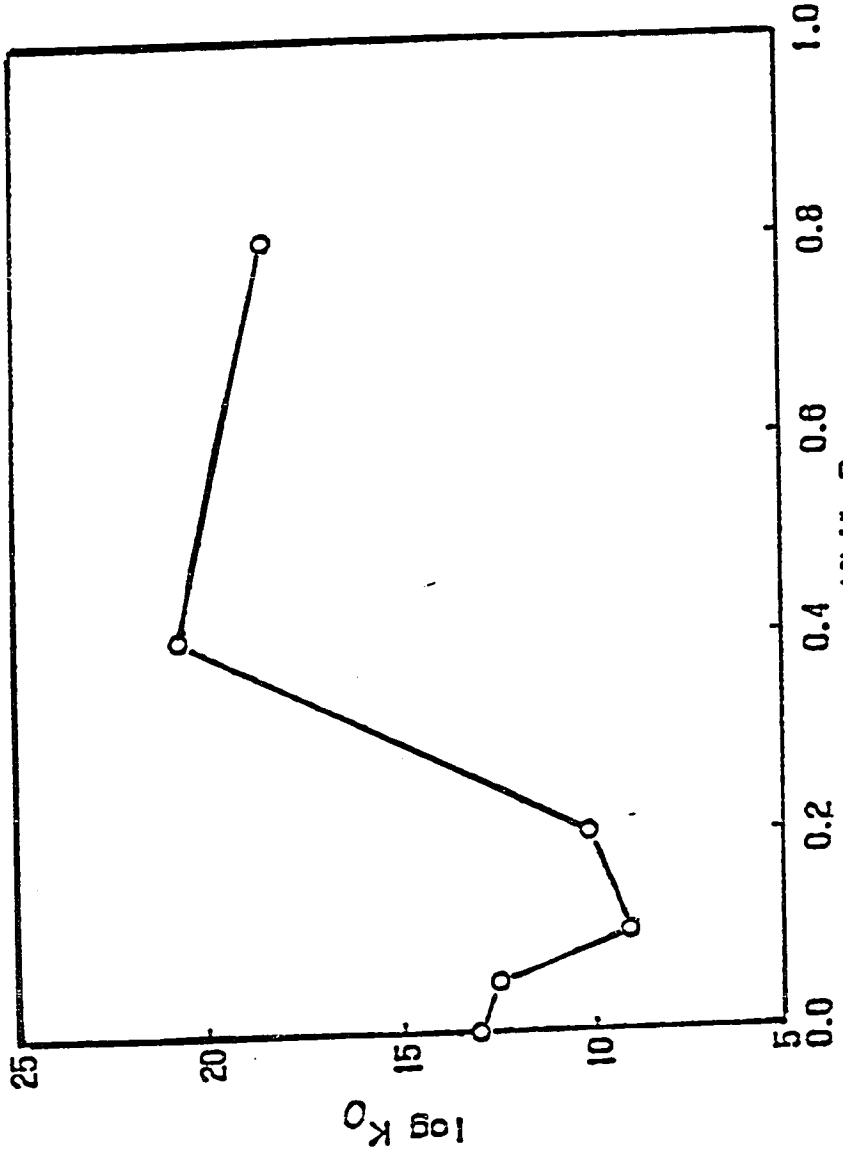

Figure IV.35 - Plot of the Exponential Factor K_O versus the wt% Nb_2O_5 for the 0.11 µm ZnO + 6 wt% Bi_2O_3 + Nb_2O_5

boundaries. This does not correlate well with Gupta's [71] result of an increase of the activation energy due to K_2O segregation effects. The reason is probably related to the presence of the liquid phase and discontinuous grain growth in the systems under study.

As more Nb_2O_5 is added to the system, solid solution of the Nb^{5+} ions into the ZnO lattice creates vacancies which increase the diffusivity of the Zn^{2+} ions. This decreases the activation energy for grain growth and increases the grain growth rate. The grain growth rate controlling mechanism for the compositions corresponding to Region II in Figure IV.30 seems to be the diffusion of the Zn^{2+} ions in the ZnO lattice. The values of 35.2 kJ/mol for the composition 0.10 wt% Nb_2O_5 and 70.4 kJ/mol for the composition 0.20 wt% Nb_2O_5 are much lower than the activation energy for grain growth in pure ZnO, indicating that the diffusion of the Zn^{2+} ions in the ZnO lattice is made easier when 0.10 wt% to 0.20 wt% Nb_2O_5 is added to the system ZnO + 6 wt% Bi_2O_3. The reason for this decrease seems to be the increase in the cation vacancy concentration as previously discussed.

As the addition level of Nb_2O_5 is increased to 0.40 wt% and 0.80 wt% the activation energy, Q, and the preexponential factor, K_0, both increase to high values. As the Nb_2O_5 addition level is increased the volume fraction of the $Zn_3Nb_2O_8$ spinel phase also increases and

these high values of Q and K_0 are indicative of a grain growth process controlled by second phase drag mechanisms.

IV.2.3 - Summary of the Effects of Nb_2O_5 Addition on ZnO Grain Growth

The results of this investigation of the effects of Nb_2O_5 additions on the grain growth of ZnO in the ZnO + 6 wt% Bi_2O_3 system have shown that the grain growth process is a discontinuous one for specimens containing less than 0.40 wt% Nb_2O_5, but appears to be a normal one for those specimens which contain 0.80 wt% Nb_2O_5. It was confirmed during this study that additions of Nb_2O_5 to the ZnO + 6 wt% Bi_2O_3 system leads to the formation of the zinc niobate spinel, ($Zn_3Nb_2O_8$), as predicted by the phase diagram.

The average ZnO grain size first decreases, then increases to a maximum value with respect to increasing levels of Nb_2O_5. The existence of this maximum is believed to be related to an increase of the cation vacancy concentration introduced into the ZnO structure by the Nb_2O_5 in solid solution.

Analysis of the grain growth kinetics by the phenomenological grain growth equation revealed that the grain growth exponent, or n-value, for the ZnO + 6 wt% Bi_2O_3 specimens containing 0.80 wt% Nb_2O_5 is five. The activation energy for ZnO grain growth in the ZnO + 6 wt%

Bi_2O_3 + 0.80 wt% Nb_2O_5 composition is (355 ±50) kJ/mol. The preexponential factor, K_0 increases by five orders of magnitude with the addition of 0.80 wt% Nb_2O_5. These high values of the kinetic parameters, Q and K_0, are believed to be related to grain boundary drag mechanisms.

Analysis of the grain growth kinetics for those situations that started as a discontinuous grain growth process have revealed that the activation energies and the preexponential factors for the system ZnO + 6 wt% Bi_2O_3 change with the Nb_2O_5 content. The grain growth exponent, or n-value, for all the compositions is five. The activation energy for the 0.05 wt% Nb_2O_5 composition is 150 KJ/mol and the preexponential factor is $K_0 = 3.05 \times 10^{12}$ $\mu m^5/h$. For the 0.10 wt% composition Q = 35 kJ/mol and $K_0 = 1.25 \times 10^9$ $\mu m^5/h$. At 0.20 wt% Nb_2O_5, Q = 70 kJ/mol and $K_0 = 1.54 \times 10^{10}$ $\mu m^5/h$. For the composition 0.40 wt% Nb_2O_5, Q = 377 kJ/mol and $K_0 = 5.01 \times 10^{20}$ mm^5/h. Figure IV.36 compares the effect of the Nb_2O_5 content on the grain sizes, the activation energy and the preexponential factor. The grain growth process seems to be controlled by pore drag mechanisms. The lower values of the kinetic parameters, Q and K_0, correspond to the system with a discontinuous grain growth for which the effects of pore drag mechanisms are reduced because many pores are left behind during the earlier stages of the grain growth process.

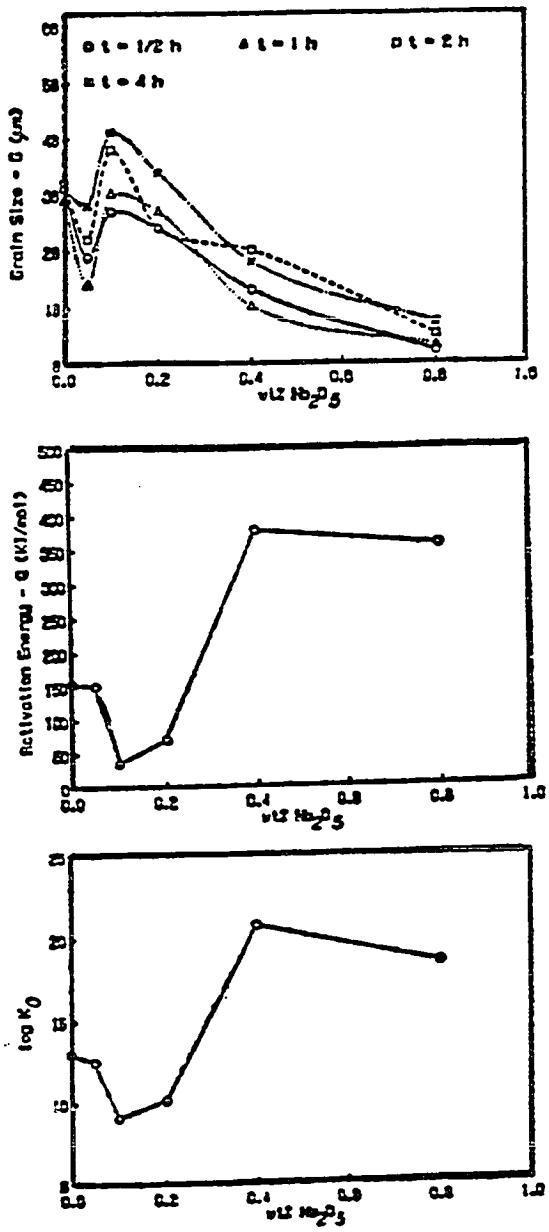

(a)

(b)

(c)

Figure IV.36 (a to c) - A Comparison Between the Effects of Nb_2O_5 Addition Levels on the (a) - Average Grain Size (b) - Activation Energy, and (c) - Preexponential Factor For the System 0.11 μm ZnO + 6 wt% Bi_2O_3 + Nb_2O_5

IV.3 - Effect of Al_2O_3 Additions

To study the effects of Al_2O_3 additions on the microstructural development of ZnO, Al_2O_3 was added to the 0.11 μm ZnO + 6 wt% Bi_2O_3 mixture at the levels of 0.10 wt%, 0.20 wt%, 0.40 wt%, and 0.80 wt%. These compositions were then fired at four different temperatures, 900°C, 1030°C, 1192°C, and 1400°C for four different times, 0.5 h, 1 h, 2 h, and 4 h for a test matrix total of 64 different specimens.

Effects of the Al_2O_3 content and the sintering temperature on the density are illustrated in Figure IV.37, as the density versus the Al_2O_3 content for for the 1 h firings. The maximum density of approximately 96% of the theoretical density was achieved for firing at 900°C. As the sintering temperature is increased, the density decreased, again probably related to the evaporation of Bi_2O_3 and ZnO. In a general sense, the level of the Al_2O_3 additions, at least between 0.10 wt% and 0.80 wt%, does not appear to significantly affect the fired density.

IV.3.1 - Microstructural Features

Figures IV.38 (a to d) illustrate the microstructures of the ZnO + 6 wt% Bi_2O_3 for the Al_2O_3 additions fired at 900°C for 4 hours. In these systems the initial ZnO particle size was 0.11 μm, which when combined with the presence of the 6wt% Bi_2O_3-rich liquid phase makes the

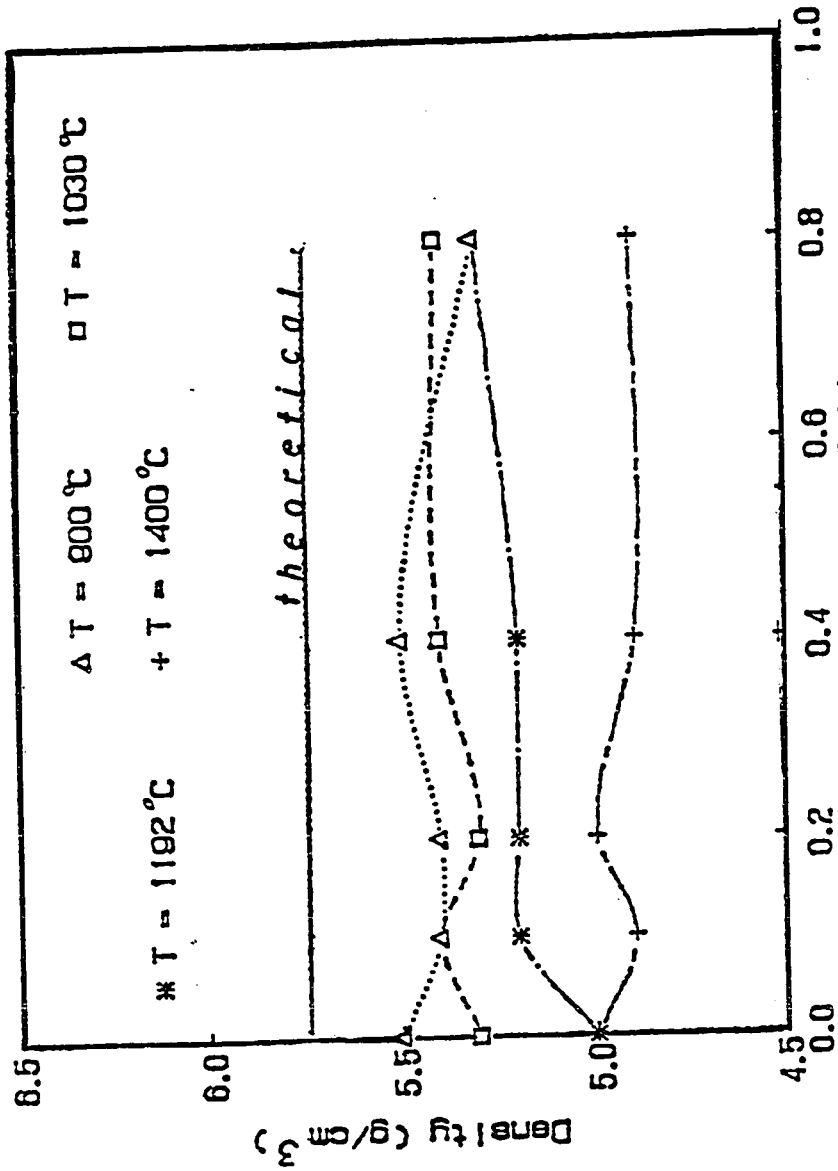

Figure IV.37 - Plots of of the Density versus wt% Al_2O_3 for the 0.11 μm ZnO + 6 wt% Bi_2O_3 + Al_2O_3 Firing Time - 1 Hour

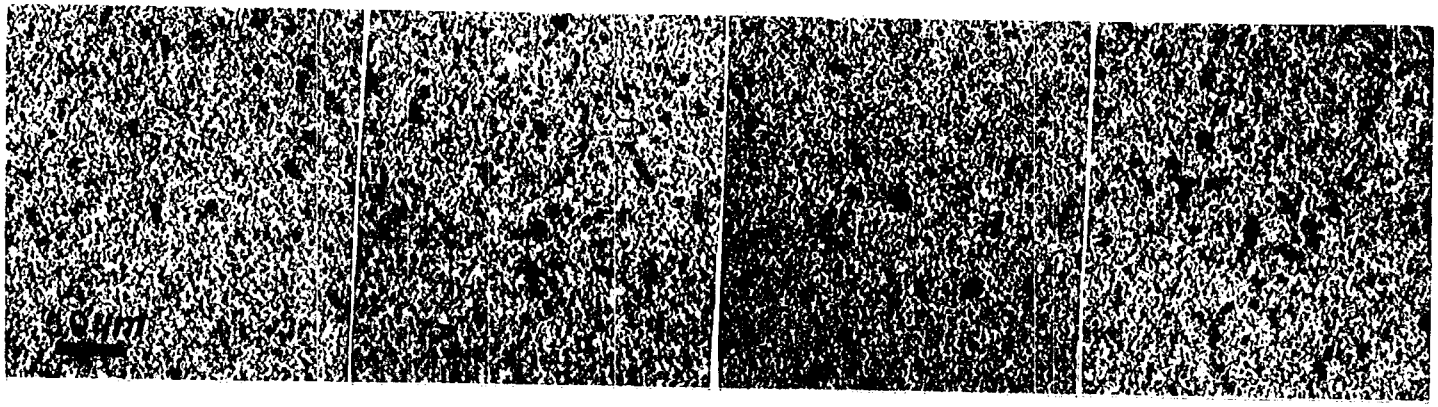

IV.38-(a)	IV.38-(b)	IV.38-(c)	IV.38-(d)
X=0.10	X=0.20	X=0.40	X=0.80
G=(2±1)μm	G=(3±1)μm	G=(2.2±1)μm	G=(1.8±1)μm

Figure IV.38 (a to d) - Optical Micrograph of the

ZnO + 6 wt% Bi_2O_3 + X wt% Al_2O_3

Fired at 900°C for 4 Hours. Initial Particle Size 0.11 μm.

Magnification 200 X

system prone to discontinuous grain growth as previously observed. However, as evident from these four microstructures, no aggregates or individual large grains are present, revealing that Al_2O_3 additions, even at a level as low as 0.10 wt% Al_2O_3, will prevent initiation of discontinuous grain growth. The average grain sizes of these microstructures vary from 2 to 3.0 μm.

Figures IV.39 (a to d) illustrate the microstructures for the specimens containing 0.10 wt% to 0.80 wt% Al_2O_3 fired at 1030°C for 4 h. These micrographs further confirm that microstructural coarsening in the Al_2O_3-doped ZnO specimens proceeds by a normal grain growth process. The average grain sizes vary from about 6 μm to 8 μm for these specimens, indicating that for these firing conditions, the variation of Al_2O_3 content in the range of 0.10 wt% to 0.80 wt% does not seem to significantly affect the ZnO grain size.

Figure IV.40 (a to d) depict the microstructures of the specimens fired at 1192°C for 4 h. As the level of Al_2O_3 increases from 0.10 wt% to 0.80 wt% the average ZnO grain size gradually decreases from (26 ± 7)μm for the specimen containing just 0.10 wt% Al_2O_3 to (18 ± 3)μm for the specimen with 0.80 wt% Al_2O_3. It is evident that the Al_2O_3 additions have a strong inhibiting effect on the ZnO grain growth.

Figures IV.41 (a to d) illustrate the microstructures

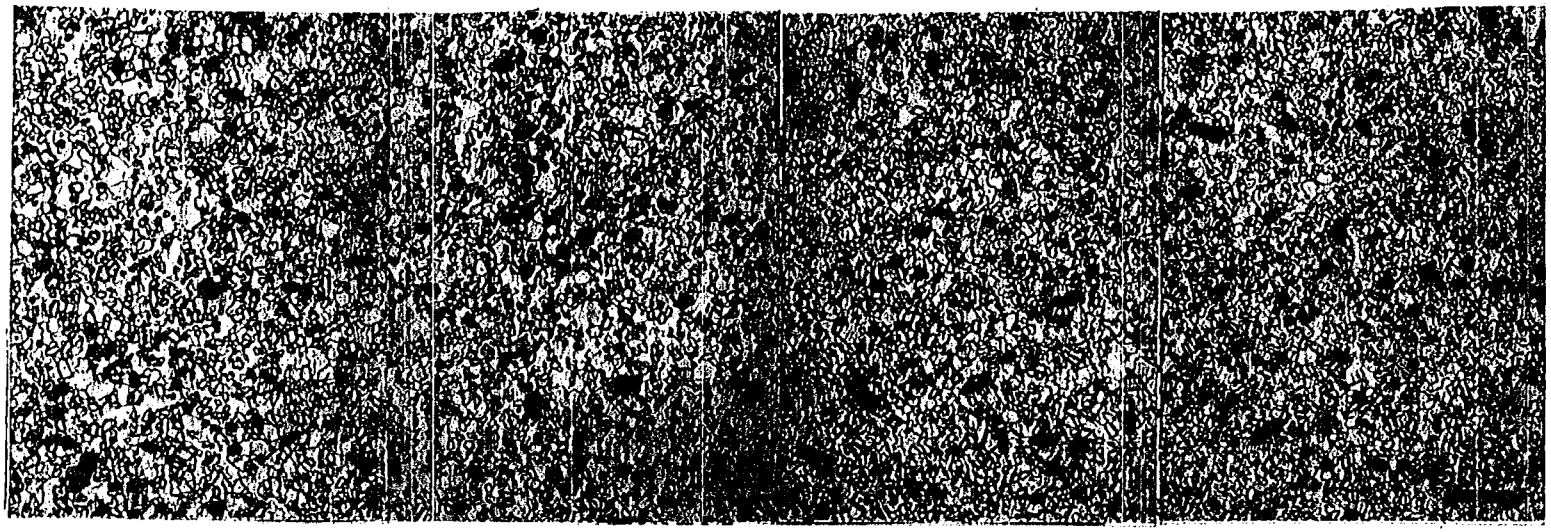

IV.39-(a)
X=0.10
G=(7±3)μm

IV.39-(b)
X=0.20
G=(8±2)μm

IV.39-(c)
X=0.40
G=(6±3)μm

IV.39-(d)
X=0.80
G=(6±2)μm

Figure IV.39 (a to d) - Optical Micrograph of the

ZnO + 6 wt% Bi_2O_3 + X wt% Al_2O_3

Fired at 1030°C for 4 Hours. Initial Particle Size 0.11 μm.

Magnification 200 X

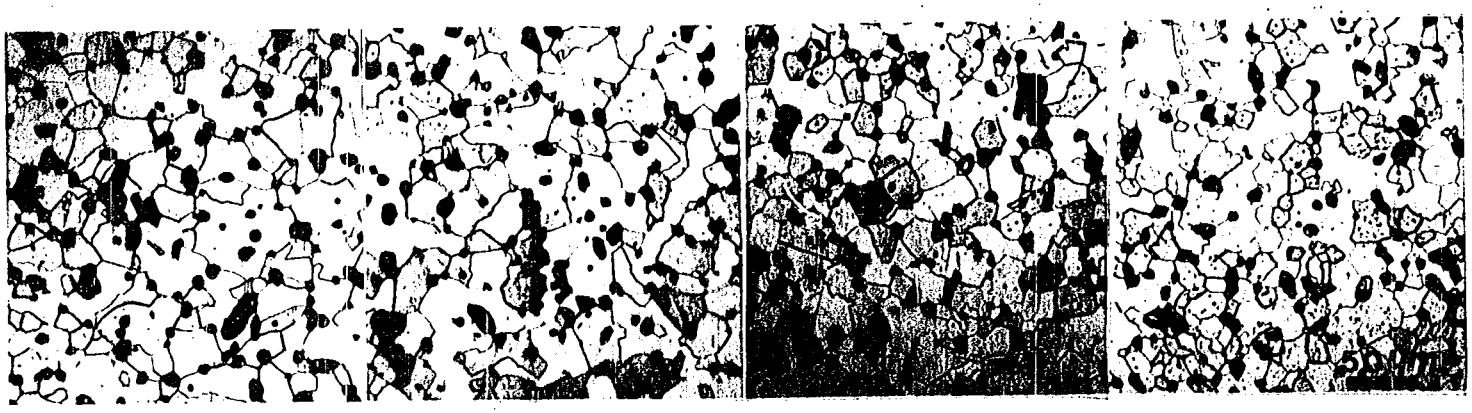

IV.40-(a)	IV.40-(b)	IV.40-(c)	IV.40-(d)
X=0.10	X=0.20	X=0.40	X=0.80
G=(26±7) μm	G=(30±5) μm	G=(21±5) μm	G=(18±3) μm

Figure IV.40 (a to d) - Optical Micrograph of the

ZnO + 6 wt% Bi_2O_3 + X wt% Al_2O_3

Fired at 1192°C for 4 Hours. Initial Particle Size 0.11 μm.

Magnification 200 X

of those specimens fired at 1400°C for 4 hours. Figure IV.41 (a) of the specimen containing 0.10 wt% Al_2O_3 shows that pores have migrated along with the grain boundaries and gradually accumulated at the corners and along the grain boundaries. The average grain size is (40 ± 8) μm.

Figure IV.41 (b) is of the specimen with 0.20 wt% Al_2O_3, its average grain size is (45 ± 8)μm. Figure IV.41 (c) is of the specimen containing 0.40 wt Al_2O_3 which has an average grain size of (33 ± 7) μm and Figure IV.41 (d) is for the 0.80 wt% Al_2O_3 specimen. The highest Al_2O_3 content has the smallest average grain size, (32 ± 8)μm. A common feature of all of these micrographs is the presence of pores at the grain corners and the large size of those pores. This agrees with the lower densities for those specimens fired at 1400°C.

When the effects of Al_2O_3 additions on the microstructural development of the ZnO are compared with the effects of the Nb_2O_5 additions, it is apparent that small amounts of those two additives have exactly opposite affects on the ZnO grain growth process. Small addition levels of Nb_2O_5 promoted a discontinuous grain growth process while small additions of Al_2O_3 prevented that phenomenon.

In Figure IV.42 the average grain sizes are plotted versus the Al_2O_3 content for the specimens fired at 900°C. Similarly, in Figure IV.43 the average grain sizes are

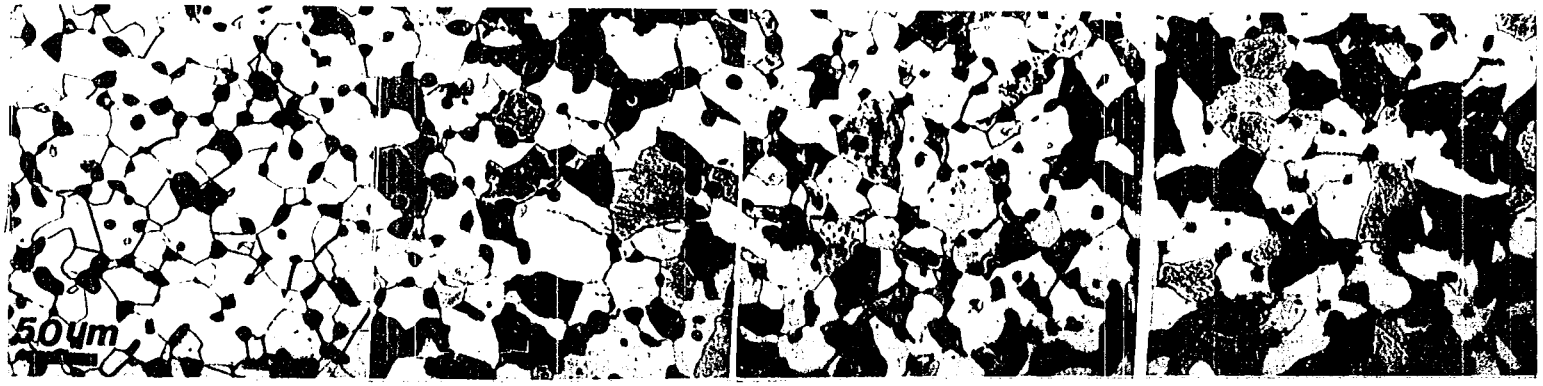

IV.41-(a)	IV.41-(b)	IV.41-(c)	IV.41-(d)
X=0.10	X=0.20	X=0.40	X=0.80
G=(40±8)µm	G=(45±8)µm	G=(33±7)µm	G=(32±8)µm

Figure IV.41 (a to d) - Optical Micrograph of the

ZnO + 6 wt% Bi_2O_3 + X wt% Al_2O_3

Fired at 1400°C for 4 Hours. Initial Particle Size 0.11 µm.

Magnification 200 X

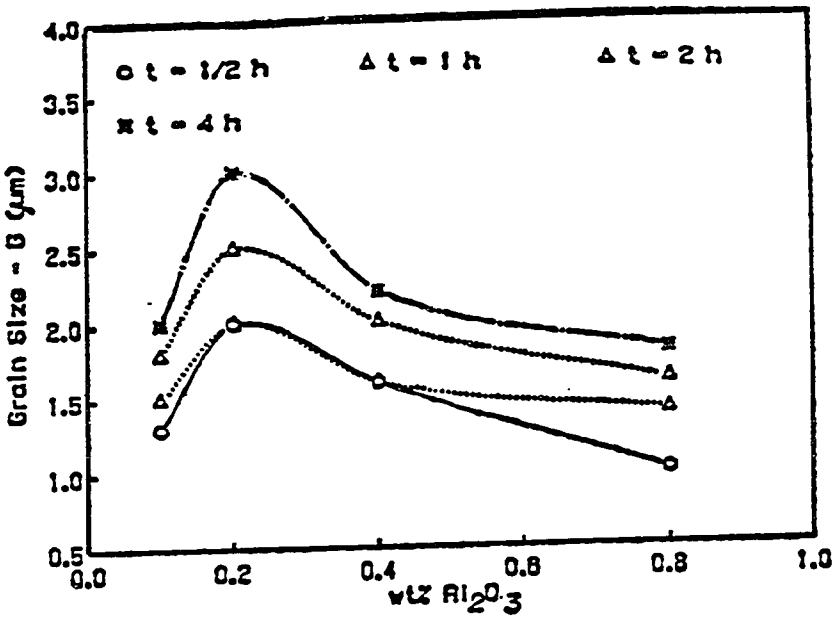

Figure IV.42 - Plots of the Average Grain Size versus wt% Al_2O_3 for the 0.11 μm + ZnO + 6 wt% Bi_2O_3 + Al_2O_3 Firing Temperature - T = 900°C.

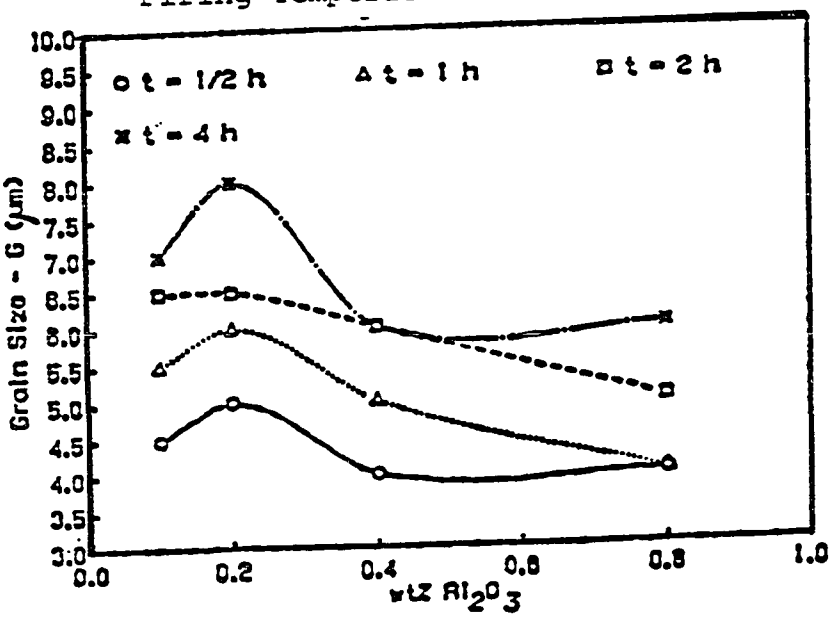

Figure IV.43 - Plots of the Average Grain Size versus the wt% Al_2O_3 for the 0.11 μm + ZnO + 6 wt% Bi_2O_3 + Al_2O_3 Firing Temperature - T = 1030°C

plotted versus the Al_2O_3 content for a firing temperature of 1030°C. For these two plots it was not possible to include the point for the zero Al_2O_3 content specimens because those specimens without Al_2O_3 experienced discontinuous grain growth and exhibit a bimodal grain size distribution. These figures indicate that the average ZnO grain size achieves a maximum value at about the 0.20 wt% Al_2O_3 composition for both firing temperatures.

In Figure IV.44 the average grain sizes are plotted versus the Al_2O_3 contents for the specimens fired at 1192°C for times of 0.5 h to 4 h. At this higher firing temperatures those specimens without Al_2O_3 yielded a microstructure consisting only of large grains which had already consumed all of the finer matrix grains, therefore for firing at the temperatures of 1192°C and 1400°C it was possible to include in these plots a point corresponding to zero content Al_2O_3. It is obvious that even for only small additions of Al_2O_3 to the ZnO + 6 wt% Bi_2O_3 binary system, a considerable decrease of the average ZnO grain size occurs. For example, when fired for 4 hours at 1192°C the grain size is reduced from (39 ±19)μm to (26 ± 12)μm when only 0.10 wt% Al_2O_3 is added. It is also evident from this figure that a small increase of the grain size occurs for the 0.20 wt% Al_2O_3 addition, but that further additions of Al_2O_3 consistently decrease the

average grain size. It is obvious that the addition of Al_2O_3 has a distinct grain growth inhibition effect on the ZnO + 6 wt% Bi_2O_3.

In Figure IV.45 the average grain sizes are plotted versus the of Al_2O_3 content for the specimens fired at 1400°C for the four different times. The grain size curves at 1400°C are very similar to the curves previously obtained for 1192°C. With the initial alumina addition there is a sharp decrease of the average grain size, from (64 ± 5)μm to (40 ± 8)μm, after which the grain size slightly increases for the 0.20 wt% Al_2O_3 addition, and then decreases with increasing Al_2O_3 contents.

As observed in Figures IV.44 and IV.45 for firing at 1192°C and 1400°C the plots of the average grain size as a function of the Al_2O_3 content follow the same general trends that were previously observed for the case of the Nb_2O_5 additions and which are represented schematically in Figure IV.30. The initial addition of Al_2O_3, at only the 0.10 wt% Al_2O_3 inhibits the ZnO grain growth (Region I), then as the Al_2O_3 content is increased to 0.20 wt% a region of grain growth enhancement is observed (Region II). Finally at higher levels of Al_2O_3, the result is grain growth inhibition (Region III). The same general behavior of three distinct grain growth/composition regions as previously discussed for the case of the Nb_2O_5 exists for the Al_2O_3 additions.

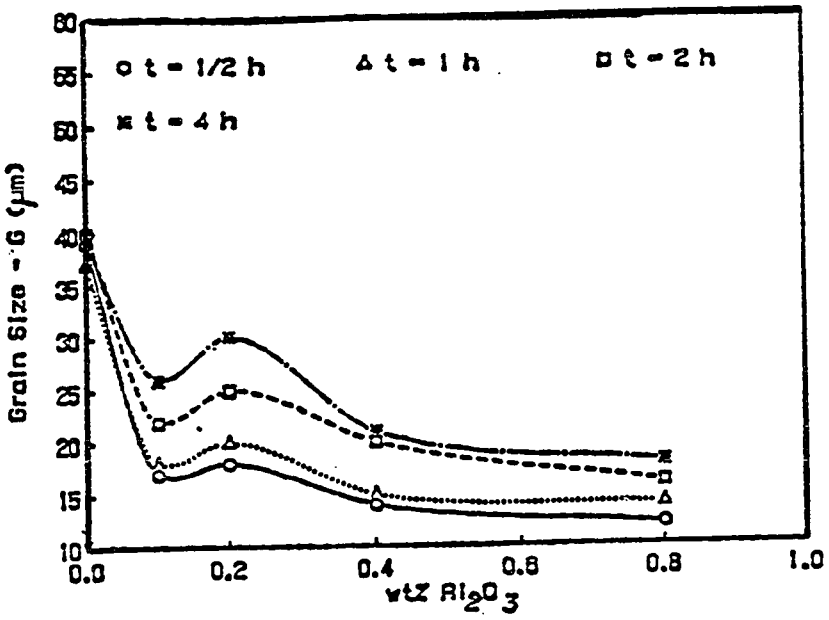

Figure IV.44 - Plots of the Average Grain Size versus the wt% Al_2O_3 for the 0.11 μm + ZnO + 6 wt% Bi_2O_3 + Al_2O_3 Firing Temperature - T = 1192°C

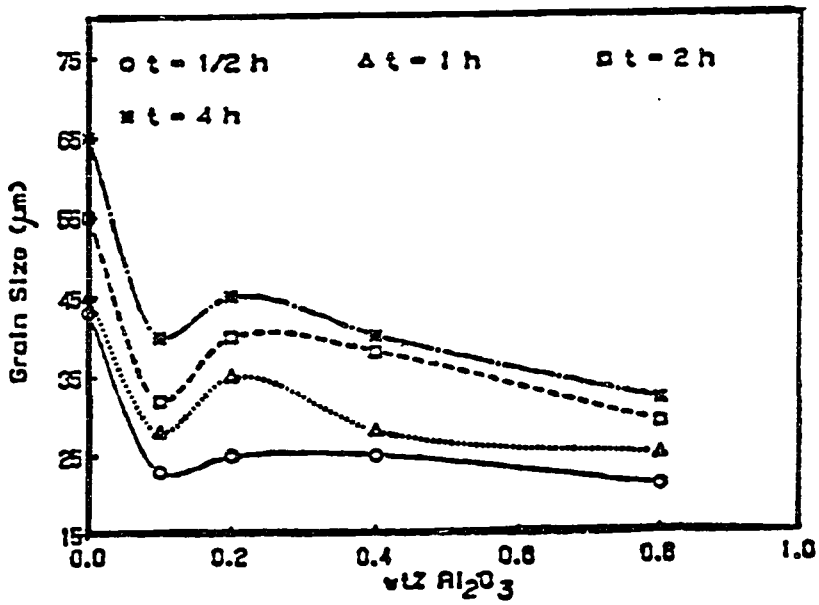

Figure IV.45 - Plots of the Average Grain Size versus the wt% Al_2O_3 for the 0.11 μm + ZnO + 6 wt% Bi_2O_3 + Al_2O_3 Firing Temperature - T = 1400°C

The initial inhibition of the ZnO grain growth is probably related to the segregation of the solute atoms to the grain boundaries, as suggested by Gupta [71] for K_2O additions to ZnO, and by Johnson and Stein [82] in the case of additions of CaO to Al_2O_3. Gupta [71] has reported the inhibition of ZnO grain growth by K_2O additions similar to the effect of the 0.10 wt% Al_2O_3 additions observed in this study. He found that with only a 0.12 wt% K_2O addition, the ZnO grain sizes were much smaller, by about a factor of two, than those for "pure" ZnO. Gupta did not detect any K_2O-containing second phases and suggested that the ZnO grain growth inhibition by the K_2O addition may have been one of solute segregation at the grain boundaries.

The radius of the Zn^{2+} is 0.74 A° and the radius of the Al^{3+} ion is 0.51 A° which resuls in a ionic size ratio of 31%. This large size factor (>> 15%) suggests that solid solution of Al_2O_3 in ZnO is not favored. Also, from the electronic considerations, since the solid solution of Al_2O_3 in ZnO requires the formation of vacancies, segregation of Al^{3+} to the grain boundaries is expected, although some solid solution certainly must exist. When comparing the segregation and solid solution behavior of the Al^{3+} ions and the Nb^{5+} ions it is seen that they have opposite tendencies, while the solid solution is more favorable for the Nb^{5+} ions, the Al^{3+} are expected to

segregate to the grain boundaries. This might explain why the Al_2O_3 addition promptly prevents discontinuous grain growth and also is a very good inhibitor of the normal grain growth process.

It was suggested for Nb_2O_5 additions in this study that the grain growth enhancement in Region II is related to the increase of the cation diffusivity caused by an increase in the cation lattice site vacancy concentration. When the Al_2O_3 goes into solid solution in the ZnO lattice, to maintain charge balance, 2 Al^{3+} must replace 3 Zn^{2+} ions leaving one vacant Zn^{2+} lattice site according to Equation (37) previously presented. This increases the cation vacancy concentration and favors material transport. As pointed out by Chiang and Kingery [74] the presence of the defects, which accommodate the lattice stoichiometry, can cause diffusion enhancement which in turn can affect the grain boundary mobility and the grain growth rate. This mechanism appears to be prevalent in Region II for Al_2O_3 additions to ZnO.

The solid solutions of Nb_2O_5 and Al_2O_3 in the ZnO structure create vacancies according to Equations (37) and (38) as previously discussed. Addition of Nb_2O_5 creates more vacancies than the additions of Al_2O_3, therefore Nb_2O_5 is expected to cause a higher enhancement of the diffusion coefficient than the Al_2O_3 and consequently a higher enhancement of grain growth in Region II. These

differences between the effects of the Nb_2O_5 and the Al_2O_3 solid solutions on the grain growth of the ZnO can be observed by comparing Figures IV.27 and IV.44 for firing at 1192°C, and Figures IV.28 and IV.45 for firing at 1400°C. These figures depicted the average grain sizes as a function of the additive oxide level and confirm that the enhancement of grain growth corresponding to Region II indeed is much greater for the Nb_2O_5 additions.

Comparison of these figures also reveals that Al_2O_3 is a much more efficient ZnO grain growth inhibitor than the Nb_2O_5. Besides the fact that the Nb_2O_5 in solid solution in ZnO creates more vacancies than the Al_2O_3, another factor that represents a major contribution to the difference observed in Region II is that Al^{3+} ions tend to segregate to the grain boundaries while the solid solution of Nb_2O_5 in ZnO is more favorable.

Inhibition of ZnO grain growth by the higher level of additions of Al_2O_3 observed in Region III is related to the presence of the $ZnAl_2O_4$ spinel phase through the second phase particle drag mechanism. The ZnO-Al_2O_3 phase diagram presented earlier in Figure II.4.4 indicates that Al_2O_3 reacts with the ZnO to form the spinel phase $ZnAl_2O_4$ and the presence of the $ZnAl_2O_4$ in the ZnO-Al_2O_3 system has been reported in the literature [7]. Figure IV.46 shows the XRD pattern for the specimen of ZnO + 6 wt% Bi_2O_3 + 0.80 wt% Al_2O_3 sintered for 2 hours at 1400°C.

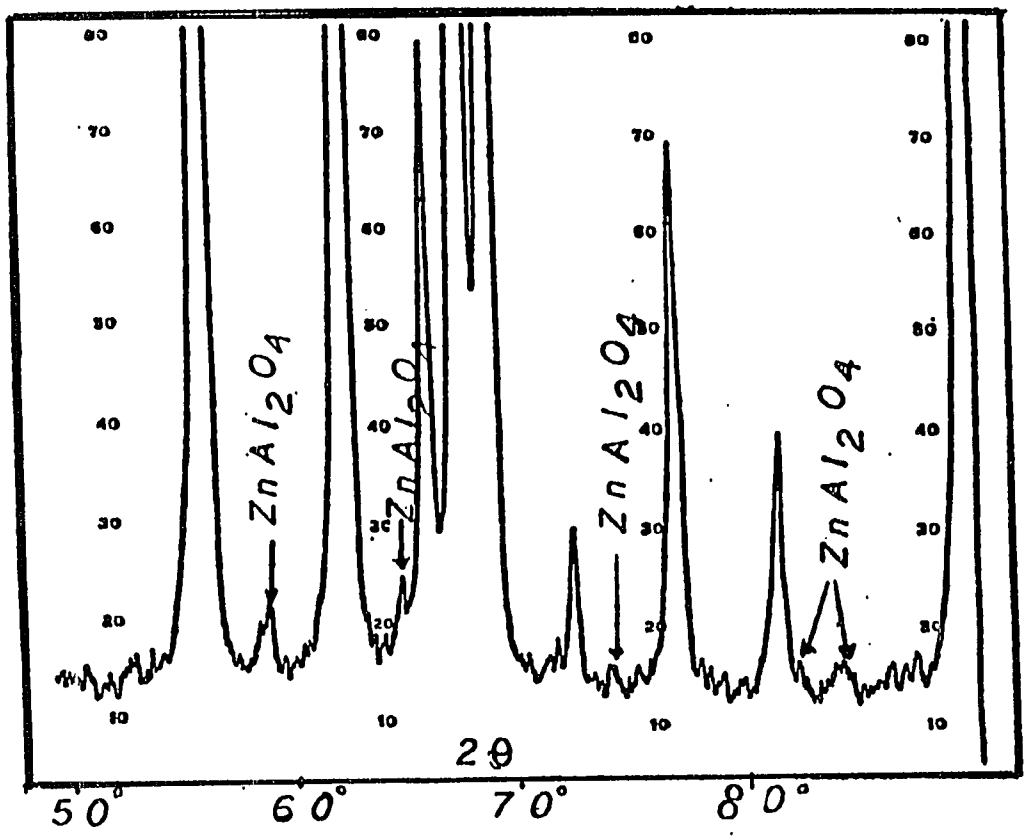

Figure IV.46 - Peaks Corresponding to the Spinel Phase $ZnAl_2O_4$ on the X-Ray Diffraction Pattern of the 0.11 μm ZnO + 6 wt% Bi_2O_3 + 0.80 wt%Al_2O_3 Fired at 1400°C for 2 Hours.

The presence of the $ZnAl_2O_4$ spinel phase is clearly revealed.

Quadir and Readey [7] have studied the effects of Al_2O_3 on the grain growth of pure ZnO at addition levels of 0.5 mol% to 5 mol%. They have attributed the inhibition of the ZnO grain growth to be related to the presence of the $ZnAl_2O_4$ spinel phase, which would reduce the grain boundary mobility by a pinning process or second phase drag process.

The inhibition of the grain growth of ZnO by additions of Sb_2O_3 has also been observed by previous workers [1,2,70] and the presence of the $Zn_7Sb_2O_{12}$ spinel phase in these systems has been confirmed [11,69,70]. However, Senda and Bradt [70] are the only who have attempted a quantitative evaluation of the effects of the $Zn_7Sb_2O_{12}$ inclusions on the grain growth process. They applied the "back stress model" suggested by Zener [44] which predicted that the limiting grain size should be directly proportional to the inclusion particle size and inversely proportional to the volume fraction of the second phase. Although their calculations resulted in final grain sizes about an order of magnitude larger than the experimentally observed grain sizes, they argued that these differences were probably reasonable, considering that their specimens probably had not yet reached the limiting grain size. The second phase particle drag

mechanism has also been reported for several other ceramic systems [80-86].

It is evident from the photomicrograph that the Al_2O_3-containing specimens have numerous pores at the grain boundaries. Probably the most important mechanism to the grain boundary drag process in the Al_2O_3-containing specimens is that of pore drag. When the pores are pinned to the grain boundaries, they can reduce the rate of grain growth. As most of the pores appear to be located at the grain boundaries, this seem to be indicative of the fact that the pores are indeed pinned to the boundaries, or vice versa, and are moving along with them. This further supports the conclusion that a pore drag mechanism is a controlling process, reducing grain growth.

In summary, the general behavior for the curve of grain size versus composition for the Al_2O_3 additions to ZnO can be attributed to three different mechanisms:

a) - Inhibition of grain growth due to solute segregation at and drag on the grain boundaries (Region I).

b) - Enhancement of grain growth due to solute solubility and increased vacancy concentrations causing increased cation diffusivity (Region II).

c) - Inhibition of grain growth due to a combination

of second phase spinel drag and pore drag mechanisms (Region III).

IV.3.2 - The Grain Growth Kinetics

Additions of Al_2O_3 to the 0.11μm ZnO + 6 wt% Bi_2O_3 suppress discontinuous grain growth. This results in normal grain growth to which the phenomenological grain growth expression of Equation (32) can be applied for a quantitative analysis of the ZnO grain growth kinetics.

IV.3.2.1 - The Grain Growth Exponent

Grain growth of ZnO for the ternary 0.11 μm ZnO + 6 wt% Bi_2O_3 + 0.10 wt% Al_2O_3 is depicted in Figure IV.47 in the form of the log (grain size) versus log (time) plot for the four different firing temperatures. The slopes of these lines are (0.226 ± 0.051) at 900°C, (0.220 ± 0.084) at 1030°C, (0.213 ± 0.079) at 1192°C, and (0.260 ± 0.070) at 1400°C. The values of the kinetic exponents, n-values, determined from the slopes of these lines are: (4.43 ± 1.01) at 900°C, (4.36 ± 1.64) at 1030°C, (4.70 ± 1.84) at 1192°C, and (3.84 ± 1.04) at 1400°C. The integer grain growth exponent for this composition is four.

Grain growth of the ZnO in the ternary ZnO + 6 wt% Bi_2O_3 + 0.20 wt% Al_2O_3 is depicted in Figure IV.48 in the form of log (grain size) versus log (time) plots for different firing temperatures. The slopes of the lines

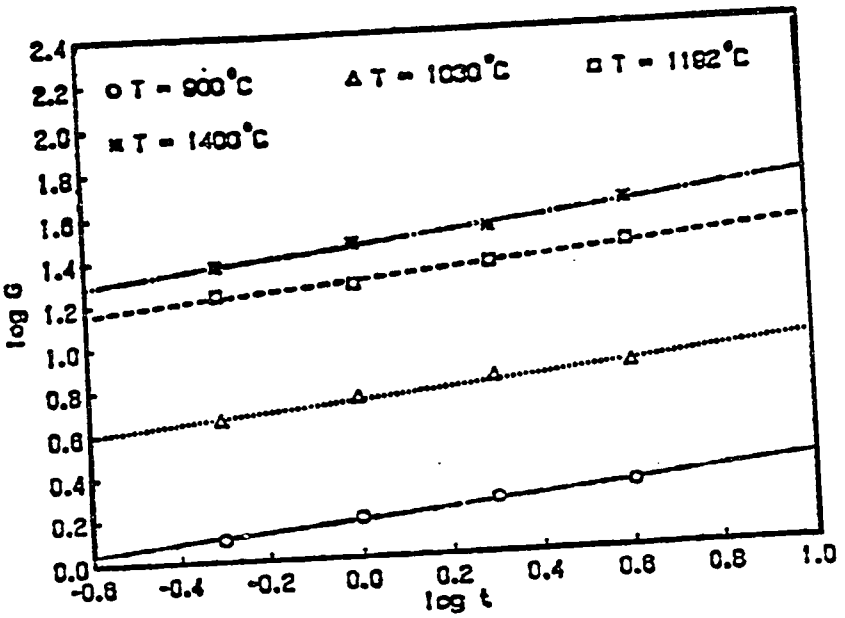

Figure IV.47 - Plots of Log (Grain Size) versus Log (Time) for the 0.11 μm ZnO + 6 wt% Bi_2O_3 + 0.10 wt% Al_2O_3

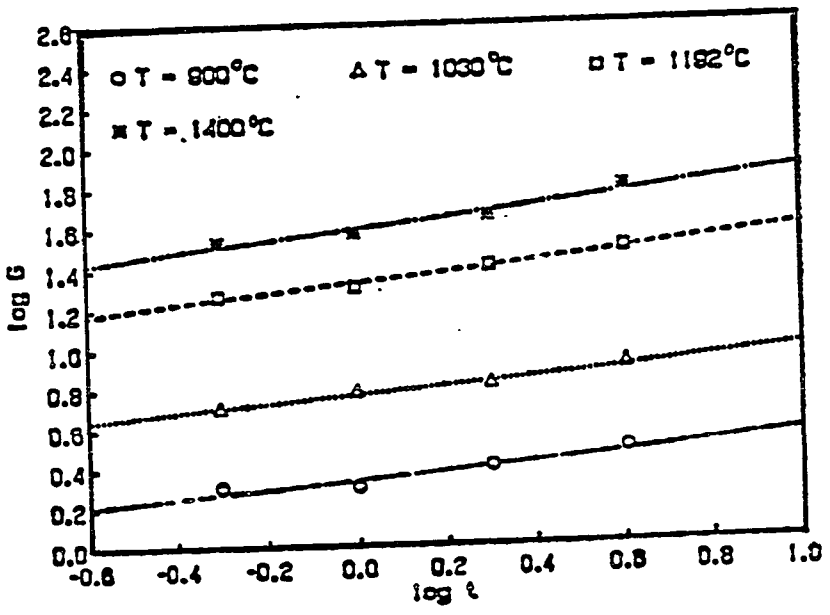

Figure IV.48 - Plots of Log (Grain Size) versus Log (Time) for the 0.11 μm ZnO + 6 wt% Bi_2O_3 + 0.20 wt% Al_2O_3

are (0.238 ±0.184) at 900°C, (0.216 ±0.084) at 1030°C, (0.260 ±0.090) at 1192°C, and (0.293± 0.151) at 1400°C. The kinetic exponents are (4.21 ±1.18) at 900°C, (4.62 ± 1.85) at 1030°C, (3.85 ±1.37) at 1192°C, and (3.41 ±1.86) at 1400°C. The average n-value estimated from these values is 4.02, so that similar to the 0.10 wt% Al_2O_3 composition an integer n-value of four is appropriate.

Grain growth for the ZnO in the ZnO + 6 wt% Bi_2O_3 + 0.40 wt% Al_2O_3 composition is depicted in Figure IV.49 in the form of log (grain size) versus log (time) for different firing temperatures. The slopes of the lines are (0.204 ±0.140) at 900°C, (0.235 ±0.174) at 1030°C, (0.229 ±0.143) at 1192°C, and (0.297 ±0.192) at 1400°C. The n-values determined from these lines are : (4.89 ± 1.74) at 900°C, (4.25 ±1.57) at 1030°C, (4.36 ±1.98) at 1192°C, and (3.37 ±1.39) at 1400°C. Again the integer n-value is four.

Grain growth of the ternary ZnO + 6 wt% Bi_2O_3 + 0.80 wt% Al_2O_3 is depicted in Figure IV.50 in the form of log (grain size) versus log (time) plots for the four different firing temperatures. The slopes of the lines are (0.292 ±0.184) at 900°C, (0.238 ±0.162) at 1030°C, (0.197 ±0.028) at 1192°C, and (0.212 ±0.051) at 1400°C. The kinetic exponent has the following values : (3.43 ± 1.36) at 900°C, (4.21 ±1.18) at 1030°C, (5.06 ±0.72) at 1192°C, and (4.71 ±1.14) at 1400°C. There exists more

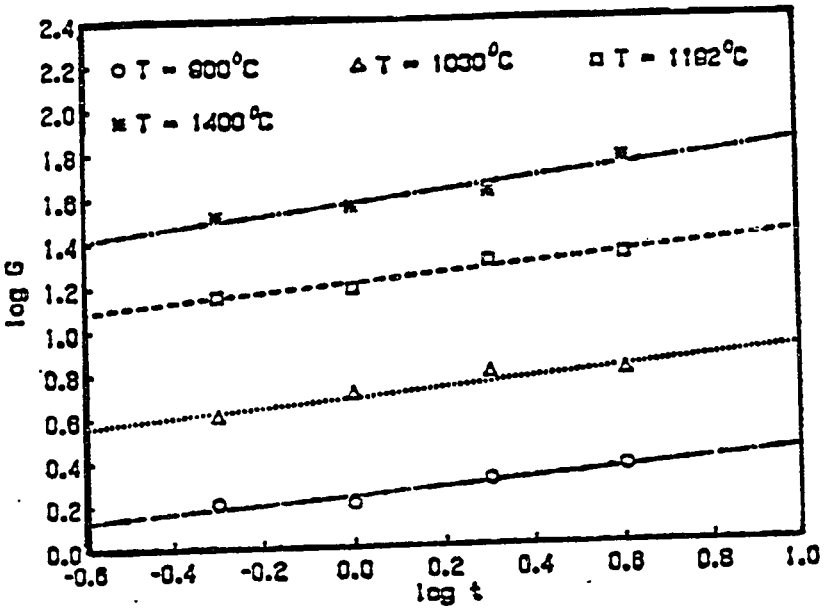

Figure IV.49 - Plots of Log (Grain Size) versus Log(Time) for the 0.11 μm ZnO + 6 wt% Bi_2O_3 + 0.40 wt% Al_2O_3

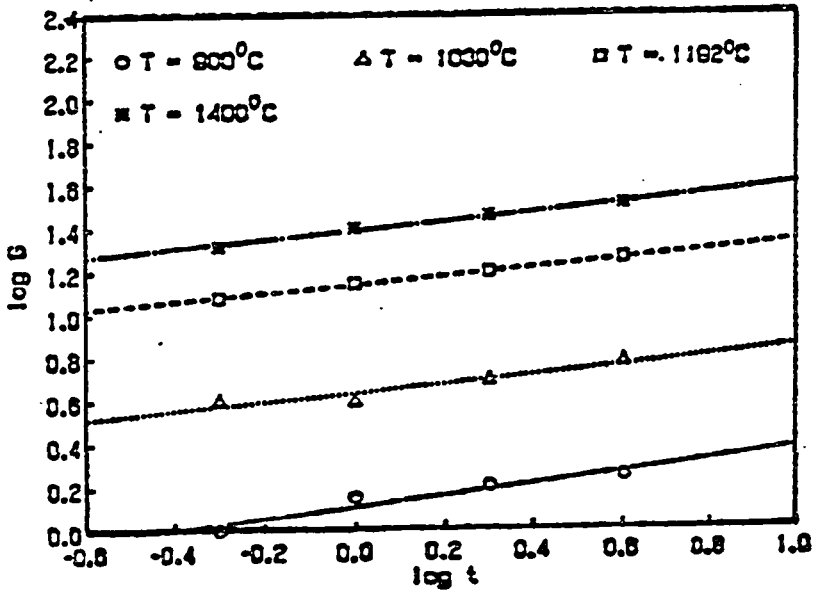

Figure IV.50 - Plots of Log (Grain Size) versus Log (Time) for the 0.11 μm ZnO + 6 wt% Bi_2O_3 + 0.80 wt% Al_2O_3

scatter on these n-values but an integer four also seems appropriate for this case.

By comparing the the grain growth exponents for all of the specimens containing Al_2O_3, it is seen that the most reasonable integer value for the kinetic exponent for all of these compositions is four. In general, according to results in the literature and the experimental results obtained in this study, the grain growth exponent or n-value increases from three for "pure" ZnO to four, five or six in the presence of various oxide additives. As discussed earlier, as the grain growth rate decreases the grain growth exponent increases. In the case of the compositions containing Al_2O_3 the grain boundary and triple point porosity and the presence of the $ZnAl_2O_4$ spinel phase are probably the main factors contributing to the reduction of the grain boundary mobility, the inhibition of grain growth and the increase of the grain growth exponent from three to four.

IV.3.2.2 - The Activation Energy for Grain Growth of ZnO in the Presence of Al_2O_3

The activation energies for the ZnO grain growth process are readily determined from the slopes of plots of log (G^n/t) versus 1/T. Figures IV.51 (a to d) show log (G^4/t) versus 1/T for the ZnO + 6 wt% Bi_2O_3 + Al_2O_3. Figure IV.51 (a) is for the composition 0.10 wt% Al_2O_3.

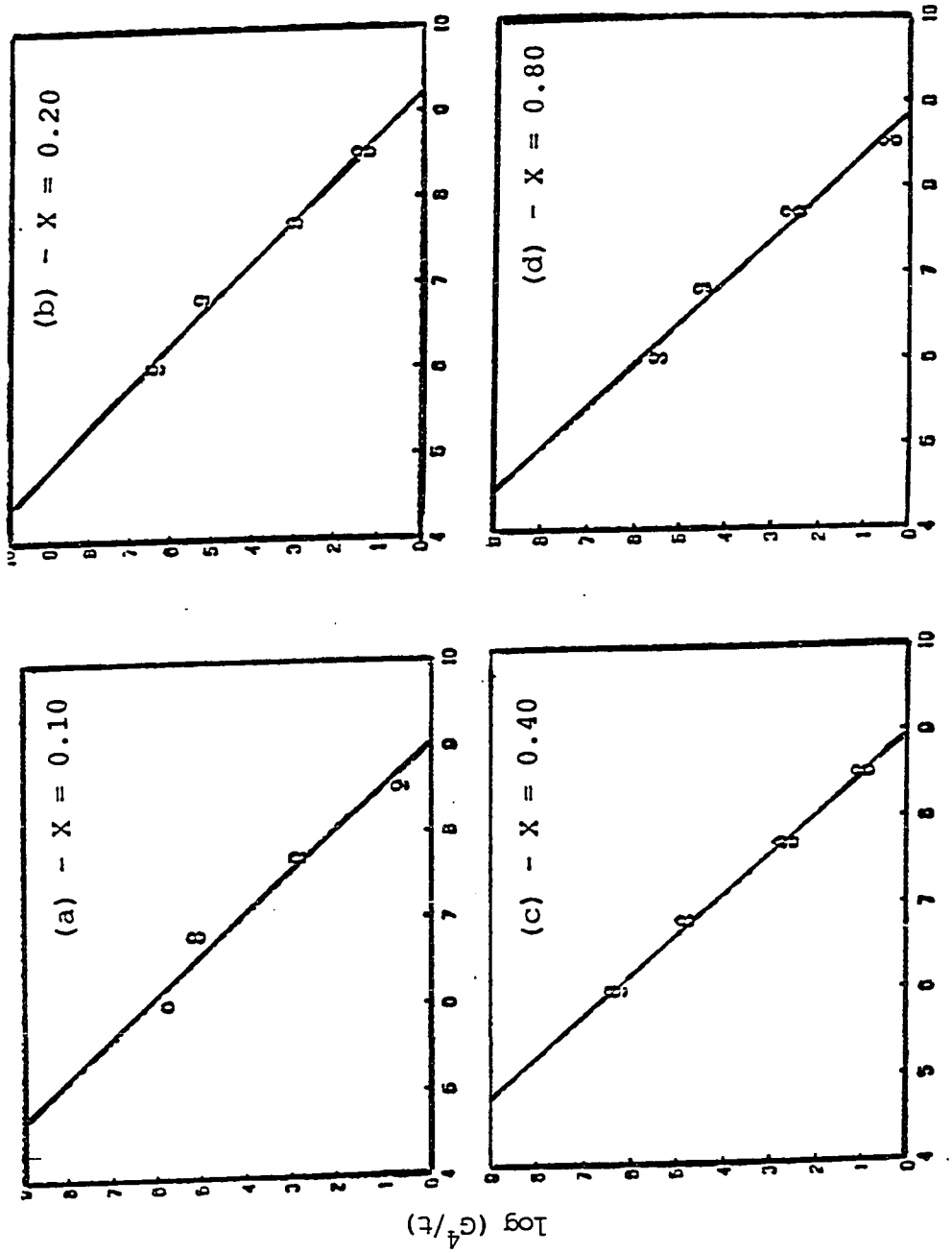

Figure IV.51 (a to d) - Arrhenius Plots - log (G^4/t) versus 1/T for the 0.11 um ZnO + 6 wt% Bi_2O_3 + X wt% Al_2O_3

This plot was constructed assuming the n-value to be equal to four. The activation energy calculated from the slope of this regression line is (399 ± 47) kJ/mol. Similarly, the Arrhenius plot for the composition of ZnO + 6 wt% Bi_2O_3 + 0.20 wt% Al_2O_3 was also constructed assuming an n-value of four. It is depicted in Figure IV.51 (b). The activation energy determined from the slope of this plot is (398 ± 26) kJ/mol, almost identical to the 0.10 wt% Al_2O_3 composition.

The Arrhenius plots for the ternary systems ZnO + 6 wt% Bi_2O_3 + 0.40 wt% Al_2O_3 and ZnO + 6 wt% Bi_2O_3 + 0.80 wt% Al_2O_3 were also constructed assuming that n is equal to four. These are depicted in Figures IV.51 (c and d). The activation energies determined from the slopes of the two lines are (416 ± 18) kJ/mol and (395 ± 34) kJ/mol respectively. The activation energies are plotted in Figure IV.52 versus the Al_2O_3 content. It is observed that the activation energy for grain growth for the ZnO + 6 wt% Bi_2O_3 specimens with Al_2O_3 additions does not vary with the Al_2O_3 content. It can be concluded that the activation energy for ZnO grain growth is independent of the Al_2O_3 content and that the small variations observed are due to the statistical nature of the experiments.

The preexponential factor, K_0, was calculated from the intercept, log K_0, of the lines in Figures IV.51 (a to d). The intercept determined from Figure IV.51 (a) is log K_0 = (18.7 ±1.8), so that the preexponetial factor for the specimen containing 0.10 wt% Al_2O_3 is 5.01 x 10^{18} $\mu m^4/h$, while for the 0.20 wt% Al_2O_3, log K_0 = (19.0 ± 0.99) and K_0 is 1.0 x 10^{19} $\mu m^4/h$. Similarly, the for the 0.40 wt% Al_2O_3, log K_0 = (19.4 ±0.68) and K_0 is 2.5 x 10^{19} $\mu m^4/h$ and for the 0.80 wt% Al_2O_3, log K_0 = (18.2 ± 1.28) and K_0 is 1.58 x 10^{18} $\mu m^4/h$. These values are summarized in Table IV.3.1 (a to d).

Senda and Bradt have also determined the preexponential factors for the "pure" ZnO and for the binary systems ZnO + Bi_2O_3 [61] and ZnO + Sb_2O_3 [70]. However, it is not possible to directly compare all of these K_0 values because of the differences in the units depending on the individual grain growth exponents, n-values. However, one comparison that can be made is between the binary system 2.0μm ZnO +Bi_2O_3 and the ternary system ZnO + 6 wt% Bi_2O_3 + Al_2O_3 analysed in this study. This comparison is possible because these two systems both have grain growth exponents of four and thus the units for K_0 are the same ($\mu m^4/h$). The value of K_0 for the binary 2.0μm ZnO + Bi_2O_3 is approximately 10^{17} ($\mu m^4/h$) and for the ternary ZnO + 6 wt% Bi_2O_3 + Al_2O_3 it is about 10^{18} to 10^{19} ($\mu m^4/h$).

Table IV.3.1(a) - Grain Growth Parameters for the

$ZnO + 6$ wt% $Bi_2O_3 + 0.10$ wt% Al_2O_3

Slopes	(0.22 ±0.05) at 900°C
	(0.23 ±0.08) at 1030°C
	(0.21 ±0.08) at 1192°C
	(0.26 ±0.07) at 1400°C
Grain Growth Exponent (n-value)	(4.43 ±1.0) at 900°C
	(4.36 ±1.64) at 1030°C
	(4.70 ±1.84) at 1192°C
	(3.84 ±1.04) at 1400°C
Activation Energy	Q = (399 ±47) kJ/mol
Intercept	$\log K_0$ = (18.7 ±1.8)
Preexponential Factor	$K_0 = 5.01 \times 10^{18} \mu m^4/h$

Table IV.3.1 (b) - Grain Growth Parameters for the

$ZnO + 6\ wt\%\ Bi_2O_3 + 0.20\ wt\%\ Al_2O_3$

Slopes	(0.24 ±0.18) at 900°C
	(0.22 ±0.08) at 1030°C
	(0.26 ±0.09) at 1192°C
	(0.29 ±0.15) at 1400°C
Grain Growth Exponent (n-value)	(4.21 ±1.18) at 900°C
	(4.62 ±1.85) at 1030°C
	(3.85 ±1.37) at 1192°C
	(3.41 ±1.86) at 1400°C
Activation Energy	Q = (398 ±26) kJ/mol
Intercept	$\log K_0$ = (19.0 ±0.99)
Preexponential Factor	$K_0 = 1 \times 10^{19} \mu m^4/h$

Table IV.3.1 (c) - Grain Growth Parameters for the $ZnO + 6$ wt% $Bi_2O_3 + 0.40$ wt% Al_2O_3

Slopes	(0.20 ± 0.14) at 900°C
	(0.24 ± 0.17) at 1030°C
	(0.23 ± 0.14) at 1192°C
	(0.30 ± 0.19) at 1400°C
Grain Growth Exponents (n-value)	(4.89 ± 1.74) at 900°C
	(4.25 ± 1.57) at 1030°C
	(4.36 ± 1.98) at 1192°C
	(3.37 ± 1.39) at 1400°C
Activation Energy	$Q = (416 \pm 78)$ kJ/mol
Intercept	$\log K_0 = (19.4 \pm 0.68)$
Preexponential Factor	$K_0 = 2.5 \times 10^{19}$ m^4/h

Table IV.3.1 (d) - Grain GRowth Parameters for the

$ZnO + 6\ wt\%\ Bi_2O_3 + 0.80\ wt\%\ Al_2O_3$

Slopes	(0.29 ± 0.18) at 900°C
	(0.23 ± 0.16) at 1030°C
	(0.20 ± 0.03) at 1192°C
	(0.21 ± 0.05) at 1400°C
Grain Growth Exponent	(3.43 ± 1.36) at 900°C
	(4.21 ± 1.18) at 1030°C
	(5.06 ± 0.72) at 1192°C
	(4.71 ± 1.14) at 1400°C
Activation Energy	Q = (395 ± 34) kJ/mol
Intercept	$\log K_0$ = (18.2 ± 1.28)
Preexponential Factor	$K_0 = 1.58 \times 10^{18} \mu m^4/h$

Equation (30) shows that the rate constant is a function of the diffusion coefficient and it is then evident that several factors which affect the diffusion coefficient will also affect the preexponential factor K_0. However, the experimental values of the kinetic grain growth parameters reflect the contributions of many different superimposed factors, all of which affect the grain boundary migration. These include solutes, second phases, and pore drag processes. Usually, it is not possible to discern with absolute certainty the individual contributions of each of the several competing processes. The experimental values of the kinetic parameters were obtained from measurements of the average grain sizes and therefore they represent an average of all the factors involved in the grain growth process. Since the overall effect of all the processes resulting in the grain growth is the grain boundary migration, the experimental values of n, Q, and K_0 should be related to the average grain boundary mobility.

IV.3.3 - Summary of the Effects of the Al_2O_3 Additions

This study of the effects of the Al_2O_3 additions on the grain growth of ZnO in the ZnO + Bi_2O_3 systems have revealed that the discontinuous grain growth process is suppressed by additions of Al_2O_3. This is probably due to segregation of Al^{3+} ions at the grain boundaries.

The average grain size varies with Al_2O_3 content, similar to that for Nb_2O_5 additions, as indicated in the general curve of Figure IV.30. However, for the systems containing Al_2O_3, the increase in grain size observed in Region II is much smaller, indicating that the solid solution of Al_2O_3 in ZnO is not as effective as the Nb_2O_5 one. It was also observed in this study that higher level additions of Al_2O_3 inhibit normal grain growth, which is believed due to the spinel phase drag mechanism. The formation of the spinel phase $ZnAl_2O_4$ as predicted by the phase diagram was confirmed by X-ray diffraction.

The study of the kinetics of grain growth for the ternary system ZnO + 6 wt% Bi_2O_3 + Al_2O_3 revealed that the grain growth exponent is four, the activation energy for grain growth is approximately 400 kJ/mol and that the preexponential factor, K_0, is about $10^{18}\mu m^4/h$ to $10^{19}\mu m^4/h$. The activation energy, Q, and the preexponential factor, K_0, do not vary with the Al_2O_3 content (above 0.10 wt% Al_2O_3) as indicated in Figures IV.52 and IV.53. The value of the grain growth exponent of four is associated with pore drag mechanisms. The high value of the activation energy, 400 kJ/mol, is indicative of a normal grain growth process, with pores located mainly at the grain boundaries, and can also be attributed to grain growth processes controlled by pore drag mechanisms. The activation energy for the Al_2O_3-

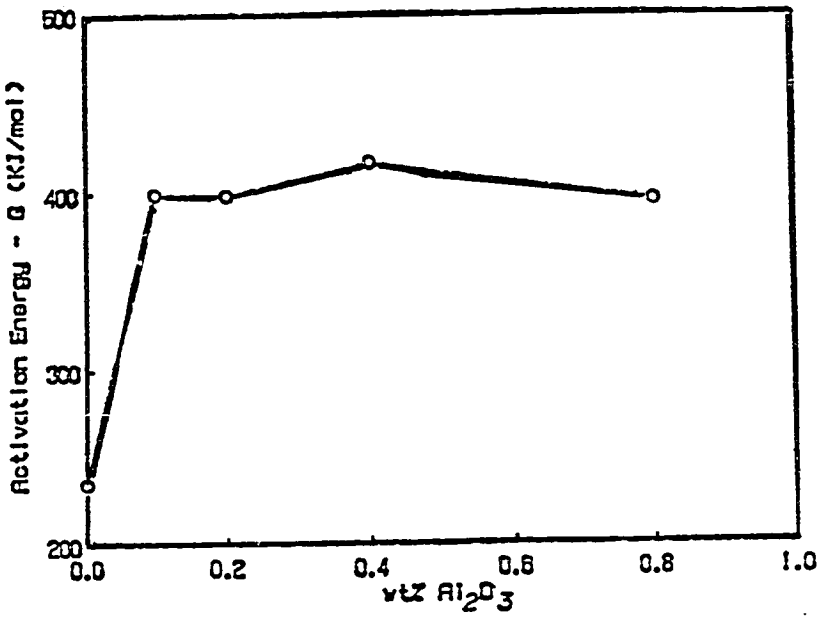

Figure IV.52 - Plot of the Activation Energy For Grain Growth versus the wt% Al_2O_3 for the 0.11 μm ZnO + 6 wt% Bi_2O_3 + Al_2O_3

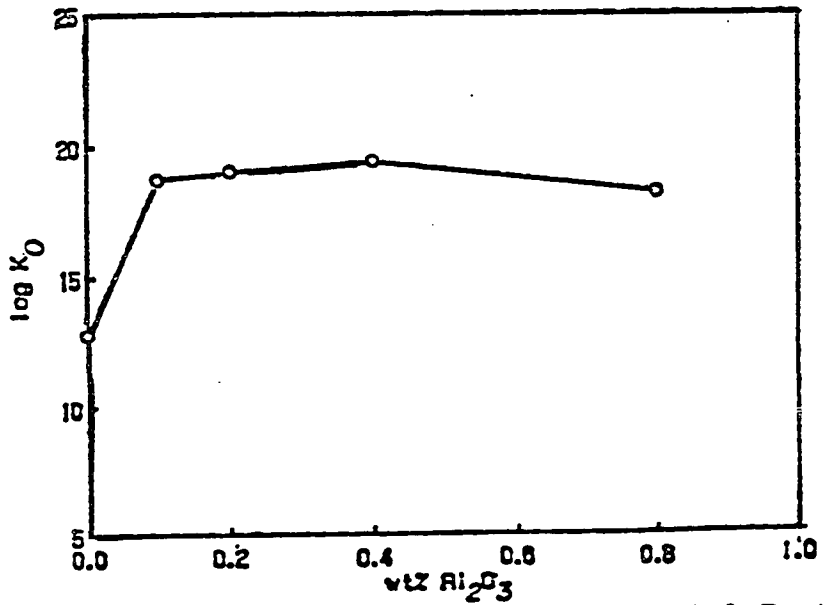

Figure IV.53 - Plot of the Log (Preexponential Factor) versus the wt% Al_2O_3 for the 0.11 μm ZnO + 6 wt% Bi_2O_3 + Al_2O_3

containing specimens is somewhat higher than the 360 kJ/mol determined for the activation energy for the specimens containing higher levels of Nb_2O_5 or for specimens consolidate with the 2.0 μm ZnO, which also presented a normal grain growth process. This higher value of the activation energy for the specimens containing Al_2O_3 can be attributed to the additional contribution to the grain boundary drag mechanisms due to the segregation of the Al_2O_3 to the grain boundary, and to the presence of the spinel phase $ZnAl_2O_4$ at the boundaries.

Chapter V - SUMMARY AND CONCLUSIONS

The effects of the initial ZnO powder particle size and the spinel forming additives, Nb_2O_5 and Al_2O_3, on the grain growth kinetics of ZnO in varistor-type ceramics were studied in a systematic fashion. Two different ZnO initial particle sizes, 0.11 μm and 2.0 μm, four different firing temperatures (900°C, 1030°C, 1192°C, and 1400°C), and four different firing times (0.5h, 1h, 2h, and 4h) were used for series of compositions.

The objective was to understand how the initial ZnO particle size and the spinel forming additives affect the microstructural development of ZnO and to determine the grain growth kinetic parameters for future use in the compositional and microstructural design of ZnO varistor ceramics.

The kinetics of grain growth was analysed through the phenomenological rate equation:

$$G^n - G_0^n = K_0 \ (t-t_0) \ \exp(\ -Q/RT) \qquad (32')$$

For the cases that exhibited normal grain growth from the initial stages, the G_0 value was much less than the G, and the factor G_0^n could be neglected. But, for those cases that began with a discontinuous grain growth process, the microstructure was initially bimodal, consisting of large

very rapidly growing grains within a matrix of very fine grains. For these cases Equation (32') can only be applied after the large grains have experienced sufficient growth to consume all the matrix grains and collide with one another. Therefore, for the analysis the initial time, t_0, cannot be zero and the grain size G_0 is not significantly smaller than the average grain size, G. The factor G_0^n cannot be neglected with respect to G^n.

For the cases where the grain growth process was normal the grain growth exponent, or n-value, could be determined directly from the slopes of the plots of log G versus log t. For those cases that started as discontinuous grain growth, the grain growth exponent, n, had to be determined by trial and error methods after the grains collided. The activation energy, Q, and the preexponential factor, K_0, were determined from Arrhenius plots of log $[(G^n - G_0^n)/(t-t_0)]$ versus 1/T. The activation energy, Q, was determined from the slope and the preexponential factor, K_0, was determined from the intercept of those plots.

This research was divided into several sections according to the different variables and the different systems that were considered. First, the effects of the starting ZnO particle size was considered in two different systems, one a solid state system and the other containing a liquid phase. Second, the effects of Nb_2O_5 additions

were analysed for systems containing a Bi_2O_3-rich liquid phase and finally, the effects of Al_2O_3 additions were studied, also in systems that contained a Bi_2O_3-rich liquid phase during sintering.

For the study of the effect of the initial ZnO particle size in solid state sintering, the system consisted of "pure" ZnO. It was observed that the grain growth process is a normal one and that the final microstructures consisted of grains that were very regular in size and shape. The initial ZnO particle size had a profound influence on the final microstructure of the fired bodies. The larger initial ZnO particle size resulted in a much smaller final grain size.

These experimental results were explained in terms of two different effects of the initial particle size. First, is the effect of the initial particle size on the rearrangement and densification rates. Smaller initial particle sizes result in higher rates of particle rearrangement during the initial stages of sintering and in higher densification rates due to stronger capillary forces. The second effect of the initial particle size is related to the driving force for grain growth which is the reduction of the surface area. The surface area per unit volume is larger for the smaller particles so that their driving force for grain growth is higher. As the force acting on the boundaries is higher the grain boundaries

are able to detach themselves from the pores more readily in the initial stages of the grain growth process, thus reducing the effects of pore drag mechanisms. Therefore, the system consolidated with the smaller initial ZnO particle size has lower volume fraction of pores and less pores located at the grain boundaries which result in a higher grain boundary mobility. Equation (44) which relates the grain growth rate to the driving force and to the grain boundary mobility shows that the grain growth rate of the specimen consolidated with the smaller initial particle sizes is larger at all stages, due to higher driving forces and to higher grain boundary mobilities, which results in larger final average grain sizes as observed experimentally.

For the study of the effect of the initial ZnO particle size in the presence of a liquid phase during sintering, the system consisted of ZnO + Bi_2O_3. It was observed that the influence of the liquid phase on the grain growth process also depended on the initial ZnO particle size. When the initial particle size was small, (0.11 μm, 0.20 μm, and 0.30 μm), the grain growth process was a discontinuous one consisting of a few large grains growing very fast and eventually consuming the matrix of fine grains. The resulting microstructure consisted of large grains that were very irregular in size and shape, with numerous pores located inside the grains as well as

at the grain boundaries. In contrast, as the initial particle size was increased to 2.0 μm, the grain growth process changed from a discontinuous one to a normal grain growth process and the final microstructure was a much finer one.

The equation for capillary forces between particles:

$$F_C = (2 \pi X^2 \gamma_{LV})/r + (2 \pi X \gamma_{LV} \cos \psi) \qquad (40)$$

was used to explain the occurrence of the discontinuous grain growth in the presence of the Bi_2O_3-rich liquid phase. Equation (40) which specifies the attractive capillary force between two particles connected by a wetting liquid meniscus, to the particle sizes describes how the particles are attracted. The strong attractive capillary forces cause particle clustering to occur during liquid phase sintering as a consequence of local melt formation. These clusters of wetted particles with closer packing and a higher volume fraction of solids develop a much higher grain growth rate than the rest of the matrix, initiating the discontinuous grain growth process.

The experimental observation that when the initial ZnO powder particle size is increased from 0.11 μm to 2.0 μm then the grain growth process changes from a discontinuous one to a normal one is also satisfactorily explained by Equation (40). The attractive capillary

force F_c decreases as the radius, r, of the solid particles increases. For sufficiently large initial ZnO powder particle sizes the capillary forces are just not strong enough to form the clusters and the discontinuous grain growth process does not occur.

To investigate the role of the content of the Bi_2O_3-rich liquid phase, the study of the effects of the initial ZnO particle size was carried out in systems containing Bi_2O_3 at the 3 wt% and 6 wt% levels. Similar results were obtained for both compositions and it was concluded that the onset of the discontinuous grain growth process is not critically dependent on the content of the liquid phase at these higher levels of Bi_2O_3.

The effect of the ZnO initial particle size on the kinetics of grain growth has revealed that the initial ZnO particle size affects the grain growth parameters in the system ZnO + Bi_2O_3. As the ZnO initial particle size is increased from 0.11 μm to 2.0 μm the activation energy for grain growth increases from 150 kJ/mol to 360 KJ/mol. This increase in the activation energy is consistent with the decrease observed in the final grain size when the discontinuous grain growth is suppressed and the grain growth process becomes normal, with more pores pinned to the boundaries and less mobile grain boundaries result.

Having determined the effects of the ZnO initial particle size, the research proceeded by analysing the

effects of the two spinel forming additives, Nb_2O_5 and Al_2O_3, on the grain growth of ZnO. When Nb_2O_5 was added to the 0.11 μm ZnO + 6 wt% Bi_2O_3 system, for additions of 0.40 wt% and less, the grain growth process was a discontinuous one, but at the 0.80 wt% Nb_2O_5 level the ZnO grain growth process was a normal one. At 0.05 wt%, Nb_2O_5 was found to inhibit the ZnO grain growth and it is suggested that this grain growth inhibition is a result of the segregation of the Nb^{5+} ions to the grain boundaries. As the Nb_2O_5 additions were increased to 0.20 wt% the final ZnO grain size also increased, revealing that at these levels the Nb_2O_5 promotes ZnO grain growth. Since solid solution of Nb_2O_5 in ZnO is favored by the cation size, the increase in the final ZnO grain size was attributed to a diffusivity enhancement caused by an increase in the cation vacancy concentration from the Nb^{5+} in solid solution. Further increases of the Nb_2O_5 additions to the 0.80 wt% level inhibit the ZnO grain growth process. This was explained in terms of a second phase drag mechanism from the presence of the $Zn_3Nb_2O_8$ spinel phase at the grain boundaries.

The study of the effect of the spinel forming additive Nb_2O_5 on the grain growth kinetic parameters of the system 0.11 μm ZnO + 6 wt% Bi_2O_3 revealed that the activation energy for grain growth, Q, and the preexponential factor, K_0, are both very strongly

dependent on the Nb_2O_5 levels. However, the grain growth exponent or n-value is five, independent of the Nb_2O_5 content. The 0.10 wt% and 0.20 wt% Nb_2O_5 compositions which presented the largest grain sizes corresponded to the lowest values of the activation energy and the preexponential factor. For the 0.40 wt% and 0.80 wt% Nb_2O_5 compositions the activation parameters increase corresponding to the grain growth inhibition observed at these Nb_2O_5 levels. It was concluded that the values of the parameters, Q and K_0, vary inversely to the grain boundary migration rate, i.e., when the grain boundary migration is enhanced, Q and K_0 are observed to decrease but when the grain boundary motion is inhibited Q and K_0 both increase.

Study of the spinel forming additive Al_2O_3 on the ZnO grain growth processes and on the kinetics of grain growth revealed that Al_2O_3 additions prevent the occurrence of discontinuous grain growth even at levels as low as 0.10 wt% Al_2O_3. Al_2O_3 inhibits normal grain growth of ZnO as well. This was explained in terms of the segregation of the Al^{3+} ions to the grain boundaries since solid solution of Al^{3+} in the ZnO is not favored by the cation size factor. The presence of the Al^{3+} cations restrains the grain boundary motion and prevents the discontinuous grain growth. A slight increase of the final ZnO grain size occurred for the 0.10 wt% and 0.20 wt% Al_2O_3 compositions

indicating that some solid solution of Al_2O_3 into the ZnO may have occurred. Increases in the levels of Al_2O_3 additions to 0.40 wt% and 0.80 wt% resulted in further grain growth inhibition due to the formation of the $ZnAl_2O_4$ spinel phase and second phase drag mechanisms.

Analysis of the effect of the Al_2O_3 on the grain growth kinetic parameters indicated that the grain growth activation energy, Q, and the preexponential factor, K_0, do not vary with the Al_2O_3 content. This result is consistent with the observations that the average grain sizes do not vary significantly with the level of Al_2O_3 addition.

Table V.1.1 summarizes the grain growth kinetic parameters determined in this study. The higher values of the activation energies, from 350 kJ/mol to 400 kJ/mol, are encountered for the systems in which the grain growth process is normal and inhibited while the lower values, from 150 kJ/mol to 35 kJ/mol, are for the systems with a discontinuous grain growth.

The effects of the spinel forming additives, Nb_2O_5 and Al_2O_3, are expressed in terms of a generalized schematic diagram containing three regions. In the first region, grain growth is inhibited through solute segregation to grain boundaries creating reduced grain boundary mobility through a solute drag mechanism. In the second region, additive solubility was accompanied by

increased lattice vacancy concentration and enhanced diffusivity leading to an increased rate of grain growth. The third region was that of grain boundary pinning by spinel crystals at the boundaries, inhibiting grain growth.

Table V.1.1 - Grain Growth Parameters For ZnO + Additives Determined In This Study

Composition (wt%)	Q(kJ/mol)	$\log K_0$	K_0
0.11μm ZnO + 6 wt% Bi_2O_3 + X wt% Additive			
		n = 5	($\mu m^5/h$)
0	154.5	13.0	1.04×10^{13}
0.05wt%Nb_2O_5	149.6	12.49	3.05×10^{12}
0.10wt%Nb_2O_5	35.2	9.10	1.25×10^{9}
0.20wt%Nb_2O_5	70.4	10.19	1.54×10^{10}
0.40wt%Nb_2O_5	376.8	20.7	5.01×10^{20}
0.80wt%Nb_2O_5	355	18.4	2.51×10^{18}
		n = 4	($\mu m^4/h$)
0.10wt%Al_2O_3	399	18.7	5.01×10^{18}
0.20wt%Al_2O_3	398	19.0	1.00×10^{19}
0.40wt%Al_2O_3	416	19.4	2.51×10^{19}
0.80wt%Al_2O_3	395	18.2	1.58×10^{18}
		n = 4	($\mu m^4/h$)
2.0 μm ZnO + 6 wt% Bi_2O_3	360	17	1.93×10^{17}

REFERENCES

1- M.Matsuoka, "Nonohmic Properties of Zinc Oxide Ceramics", Jpn.J.Appl. Phys. 10 736 (1971).

2- T.Asokan, G.N.K.Iyengar, and G.R.Nagabhushana, "Influence of Process Variables on Microstructure and V-I Characteristics of Multi component ZnO-Based Nonlinear Resistors", J.Amer. Ceram.Soc., 70 (9) 643-50 (1987).

3- T.Asokan, G.N.K.Iyengar, and G.R.Nagabhushana, "Studies on Microstructure and Density of Sintered ZnO-Based Nonlinear Resistors", J.Mat.Sci. 22 (6) 2229-36 (1987).

4- T.Asokan, G.N.K.Iyengar, and G.R.Nagabhushana, "Inhomogeneity in Sintered ZnO-Based Non-Linear Resistors", Ceram.Inter. 14 35-41 (1988).

5- T.Asokan, G.N.K.Iyengar and, G.R.Nagabhushana, "Non-Ohmic Behavior of the Binary ZnO-Nb_2O_5 System", J.Mat.Sci. 22 1019-1023 (1987).

6- P.Palanisamy and T.Asokan, "Intelligent Processing of ZnO-Based Ceramics", Cer.Bull.67 (10) 1695-98 (1988).

7- T.Quadir, D.W.Readey, "Microstructure Development of ZnO in Hydrogen", J. Am. Cer. Soc., 72 (2) 297-302 (1989).

8- W.Komatsu, M.Miyamoto, S.Hujita and Y.Moriyoshi,

"Effects of Dopants on Sintering of Zinc Oxide and Nickel Oxide", Yogyo Kyokai Shi 76 (12) 407-12 (1968).

9- W.Komatsu, Y.Moriyoshi and N.Sato, "Synergetic Effect on Sintering of ZnO with Different Dopants ", ibid. 77 (10) 347-53 (1969).

10- H.Cerva and W.Russwurm, "Microstructure and Crystal Structure of Bismuth Oxide Phases in Zinc Oxide Varistor Ceramics", J.Amer.Ceram.Soc. 71 (7) 522-30 (1988).

11- L.M.Levinson and H.R.Philipp, "Zinc Oxide Varistors A Review",Cer.Bull. 65 (4) 639-46 (1986).

12- K.Eda, "Conduction Mechanism of Non-Ohmic Zinc Oxide Ceramics", J. Appl. Phys. 49 (5) 2964-71 (1978).

13- M.Sumiyoshi, "Ceramic Varistor" F.C., Annual Report for Overseas Readers, Fine Ceramics for Future Creation, March 1988 p. 42-50, Japan Fine Ceramics Association.

14- D.A.Porter, and K.E.Easterling,."Phase Transformation in Metals and Alloys" pg 136 Van Nostrand,Reinhold Publisher, Berkishire, England, 1985.

15- F.N.Rhines and K.R.Craig, "Mechanism of Steady-State Grain Growth in Aluminum", Metall. Trans.

5A 413 (1974).

16- R.M.German, "Liquid Phase Sintering", Plenum Press. New York (1985) pp 149.

17 M.Hillert, "On the Theory of Normal and Abnormal Grain Growth", Acta Met. 13 227-238 (1965).

18 K.W.Lay, "Grain Growth of UO_2-Al_2O_3 in the Presence of a Liquid Phase",J. Am. Cer. Soc. 51 (7) 373-76 (1968).

19- J.K.Burke and D.Turnbull, "Recrystallization and Grain Growth", Prog.Metal.Phys. 3 220 (1952).

20- C.S.Smith, Metal Interfaces, P.65 ASM, Cleveland, OH (1952).

21- P.Felthan, "Grain Growth in Metals", Acta Metall. 5 97 (1957).

22- N.P.Louat, "On the Theory of Normal Grain Growth", Acta Metall. 22 721 (1974).

23- J.E.Morral and M.F.Ashby," Dislocated Cellular Structures", Acta Metall. 22 567 (1974).

24- R.D.Doherty, Discussion of "Mechanism of Steady-State Grain Growth in Aluminum", Metall. Trans. 6A 588 (1975).

25- O.Hunderi, "Steady State Grain Growth:A Note on the Kinetics", Acta Metall. 27 167 (1979).

26- S.K.Kurtz and F.M.A.Carpay, "Microstructure and Normal Grain Growth in Metals and Ceramics.Part II.Experiment.".J.Appl.Phys. 51 5745 (1980).

27- P.W.Voorhees and E.Glicksman, "Ostwald Ripening During Liquid Phase Sintering - Effect of Volume Fraction on Coarsening Kinetics, "Metall.Trans.A 15A 1081-1088 (1984).

28- P.W.Voorhees and M.E.Glicksman, "Solution to the Multi-Particle Diffusion Problem with Applications to Ostwald Ripening I-Theory", Acta Met. 32 2001-11 (1984).

29- P.W.Voorhees and M.E.Glicksman, "Solution to the Multi-Particle Diffusion Problem with Applications to Ostwald Ripening-II. Computer Simulations", Acta Met.32 2013-2030 (1984).

30- D.J.Srolovitz, M.P.Anderson, P.S.Sahn and G.S.Grest, "Computer Simulation of Grain Growth II:Grain Size Distribution, Topology and Local Dynamics", Acta Metall. 32 793 (1984).

31- C.Wagner, "Theory of Precipitate Change by Redissolution", Z. Elektrochem. 65 (7-8) 581-91 (1961).

32- I.M.Lifshitz and V.V.Slyozov, "The Kinetics of Precipitation from Supersaturate Solid Solutions", J.Phys. Chem. Sol. 19 35-50 (1961).

33- G.W.Greenwood, "The Growth of Dispersed Precipitates in Solutions", Acta Met. 4 243-248 (1956).

34- K.Tsumuraya, "Coarsening Models Incorporating

Both Diffusion Geometry and Volume Fraction of Particles", Acta Met. 31 437-452 (1983).

35- A.J.Ardell, "The Effect of Volume Fraction on Particle Coarsening: Theoretical Considerations", Acta Met. 20 61-71 (1972).

36- C.K.L.Davies, P.Nash and R.N.Stevens, "The Effect of Volume Fraction of Precipitate on Ostwald Ripening, "Acta Met. 28 179-189 (1980).

37- A.D.Braisford and P.Wyenblatt, "The Dependence of Ostwald Ripening Kinetics on Particle Volume Fraction", Acta Met. 27 489-497 (1979).

38- S.Sarian and H.W.Weart, "Kinetics of Coarsening of Spherical Particles in a Liquid Matrix", J.Appl. Phys.37 1675-1681 (1966).

39- J.J.Weins and J.W.Cahn, "The Effect of Size and Distribution of Second Phase Particles and Voids on Sintering", Sintering and Related Phenomena, G.C. Kuczynski (ed), Plenum Press, New York, NY, 1973 pp 151-163.

40- R.Asimov, "Clustering Kinetics in Binary Alloys", Acta Met. 11 72-73 (1963).

41- J.A.Marquesee and J.Ross, "Theory of Ostwald Ripening: Competitive Growth and its Dependence on Volume Fraction", J.Chem. Phys. 80 536-543 (1984).

42- P.W.Voorhees, "Theory of Ostwald Ripening",

J.Stat.Phys.38 231-252 (1985).

43- M.I.Mendelson, "Average Grain Size in Polycrystalline Ceramics", J.Amer.Ceram.Soc. 52 (8) 443-46 (1969).

44- C.Zener, quoted by C.S. Smith, "Grains, Phases, and Interfaces : An Interpretation of Microstructure," Trans. Metall. Soc. AIME , 175 15-51 (1948).

45- J.W.Cahn, "The Impurity Drag Effect in Grain Boundary Motion", Acta Met. 10 789-99 (1962).

46- K.Lucke and K.Deter, "A Quantitative Theory of Grain Boundary Motion and Recrystallization in Metals in the Presence of Impurities", Acta Met. 5 628-637 (1957).

47- R.J.Brook, "Controlled Grain Growth", in Treatise on Materials Science and Technology 9, Ceramic Fabrication Processes, pp 331, edited by Wang, F.F., Academic Press, New York, (1976).

48- H.Gleiter, "Theory of Grain Boundary Migration Rate", Acta Met. 17 853-862 (1969).

49- M.Fukuhara and H.Mitani, "Mechanisms of Grain Growth in Ti(C,N)-Ni Sintered Alloys", Powder Met. 25 62-68 (1982).

50- B.Merideth and D.R.Milner, "The Liquid-Phase Sintering of Titanium Carbide", Powder Met. 19 162-170 (1976).

51- D.Y.Kim and A.Accary, "Mechanisms of Grain Growth Inhibition During Sintering of WC-Co Based Hard Metals", Sintering Processes, G.C. Kuczynski (ed), Plenum Press, New York, NY,1980 pp 235-244.

52- W.D.Kingery, H.K.Bowen, D.R.Uhlman, "Introduction to Ceramics", John Willey and Sons, New York (1976) pp. 157-162.

53- G.Kuczynski, "Science of Sintering", Sci.Sint.9 243 1977

54- T.J.Gray, "Sintering of Zinc Oxide", J.Amer.Ceram.Soc. 37 (11) 534-39 (1954).

55- D.Dollimore and P.Spooner, Sintering Studies on Zinc Oxide", Trans.Faraday Soc. 67 (9) 2750-59 (1971).

56- T.K.Gupta and R.L.Coble, "Sintering of ZnO:I", J. Amer. Ceram. Soc. 51 (9) 521-25 (1968).

57- T.Senda and R.C.Bradt, "Grain Growth in Sintered ZnO and ZnO-Bi_2O_3 Ceramics", to be published in J.Amer.Ceram.Soc.

58- G.C.Nicholson, "Grain Growth in Zinc Oxide", J.Amer.Ceram.Soc. 48 (4) 214-215 (1965).

59- S.K.Dutta and R.M.Spriggs, "Grain Growth in Fully Dense ZnO", J.Amer.Ceram.Soc. 53 (1) 61-62 (1970).

60- W.A.Weyl, "Atomistic Interpretation of the

Mechanism of Solid State Reaction and Sintering", Ceram.Age 60 (5) 28-38 (1952).

61- O.J.Whittemore and S.L.Powell, "Effects of Oxygen Pressure and Water Vapor on Sintering of ZnO", Sintering and Heterogeneous Catalysis (ed) G.C.Kuczyski, A.Miller and A.G.Sargeant, Plenum Publishing Corporation (1984).

62- V.J.Lee and G.Parravano, "Sintering Reactions of Zinc Oxide", J.Appl.Phys. 30 (11) 1735-40 (1959).

63- L.F.Norris and G.Parravano, "Sintering of Zinc Oxide", J.Amer.Ceram.Soc. 46 (9) 449-52 (1963).

64- O.J.Whittemore and J.A.Varela, "Initial Sintering of ZnO", J.Amer. Ceram. Soc.64 (11) C.154-C.155 (1981).

65- O.J.Whittemore, J.A.Varela and E.S.Tosaya, "Pore Growth During the Sintering of ZnO", 5th International Meeting on Modern Ceramics Technologies, Italy, 1982.

66- J.Wong, "Sintering and Varistor Characteristics of ZnO-Bi_2O_3 Ceramics", J.Appl. Phys. 51 (8) 4453-59 (1980).

67- J.W.Medernach and R.L.Snyder, "Powder Diffraction Patterns and Structures of Bismuth Oxides", J.Amer. Ceram.Soc. 61 (11-12) 494-97 (1978).

68- H.A.Harwig, "On the Structure of Bismuth Sesquioxide α, β, and δ Phases", Z.Anorg.Allg. Chem. 444 151-66 (1978).

69- J.Kim, T.Kimura, and T.Yamaguchi, "Sintering of ZnO Doped with Antimony Oxide and Bismuth Oxide", J. Am. Cer. Soc. 72 (8) 1390-95 (1989).

70- T.Senda and R.C.Bradt, "Grain Growth During Liquid Phase Sintering of ZnO-Sb_2O_3 Ceramics", to be published.

71- T.K.Gupta, "Inhibition of Grain Growth in ZnO", J.Amer.Ceram.Soc. 54 (8) 413-414 (1971)

72- F.M.Levin, C.R.Robbins and H.F.McMurdie, "Phase Diagrams For Ceramists" Compiled at the National Bureau of Standards, Edited and Published by The American Ceramic Society Inc. (1964).

73- J.P.Gambino et al, "Effect of Heat Treatments on the Wetting Behavior of Bismuth Rich Intergranular Phases in ZnO:Bi:Co Varistors" J. Am. Ceram. Soc. 72 (4) 642-45 (1989).

74- Y.M.Chiang and W.D.Kingery, " Grain Boundary Migration in Nonstoichiometric Solid Solutions od Magnesium Aluminate Spinel: I, Grain Growth Studies" J. Am. Cer. Soc. 72 (2) 271-77 (1988).

75- J.B.Baldo. "Grain Growth in Refractory Dolomites", PhD Thesis, Dept. of M.S.E. University of Washington, 1986

76- C.Greskovich and K.W.Lay, "Grain Growth in Very Porous Al_2O_3 Compacts," J.Am.Cer.Soc.,55 [3] 142-46 (1972).

77- F.A.Nichols, "Theory of Grain Growth in Porous Compacts", J.Appl.Phys. 37 (13) 4599-4602 (1966).

78- O.Milosenic, P.Kostic, V.Petrovic, D.Uskokovic, "The Study of the Grain Growth and Electric Properties of ZnO Varistor Ceramics" Science of Sintering 15 [3] 121-130 (1983)

79- J.Wong, "Microstructure and Phase Transformation in a Highly Non-Ohmic Metal Oxide Varistor Ceramic, "J. Appl. Phys., 46 [4] 1653-59 (1975)

80- N.A.Haroum, and D.W.Budworth, "Effects of Additions of MgO, ZnO and NiO on the Grain Growth in Dense Alumina", Trans. Brit. Ceram. Soc., 69 [2] 73-79 (1970).

81- A.Mocellin and W.D.Kingery, "Microstructural Changes During Heat Treatment of Sintered Al_2O_3, "J.Amer.Ceram.Soc., 56 [6] 309-14 (1973)

82- W.C.Johnson and D.F.Stein, "Additive and Impurity Distributions at Grain Boudaries in Sintered Alumina, "J. Amer. Ceram. Soc., 58 [11-12] 485-88 (1975).

83- F.F.Lange and M.M. Hirlinger, "Hindrance of Grain Growth in Al_2O_3 by ZrO_2 Inclusions,

"J.Amer.Ceram.Soc., $_{67}$ [3] 164-68.

84- D.J.Green, "Transformation Toughening and Grain Size Control in β''-Al_2O_3 / ZrO_2 Composites, "J.Mat.Sci., 20 2639-46 (1985).

85- F.F.Lange and M.M.Hirlinger, "Grain Growth in Two Phase Ceramics: Al_2O_3 Inclusions in ZrO2, "J. Amer.Ceram.Soc., 70 [11] 827-30 (1987).

86- W.H.Rhodes, "Controlled Transient Solid Second-Phase Sintering of Yttria, "J.Amer.Ceram.Soc., 64 [1] 13-19 (1981).

87- W.D.Kingery and B.Francois, "Grain Growth in Porous Compacts, "J.Amer.Ceram.Soc., 48 [10] 546-47 (1965).

88- R.J.Brook, "Pore-Grain Boundary Interactions and Grain Growth, "J.Amer.Ceram.Soc., 52 [1] 56-57 (1969).

89- F.M.A.Carpay, "The Effect of Pore Drag on Ceramic Microstructures," pp. 261-275 in Ceramic Microstructures ' 76, edited by R.M.Fulrath and J.A.Pask, Westview Press, Boulder, Co, 1977.

90- A.M.Glaeser, "Microstructure Development in Ceramics: The Role of Grain Growth, "Yogyo-Kyokai-Shi, 92 [10] 537-46 (1984).

91- G.C.Nicholson, "Grain Growth in Magnesium Oxide Containing a Liquid Phase, "J. Amer.Ceram.Soc., 48 [10] 525-528 (1965).

92- Y.Moriyoshi and W.Komatsu, "Kinetics of Initial Sintering with Grain Growth, "J.Amer.Ceram.Soc., 53 [12] 671-75 (1970)

93- R.C.Buchanan, " Ceramic Materials for Electronics" pg 380 Marcel Dekker, Inc., New York and Basel, 1986.

94- J.Zhao and M.P.Harmer, "Sintering of Ultra-High-Purity Alumina Doped Simultaneously with MgO and FeO," J.Am.Ceram.Soc., 70 [12] 860-66 (1987).

Appendix A - Average Grain Sizes, G, For Different ZnO Particle Sizes

Composition	t(h)	G (μm) Temperature (°C)			
		900	1030	1192	1400
0.11μmZnO+6wt%Bi_2O_3	0.5			37	43
	1.0			39	45
	2.0			40	54
	4.0			47	64
2.0 μmZnO+6wt%Bi_2O_3	0.5	5	7	10	23
	1.0	5	7.5	11	30
	2.0	6	8	15	34
	4.0	7	9	17	39

Appendix . B - Average Grain Size, G, For The Compositions

$ZnO + 6\ wt\%\ Bi_2O_3 + Nb_2O_5$

Composition	t(h)	G(μm) Temperature (°C)			
		900	1030	1192	1400
$ZnO+6wt\%Bi_2O_3+0.05wt\%Nb_2O_5$	0.5			22	37
	1.0			27	39
	2.0			30	46
	4.0			36	50
$ZnO+6wt\%Bi_2O_3+0.10wt\%Nb_2O_5$	0.5			35	36
	1.0			38	40
	2.0			46	47
	4.0			49	53
$ZnO+6wt\%Bi_2O_3+0.20wt\%Nb_2O_5$	0.5			32	37
	1.0			35	41
	2.0			43	44
	4.0			45	57
$ZnO+6wt\%Bi_2O_3+0.40wt\%Nb_2O_5$	0.5			18	33
	1.0			21	43
	2.0			26	52
	4.0			28	55
$ZnO+6wt\%Bi_2O_3+0.80wt\%Nb_2O_5$	0.5	3	7	10	29
	1.0	3	8	11	32
	2.0	4	9	13	34
	4.0	4	11	15	46

Appendix C - Average Grain Size, G, For The Composition

$ZnO + 6\ wt\%\ Bi_2O_3 + Al_2O_3$

Composition	t(h)	G(μm) Temperature (°C)			
		900	1030	1192	1400
$ZnO+6wt\%Bi_2O_3+0.10wt\%Al_2O_3$	0.5	1.3	4.5	17	23
	1.0	1.5	5.5	18	28
	2.0	1.8	6.5	22	32
	4.0	2.0	7.0	26	40
$ZnO+6wt\%Bi_2O_3+0.20wt\%Al_2O_3$	0.5	2.0	5.0	18	25
	1.0	2.0	6.0	20	32
	2.0	2.5	6.5	25	40
	4.0	3.0	8.0	30	45
$ZnO+6wt\%Bi_2O_3+0.40wt\%Al_2O_3$	0.5	1.6	4.0	14	20
	1.0	1.6	5.0	15	25
	2.0	2.0	6.0	20	30
	4.0	2.2	6.0	21	33
$ZnO+6wt\%Bi_2O_3+0.80wt\%Al_2O_3$	0.5	1.0	4.0	12	21
	1.0	1.4	4.0	14	25
	2.0	1.6	5.0	16	29
	4.0	1.8	6.0	18	32

VITA

Silvia Irene Sylvestre Nunes was born on 03.17.1943 in S.Paulo, Brazil. She finished elementary, middle and high school at the "Instituto de Educação Dr. Alvaro Guião" in S. Carlos, S.P.. She entered the University of S.Paulo in 1962 where she earned a Bachelor Degree in Physics in 1968 and a Masters Degree in Solid State Physics in 1978 (thesis: Preferred Orientations in Niobium Determined by Neutron Diffraction). She earned her PhD in 1989 from the University of Washington (dissertation: Grain Growth in Sintered ZnO Ceramics).